

**Universidade de Évora - Instituto de Investigação e Formação Avançada
Università di Roma La Sapienza Aristotle University of Thessaloniki**

Mestrado em Ciência dos Materiais Arqueológicos (ARCHMAT)

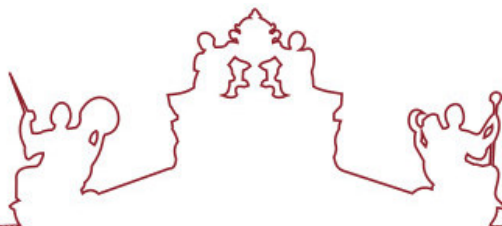
Dissertação

**Study of historical mortars from Villa Romana of Frielas |
Portugal**

Tanjil Ahmmed

Orientador(es) | Patrícia Sofia Moita
Cristina Galacho
José Carlos Quaresma

Évora 2021



**Universidade de Évora - Instituto de Investigação e Formação Avançada
Università di Roma La Sapienza Aristotle University of Thessaloniki**

Mestrado em Ciência dos Materiais Arqueológicos (ARCHMAT)

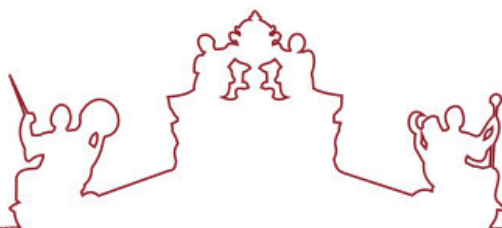
Dissertação

**Study of historical mortars from Villa Romana of Frielas |
Portugal**

Tanjil Ahmmed

Orientador(es) | Patrícia Sofia Moita
Cristina Galacho
José Carlos Quaresma

Évora 2021



A dissertação foi objeto de apreciação e discussão pública pelo seguinte júri nomeado pelo Diretor do Instituto de Investigação e Formação Avançada:

Presidente | Nicola Schiavon (Universidade de Évora)

Vogais | Carlos Alexandre Ribeiro (Universidade de Évora) (Arguente)
Cristina Galacho (Universidade de Évora) (Orientador)
Donatella Magri (Università degli Studi di Roma "La Sapienza")
Fabio Attorre (Università di Roma La Sapienza)
Panagiotis Spathis (Aristotle University of Thessaloniki)
Patrícia Sofia Moita (Universidade de Évora) (Orientador)

ABSTRACT

Study of historical mortars from the Roman villa of Frielas (Loures, Portugal)

The Roman villa of Frielas is an archaeological site from 3rd – 6th century AD located in Loures, Portugal. The villa is on excavation since 1997. The site is an area of 3500 m². The area still under excavation corresponds to the villa's urban pars. The villa has two construction phases, the first phase is very limited with structural evidence and mostly destroyed during the construction of 2nd phase. The 2nd phase has evidence of architectural features with functionality mainly, some compartments surrounding the peristyle with portico and mosaic floor passages. And its abandonment occurred at the beginning of the 7th century A.D. The abandonment phase has no remarkable architectural features, except some unfinished walls or destruction of earlier phases.

A total of eighteen mortar samples were collected from the different structures of the villa with different functional uses (render, filler, and floor) and analyzed by a multi-analytical approach by means of Optical Microscopy, (Stereo zoom and Petrographic microscope), X-ray Diffraction (XRD), Variable Pressure Scanning Electron Microscopy coupled with Energy Dispersive X-ray Spectroscopy (VP-SEM-EDS), Thermogravimetric analysis (TGA-DTG), Acid attack and Granulometric analysis.

The results revealed a similar composition of calcitic aerial binder, while differences in aggregates allowed to establish 4 groups. Raw materials are local and within a radius of 5Km. There was no prominent variation that can suggest a different chronology between the four groups. Though, it is assumed that there might be some renovation, restoration, or partial rebuilding that occurred in the same period. In terms of production technology, it is evident that the Vitruvius rules were not followed.

Key words: Mortars, Roman villa, materials, provenance, raw materials, archaeometry.

RESUMO

Estudo de argamassas históricas da villa romana de Frielas (Loures, Portugal)

A villa romana de Frielas é um sítio arqueológico do século III ao IV DC localizado em Loures, Portugal. A villa romana está em escavação desde 1997. O local tem uma área de 3500 m². A área ainda em escavação corresponde à área urbana da villa. Esta apresenta duas fases de construção sendo que a primeira fase é muito limitada com poucas evidências estruturais e/ou destruídas durante a construção da 2ª fase. A 2ª fase apresenta evidências de características arquitetónicas com funcionalidade principalmente, alguns compartimentos circundando o peristilo com passagens de pórtico e piso de mosaico. E seu abandono ocorreu no início do século 7 d.C. A fase de abandono não tem características arquitetónicas notáveis, exceto algumas paredes inacabadas ou destruição de fases anteriores.

Um total de dezoito amostras de argamassas com usos funcionais distintos (reboco, enchimento e assentamento) foram recolhidas, em diferentes estruturas da villa, e analisadas por uma abordagem multi-analítica compreendendo a Microscopia Ótica (estereomicroscopia e petrografia), a Difração de raios X (DRX), a Microscopia Eletrónica de Varrimento – Espectroscopia de Energia Dispersiva de raios X (MEV-EDS), a Análise Termogravimétrica (ATG-DTG), o Ataque Ácido e a Análise Granulométrica.

Os resultados revelaram que as argamassas estudadas apresentam uma composição semelhante, ligante de cal calcítica, enquanto que as diferenças nos agregados permitiram estabelecer 4 grupos. As matérias-primas são locais e num raio de 5km. Não se verificaram variações significativas que possam sugerir uma cronologia diferente entre os quatro grupos. Porém, presume-se que pode ter havido alguma renovação, restauro ou reconstrução parcial ocorrida no mesmo período. Em termos de tecnologia de produção, é evidente que as regras de Vitruvius não foram seguidas.

Palavras-chave: Argamassas, villa romana, materiais, proveniência, matérias-primas, arqueometria.

ACKNOWLEDGMENTS

It is through the contributions of other individuals both academic and emotional that any researcher can produce a research work. Therefore, I wish to acknowledge my gratitude to certain people without whom this thesis would not have been possible.

I record my sincere gratitude to my supervisor Professor Patricia Moita, my co supervisors Prof. Cristina Galacho and Prof. Quaresma for their constant guidance and support in the formation and completion of this thesis. Their constant support and patience with me in teaching and guiding me through the different stages of archaeometry research has made this thesis possible. I also record my heartfelt gratitude to Ana Raquel Silva for her relentless help and valuable suggestions throughout the period of this study.

I express my appreciation to all the researchers at the Hercules Lab with special thanks to Mafalda Costa, Luis Dias, and Fabio Sitizia for their support throughout the duration of my analysis. I also record my thanks to Anna Tsoupra for her support, guidance, and advice during this study.

I express deepest gratitude to Dulce Valdez and Deniz Kabil for inspiring, guiding, and helping me throughout this thesis. I also record my sincere appreciation to Ms. Sandra Velez and Ms. Aida Graça for extending their technical support whenever I needed it. I am deeply grateful to all my friends and colleagues with special mention for Carlos Andres Camara and Maria Almeida for the support and backing that they extended towards me through all the ups and downs of this research duration.

I record my thanks to Prof. Nick Schiavon and the ARCHMAT EMMC Committee, for allowing me to explore and experience a wide range of cultural exchange and opening doors for further scope in scientific studies in archaeology. My sincere appreciation to all my professors and teachers who helped me grow academically in the field of archaeometry throughout the duration of the programme.

I am forever indebted to my family who has shown never-ending support and constant backing in all my endeavours. I express my heartfelt appreciation to all my friends and colleagues for their encouragement and support given to me. Specially, I owe a great depth of gratitude to Ehsan Rahmath Ilahi for her greatest support and motivations, during this work.

Finally, it is by the grace of Almighty that this research work has been made possible hence I record my everlasting gratitude to Him.

Index

Abstract.....	I
Resumo.....	II
Acknowledgment.....	III
Table of Contents.....	i
List of Figures.....	ii
List of Tables.....	iv
List of Appendices	vii

Table of Contents

1	INTRODUCTION.....	1
1.1	Aim of the study	2
1.2	Mortars.....	3
2	ARCHAEOLOGICAL CONTEXTS	7
2.1	Historical Background.....	7
2.2	Roman villa of Frielas	10
2.2.1	The initial phase (third quarter of 1 st century AD- first quarter of 3 rd century AD)	10
2.2.2	Second Phase (First quarter of the 3 rd century AD - First quarter of the 5 th century AD)	11
2.2.3	Abandonment phase (Second quarter of the 5 th century AD - beginning of the 7 th century AD) 13	
2.3	The architecture of the villa	14
2.3.1	Peristyle.....	14
2.3.2	Compartments	14
2.3.3	Mosaic	15
2.3.4	Structures	16
2.3.5	Entrance of the passage	17
2.4	Geological context	18
3	SAMPLES AND METHODOLOGY.....	20
3.1	Analytical techniques and methods	20
3.1.1	Optical Microscopy.....	20
3.1.2	X-Ray Diffraction (XRD)	20

3.1.3	Thermogravimetric Analysis (TGA).....	22
3.1.4	Scanning Electron Microscopy coupled with Energy-Dispersive Spectroscopy (SEM-EDS) ...	23
3.1.5	Acid attack and Granulometric analysis.....	24
3.2	Sampling	25
3.3	Sample preparation.....	28
3.3.1	Powdered sample.....	29
3.3.2	Sectioned sample	30
3.3.3	Fragmented Sample	32
3.4	Experimental Conditions.....	32
3.4.1	Optical Microscopy.....	32
3.4.2	Stereo-Zoom Microscopy	32
3.4.3	X-Ray Diffraction (XRD)	33
3.4.4	Thermogravimetric Analysis (TGA-DTG).....	33
3.4.5	Scanning Electron Microscopy – Energy Dispersive X-ray Spectrometry (SEM-EDS)	34
3.4.6	Acid Attack and Granulometric Analysis.	34
4	RESULTS	36
4.1	Preliminary Observation	36
4.2	Stereo-zoom microscopy	39
4.3	Petrographic Analysis	45
4.4	X-ray Diffraction (XRD).....	48
4.5	Thermogravimetric Analysis (TGA).....	53
4.6	Scanning electron microscopy with Energy dispersive X-ray spectroscopy (SEM-EDS)	58
4.7	Acid attack and Granulometric analysis.....	65
5	DISCUSSION	73
5.1	Raw materials	74
5.1.1	Binder	74
5.1.2	Aggregates.....	77
5.2	Provenance study	79
5.3	Production Technology.....	82
6	CONCLUSIONS.....	87
7	REFERENCES.....	90
8	APPENDICES.....	94

List of Figures

Figure 1. 1- The lime cycle. A) Calcination, B) hydration and C) carbonation.	5
Figure 2. 1- Location of the Roman villa of Frielas in Google map. Yellow square marked the site.	7
Figure 2. 2- Ancient Roman trade route (left), Roman roads and secondary paths in ancient Lisbon territory (right) (the map adapted from Silva, 2012).	8
Figure 2. 3- Representative ceramic and amphorae fragments from the Roman villa of Frielas, a) Drawing of Amphorae (Haltern 70), b) Fragments of amphorae (Late roman time), c) decorated ceramic fragments (525-550 AD), d) decorated ceramic fragments, e) ceramic fragments (470-500 AD.). Images were collected from Ana Raquel and (Quaresma, 2017).	9
Figure 2. 4- Plan drawing; the Roman villa of Frielas, indicating construction phases. (The drawing adapted from Silva, 2012).	12
Figure 2. 5- Plan of the villa. (Adopted from Silva, 2000)	16
Figure 2. 6- Geological map of Frielas and its surroundings indicating 'Formação de Benfica' (ϕ_{Bf} / red brown), 'Calcário de Alfornelos' (ϕ_{Bf}^a / stripe in red brown), 'Complexo Vulcânico de Lisboa' (CVL- β^1 / dark brown), 'Formação da Bica' (C^2_{Bi} / light green), 'Formações da Gal e Caneça' (C^2_{Gc} / dark green) and sequential deposit of M_{B1} (orange), M_{B2} (stripe in Orange), M_{L1} (yellow), M_{S1} (light yellow). The nomenclature and names used for the various units correspond to those defined in the Explanatory Notice of the Geological Map of Portugal, at a scale of 1:50,000, Folha 34-B, Loures (Manuppella <i>et al.</i> , 2011).	18
Figure 3. 1- a) Schematic representation of the interference process by waves produced by the ordered arrangement of atoms in a crystal (Stuart, 2007), b) Schematic diagram of an XRD diffractometer setup (Stuart, 2007)	21
Figure 3. 2- Scheme showing the location of the sample collected from the Roman villa of Frielas.	25
Figure 3. 3- Sample collection from the Roman villa of Frielas, a) Carefully using hammer and chisel, b) water channel sidewall, c) parallel wall of water channel, d) peristyle wall, e) Overlapping floor, f) mosaic floor, g) filler mortar, h) stairs, i) compartment wall (opposite side of the mural painting).	26
Figure 3. 4- Sample preparation diagram	28
Figure 3. 5- Tools used for the preparation of the powdered samples: a) Disaggregation by mortar and pestle, b) Powdering equipment PM 100 Planetary Ball Mill (Retsch), c) Agate grinding jar and grinding balls	29
Figure 3. 6- Thin section and polished section preparation: (a) selected part of samples, (b) Struers EpoFix resin and hardener (c) Sample in resin solution, (d) hardened sample (e) cutting by discoplan-TS, (f-h) Buehler Epoxy Resin for gluing, (i-j) System Abele press Cutting out the thin sections under vacuum using a Logitech CS10 Thin Section Cut Off Saw (k) polishing thin section by hand on silicon carbide paper (l) Results of FRL-9, polished section (m) and thin section.	31
Figure 3. 7-Experimentation of the analysis: a) Preparation of HCl aqueous solution, b) Heating up the sample in HCl aqueous solution on hot plate up to boiling temperature, c) Cooling down the solution, d) Adding water to the solution, e) Filtration under vacuum using a Büchner funnel, g) Filtered wet sample using filter paper, h) Dried sample, f) Sieving using ASTM E11 test sieves.	35

Figure 4. 1- Visual observation and Photographic documentation of representative mortar samples.	37
Figure 4. 2- Type of ceramics found in each Sample. ‘Y’ axis showing visually estimated volume.	40
Figure 4. 3- XRD patterns (Global fraction) of ceramic rich samples (Group-A), (Q-quartz, C-calcite, F-feldspar, and Mi-mica).	49
Figure 4. 4- XRD patterns (Global fraction) of ceramic rich samples (Group-B), (Q-quartz, C-calcite, F-feldspar)	50
Figure 4. 5- XRD patterns (Global fraction) of basaltic and shell fragment rich samples, (Group-C) ,(Q-quartz, C-calcite, F-feldspar- ferrosilite, Au-augite, and H-hematite)	50
Figure 4. 6-XRD patterns of soil sample-FRL-13-s, (1 st phase) (Q-quartz, C-calcite, F-feldspar, Mi- mica, and Fe-	51
Figure 4. 7- XRD patterns of soil sample-FRL-16-s (abandonment phase) (Q-quartz, C-calcite, F-feldspar, Mi- mica, and	51
Figure 4. 8-Calculated percentage of CaCO ₃ in the samples of Roman Villa of Frielas from TGA results.	53
Figure 4. 9-TG/DTG curves of ceramic rich (group-A) samples FRL-1 (brown), FRL-3 (purple), FRL-5 (blue) and FRL-7-i (green), FRL- 9 (black) and FRL-10-D (red). continuous curves representing TG and dashed curves representing DTG data.	54
Figure 4. 10-TG/DTG curves of binder-rich upper layers (Group-D) samples FRL-6-U (green), FRL-8-U (blue), FRL-10-U (red), and FRL-19-U (black), continuous curves representing TG and dashed curve representing DTG data.....	55
Figure 4. 11- Soil sample (FRL-13-s) 1 st phase of the villa, Thermogram showing decomposition of CaCO ₃ , and decomposition between 200-600°C range could possibly indicate the present of clay minerals in the sample.	56
Figure 4. 12- Soil sample (FRL-16-s) abandonment phase, Thermograms showing decomposition of CaCO ₃ . 56	
Figure 4. 13-Siliceous aggregates. a) sample-FRL-12 (group-B), b) sub-angular shape aggregates in BSE image of FRL-12, c) Blue=Ca, yellow=Si, the elemental map showing Si-rich quartz in Ca-rich binder, d) Sample-FRL-3 (group-A), e) BSE image indicating crushed lime and angular shape aggregates, f) elemental image showing Ca-rich angular lime fragment and Si-rich quartz as aggregates.....	58
Figure 4. 14-Basaltic rock fragment, a) Sample-FRL-1 with rounded basaltic rock fragment, b) BSE image of basaltic rock fragments, c) multi-point analysis spectrum of the spot marked in ‘b’ image, d) elemental image of green=Mg, blue=Ca, e) orange=Al, f) blue=Na, g) red=Fe.	59
Figure 4. 15-basaltic grain as aggregates, a) Sample-FRL-19 (group-C), b) rounded basaltic grain in BSE image, c) multi-point analysis spectrum of the spot marked in image ‘b’.	60
Figure 4. 16-stratified layers, a) FRL-6-U&D, b) BSE image showing Upper and lower layer, c) elemental mapping indicating blue=Ca, yellow=Si, binder, and aggregates in both layers, d) FRL-8-U&D,(mosaic floor), e) binder (blue=Ca) rich upper layer-FRL-8, f) blue-Ca, yellow=Si, angular- subangular quartz in the lime binder (lower layer-FRL-8), g) decorative sample FRL-19-U &D, h) BSE image, i) elemental image showing upper and lower layer and aggregates distribution.....	61
Figure 4. 17- FRL-8 U & D layer, Tesserae composition, a) FRL-8, Mosaic floor, tesserae, b) multi-point analysis on tesserae, c) spectrum of the spot marked on image ‘b’, the composition of tesserae, Ca, Si, Mg, and Al. 62	

Figure 4. 18-Ceramic rich sample with cracks. a) sample-FRL-1 (group-A), b) arrows indicating cracks in the binder alongside the ceramic fragments in BSE image, c) elemental image- blue=Ca, orange=Al. 62

Figure 4. 19-Cracks in the binder. a) BSE image of sample FRL-8-U, b) blue-Ca, yellow-Si showing cracks in the binder and Si rich quartz as aggregates, c) Arrow indicating cracks in the elemental image, red=C. 62

Figure 4. 20-Lime lumps, and shell fragments, a) sample-FRL-15 (group-C), b) BSE image showing rounded lime lumps and shell fragment, e) blue=Ca, yellow=Si, orange=Al, the arrow indicating Ca-rich shell fragment a rounded lime lump, d) linear shape shell fragment, e) Ca, Al, Si, and pink=K, the elemental image showing Ca-rich shell fragments, sub-angular and poorly rounded quartz, and feldspar. 63

Figure 4. 21-Lime lump, FRL-17 (group-C) a) yellow line indicating lime lump, b) multi-point analysis spectrum of the spot marked in image 'a' 63

Figure 4. 22 -Binder composition, a) mapping in FRL-1 (group-1), b) point analysis in binder c) spectrum shows binder composition of spot marked in image 'b', d) mapping on FRL-19-D (group-C), e) multi-point analysis in the binder, f) spectrum shows binder composition of spot marked in image 'e', g) areal map on FRL-8-U (group-B), h) point analysis on the binder, i) spectrum shows binder composition with the presence of Ca with Mg, Al, Si, and K. 64

Figure 4. 23-Sample with chromatic layer, a) sample- FRL-17, with chromatic layer, b) BSE image on a pigmented layer, c) multi-point analysis spectrum of spot marked in image 'b', d) elemental mapping, yellow=Si, blue=Ca, e) elemental image of pigmented layer, orange= Al, f) map showing elements yellow=Si, blue=Ca, red=Fe..... 65

Figure 4. 24- Calculated weight (%) of soluble and insoluble residue obtained by Acid attack analysis. Sample-FRL-17 is not in the chart, due to insufficient materials, there were no acid attack analysis for this sample. 66

Figure 4. 25.a-Grain size distribution from average mean values in weight percentage. Ceramic rich sample (Group-A) marked in red, quartz rich samples (Group-B) marked in green. Group-C marked as purple, and group-D marked as orange box. 67

Figure 4. 26 - Gravel: Mud: Sand diagram obtained from the GRADISTAT software. 69

Figure 4. 27-Ceramic rich samples representative to group A 70

Figure 4. 28- Representative grain distribution images of quartz rich samples, group-B 71

Figure 4. 29- Representative grain distribution image of group-C, sample with shell and basaltic rock fragments 72

Figure 5. 1- Amount of CaCO₃ (weight %) of the studied samples. Comparison of TGA, acid attack (Soluble fraction), and XRD. XRD is giving fragile quantitative analysis from GF (Global fraction). Sample- FRL-17, could not perform the acid attack analysis due to insufficient materials therefore soluble fraction (SF) curve (blue) showed 0 percentage. 74

Figure 5. 2- Representative % of elements present in binder results from EDS analysis; Ca (blue), Mg (green), Si (yellow), K (pink), Na (light blue), and Fe (red). Samples that are not presented in the chart, due to lack of information and unavailability of the instrument. 76

Figure 5. 3- a) shows the Stratigraphy of a Roman mosaic floor according to Vitruvius’s description. (Adapted from Caldeira et. al., 2019). 1. Tessellatum, 2. Bedding, 3. Nucleus, 4. Rudus, 5. Statumen, b) section view of the sample FRL-8 (mosaic floor) in situ, from the site, c) prepared polished section of the sample FRL-8, containing stratigraphic layers of the floor. 78

Figure 5. 4- Lithographic map of Loures: Formation of Benfica (yellow) and Miocene limestone (lemon green), Lisbon volcanic complex (LVC) in brown. (Zêzere, 2020) 81

List of Table

Table 3. 1- Mortar and soil samples from the Roman Villa of Frielas 27

Table 4. 3- Distribution frequency of ceramic fragment types found in samples. 40

Table 4. 4- General aspect of the samples under stereo zoom microscope. 41

Table 4. 5- Preliminary assessment and microscopic observations. 42

Table 4. 6- Representative petrographic images of the general composition of mortars. 46

Table 4. 7- Representative petrographic images of the minerals observed under XPL (cross polarized light) and PPL (plane-polarized light)..... 47

Table 4. 8- Petrographic observation results. 48

Table 4. 9- Mineralogical composition of the fine fractions of mortars assessed by XRD 52

Table 4. 10- TGA results. Record of the mass loss percentages during structurally bound water loss, decomposition of CO₂, CaCO₃ percentage and estimated binder to aggregate ratio. 57

Table 4. 11- Description of the insoluble residue..... 69

Table 5. 1-Division or groups of samples for the result discussion. 73

Table 5. 2- Sample composition (mass %) and binder to aggregate ratio by Jedrzejewska method (Jedrzejewska, 1960) 85

Table 5. 3- Weight loss percentages of structurally bound water in the temperature range 200-600 °C, and CO₂ (600-900 °C) for understanding the hydraulic characteristic of the samples..... 86

List of Appendices

Appendix 8. 1-The Roman villa of Frielas, east to west orientation view.	94
Appendix 8. 2- The Roman villa of Frielas, west to north orientation view.	94
Appendix 8. 3-The Roman villa of Frielas. South-east corner, 1 st phase structures.	95
Appendix 8. 4-Peristyle wall with the column, surrounded by mosaic floor and the portico.	95
Appendix 8. 5- Photographs of collected samples from the Roman Villa of Frielas, after cleaning.....	96
Appendix 8. 6-Results of soluble and insoluble fractions after acid attack, and granulometric analysis performed in insoluble fractions.	99
Appendix 8. 7-Thermograms of the results of the global fraction powders of the samples from the Roman villa of Frielas.	100
Appendix 8. 8-X-ray Diffractograms of the powdered global fractions of the mortar samples from the Roman villa of Frielas.....	103
Appendix 8. 9-Insoluble residues obtained after the acid attack, observed by Stereo zoom microscope	106

1 INTRODUCTION

.....

The use of mortar is as ancient as the art of architecture; for example, the Egyptian pyramids contain mortar works dating back to at least 4000 B.C (Krumnacher, 2001). Mortars used in historical monuments contain important information about the construction technology of the time in which they were constructed, and they are as important as historical records; consequently, historical mortar analysis should be performed using a scientific approach. The information extracted from these approaches gives useful knowledge about how complex architectural structures were built and remained throughout the long periods, as well as evidence of the technological background of specific historical periods. Furthermore, mortar studies give important contributions to future restoration projects and material provenance research.

The subject of this study is the analytical characterization of historical mortars from the Roman villa of Frielas. The villa is in the northern part of the parish of Frielas, the municipality of Loures under the Lisbon District. The archaeological record reveals an occupation of this villa from the end of the 3rd century/beginning of the 4th century AD to its abandonment in the beginning of the 7th century A.D.

A multi analytical approach was made to characterize the mortar samples from this roman villa. All the results are based on analytical techniques that were used to define mortar in terms of raw materials and their provenance, production technology and manufacturing recipes.

1.1 Aim of the study

Mortar is a wide range of research area, especially when it is from the Roman period. It is worth mentioning that there is plenty of effective research in mortars already conducted and well-published. But still, the word re-search is always a new opportunity to search for more details and acquire knowledge from different historical structures. With this perspective, the Roman villa of Frielas and mortars from its construction phases can be interesting to find out the technological changes, characteristics, raw materials, and provenance study.

By using multi-analytical techniques, this study aims to provide a textural, mineralogical, and chemical characterization of the mortars combined with archaeological data. The results will provide a comprehensive knowledge of the technologies applied in their manufacture as well as the origin of the raw materials used. The results will allow for the identification of several construction phases of the villa as well as significant information about the historical background. The relationship between the selected materials and the expected results will be evaluated. The effort will also help with future restoration methods, such as the creation of appropriate repair mortars.

This archaeometric study was undertaken at the HERCULES Laboratory of the University of Évora, Portugal, as part of the Erasmus Mundus Archaeological Materials Sciences Joint Master's Degree (ARCHMAT). The acquired information will be utilized to compare the mortars to ancient construction material production formulas described by Vitruvius in his Ten Books on Architecture, as well as to comprehend the significance of the Roman villa of Frielas and its relation to other Roman villas. In order to consolidate and repair their manufacturing technologies, useful information about their technologies has been deduced.

A total number of eighteen mortar samples from the Roman villa of Frielas is collected, to characterize the samples with multi-analytical approaches. Optical Microscopy (Stereo zoom and Petrographic microscopes), X-ray Diffraction (XRD, Powder XRD), Variable Pressure Scanning Electron Microscopy coupled with Energy Dispersive X-ray Spectroscopy (VP-SEM-EDS), Thermal Gravimetric Analysis (TGA-DTG), Acid attack, and Granulometric analysis will be used to examine the samples.

1.2 Mortars

The term "mortar" refers to a composite mixture consisting of a binder and small-sized aggregate material which is commonly employed as a structural binder between masonry units such as bricks and stones (Artioli, *et al.*, 2019). Mortars can have a variety of compositional characteristics based on the raw materials employed and the manufacturing techniques used at the time (Riccardi *et al.*, 2007). Mortars are widely studied, nowadays due to the scientific advancements which help to understand their manufacturing recipes, capabilities, and durability (Ergenç and Fort, 2019). Normally, the raw materials used for manufacturing mortars are locally acquired and the application process varies depending on the function of the mortar (Artioli, 2010; Borsoi *et al.*, 2019).

In general, mortar is made up of three ingredients: aggregate, binder, and water, all of which are mixed together to make a paste (Borelli, 1999; Schnabel, 2008). In some cases, mortars have additives that provide additional features such as waterproofing. Binders help to bind the aggregate grains within the mixture. Based on the mode of setting, binders can be classified into two; aerial (non-hydraulic) binders that are set when in contact with air and hydraulic binders that set when in contact with water. Therefore, the type of binder used depends on the function of the mortar.

There are three types of binders that have been used throughout history until recent times which are mud/clay, gypsum, and lime (Elsen, 2006). The oldest examples of clay binders can be found at the walls of Jericho (Israel) dating from 8300 BC and structures in *Çatalhöyük* (Turkey) dating from 6000-7500 BC. Since no heat treatment was needed for their production, mud binders are not as durable and show less strength against the degradation caused by weathering (Rodríguez-Navarro, 2012). The other two binders, gypsum, and lime are results of heating processes in which gypsum requires lower temperatures and lime requires higher temperatures, implying that gypsum was used as a binder component earlier than lime (Elsen, Van Balen and Mertens, 2013).

The second main component of mortars are aggregates which are dependent on the region they are acquired from. The main purpose of including aggregates in mortars is to prevent shrinkage of the paste when dried. Natural sand recovered from river or sand quarry is the most common aggregate that is used in mortars, but crushed stones and shells are also used after they undergo a series of manufacturing processes (Schnabel, 2008). Through a series of examinations on the composition, size, and shape of the aggregate's origin and the source of the raw materials may be tracked since they do not significantly alter or interact with other materials in the mortar during the production steps of the mortar making (Schnabel, 2008). The study of aggregates helps understand the geological origin and recipe of the mortar fabrication (Elsen, 2006). Other aggregates include non-porous rocks and gravel, porous bricks and pottery, and organic aggregates such as charcoal and fibers which provide tensile strength to the mortar. It should be noted that a mixture of aggregates may be used depending on the function of the mortar (Elsen, 2006).

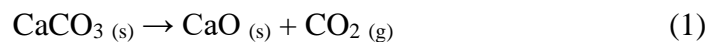
In association with aggregates, additives are a frequent component in mortars. They can be organic (straw, hair, eggs) or mineral (or pozzolanic), and they create hydration cementitious products when mixed with hydrated lime (Elsen, 2006). These pozzolanic additions can be of natural origin, as mentioned by Vitruvius in Book II, Chapter VI, and obtained from the volcanic pyroclastic rock; or they can be man-made, produced from powdered ceramic materials, most commonly tiles and pottery (Elsen,2006).

The employment of *opus signinum* coating in Roman mortars connected to water-bearing and hydraulic constructions is a unique feature. The use of *opus signinum* in water facilities has been observed at the Roman sites of *Pisões* (Borsoi *et al*, 2019), *Ammaia* (Cardoso *et al*, 2014), *Augusta Emerita* (Robador *et al*, 2010), *Conmbriga* (Velosa *et al*,2007), *Tróia* (Silva *et al*, 2006), *Mérida* (Franquelo *et al*, 2008; Robador *et al.*, 2013). This form of waterproofing coating is made by combining lime-based mortars with fine sand and a high proportion of *cocciopesto* (ceramic pieces or broken pottery, which may also be used as a coating, such as in pavements) (Borsoi *et al*, 2019). Crushed ceramics have been employed for constructions associated with water-bearing features such as baths, canals, and aqueducts since early Hellenistic to early Byzantine periods (Elsen,2006), mostly to protect the walls from dampness.

Among the Roman mortars, lime has been considered the most common mortar binder in the historical context (Schnabel, 2008). Lime-based binders get their strength due to a series of chemical reactions given by the nature of the components and their interaction. The lime cycle plays the most important role, and it consists of three main steps: a) calcination, b) hydration or slaking, and c) carbonation or hardening. (Delatte, 2001; Elsen, 2006; Rodríguez-Navarro, 2009).

1. Calcination (A)

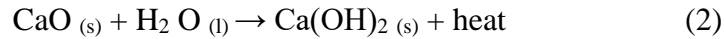
The calcite (CaCO_3) in the limestone decomposes at high temperatures (900 - 1000°C) during the calcination process, generating calcium oxide (CaO), commonly known as quicklime, and releasing carbon dioxide (CO_2) as stated in equation (1). This procedure takes place in a kiln with limestone from a quarry, and the final product is known as burned lime or lump lime.



2. Hydration (B)

The second process, known as hydration which occurs after the quicklime is produced. Water (H_2O) is added to the quicklime during this process to hydrate it, creating calcium hydroxide (Ca (OH)_2) and generating heat, as stated in equation (2). The hydration process might result in the formation of a dry powder, or a lime paste in one of two ways. When just enough water

is used in the slaking process, the dry powder known as hydrated lime is created. Lime pastes or lime putty, commonly known as slaked lime, are made by adding extra water to lime (Rodríguez-Navarro, 2012).



3. Carbonation (C)

Carbonation is the last phase in the lime cycle when the slaked lime generated by hydration is converted back into calcium carbonate (CaCO_3) by collecting carbon dioxide from the atmosphere and producing water, as indicated in equation (3).

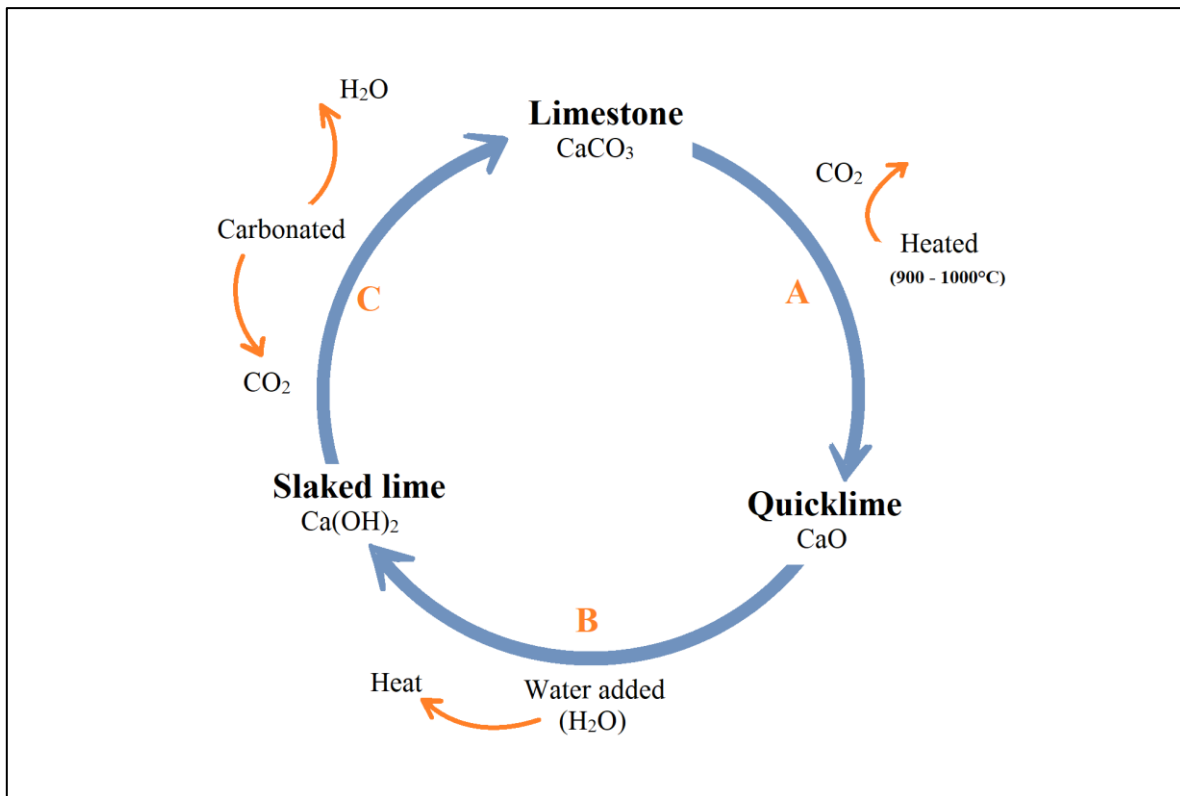
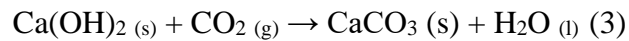


Figure 1. 1- The lime cycle. A) Calcination, B) hydration and C) carbonation.

When calcium carbonate hardens, all the components in the mixture come together to form a hard and solid mixture with a finely crystallized calcite matrix (Elsen, 2006; Rodríguez-Navarro, 2009). The size of the calcite crystals and their textural characteristics may be affected by external circumstances during the carbonation process (Elsen, 2006). The limestone used for the burning may have both calcium and magnesium carbonate in its

composition. Because they operate somewhat differently owing to their magnesium concentration, such a scenario may influence the temperature of the calcination. In comparison to calcitic limes, dolomitic limes would slake more slowly (Schnabel, 2008).

Some binder-related particles are associated with the type of limestone used and the burning conditions, resulting in lime-lumps which are formed due to lack of water or time during slaking, that when underburned, can reveal the raw material used, and when over-burned, can reveal the calcination temperature (Elsen, 2006).

They can be observed in the final binder composition as rounded porous inclusions within the matrix (Elsen, 2006). They represent the initial raw material and therefore can be used for understanding the provenance of the raw materials and the lime production technology.

Previous research has demonstrated the early use of quicklime in the Hayonim Cave since 10,400 BC and lime plaster in the Neolithic sites of the Levant region since 8,700-7,000 BC (Artioli, 2010), and that most probably the lime-plaster diffusion was made through Greece to the Etruscans and then followed to the Roman Empire (Artioli, 2010). Certain ancient works such as *'the ten books on Architecture'* and *'Natural history'* written by scholars Vitruvius and Pliny respectively mention provenance and quality of materials and recipes for different uses of mortars. Vitruvius suggests using white and hard stone to burn to make lime for building structural parts and porous rocks for stucco and rendering in the fifth chapter of Book II of *'Vitruvius De Architectura'* (Morgan, 1914).

Vitruvius suggests the use of clean pit sand, freshly taken from the sandpits, riverbeds, gravel, or sea sand to prevent weathering, and warns on the use of sea sand and the related possible problems, such as gradual drying and surface degrading, in his treatise *'The ten books on Architecture'*. Specifically, he defines the binder-to-aggregate ratios based on the sand's source: *"After slaking it, mix the mortar with 3 parts of pit sand and one of lime; for river or sea-sand, 2 parts of sand and one of lime. Using river or sea sand, the third part of burnt brick pounded up and sifted can be added to make a better composition"* (Book II, Chapter V, Vitruvius).

2 ARCHAEOLOGICAL CONTEXTS

2.1 Historical Background

The Roman villa of Frielas (*Villa Romana de Frielas*), which was named after the town it is located in, is an archaeological site that is on excavation since 1997, as a result of an investigation conducted by the municipality of Loures. The villa is in the northern part of the parish of Frielas, municipality of Loures under Lisbon District (38°49'37.1" N-9°08'37.9" W) and on the right bank of Póvoa stream (*Ribeira da Póvoa*), at 7-10 m distance and on the right of the Tagus River across the Trancão River. It was part of the territory of *Olisipo* (present-day Lisbon) which included a vast area ranging from *Torres Vedras* to the north, to the vicinity of *Alenquer* in the east during the roman time (Silva, 2004; Quaresma, 2017).

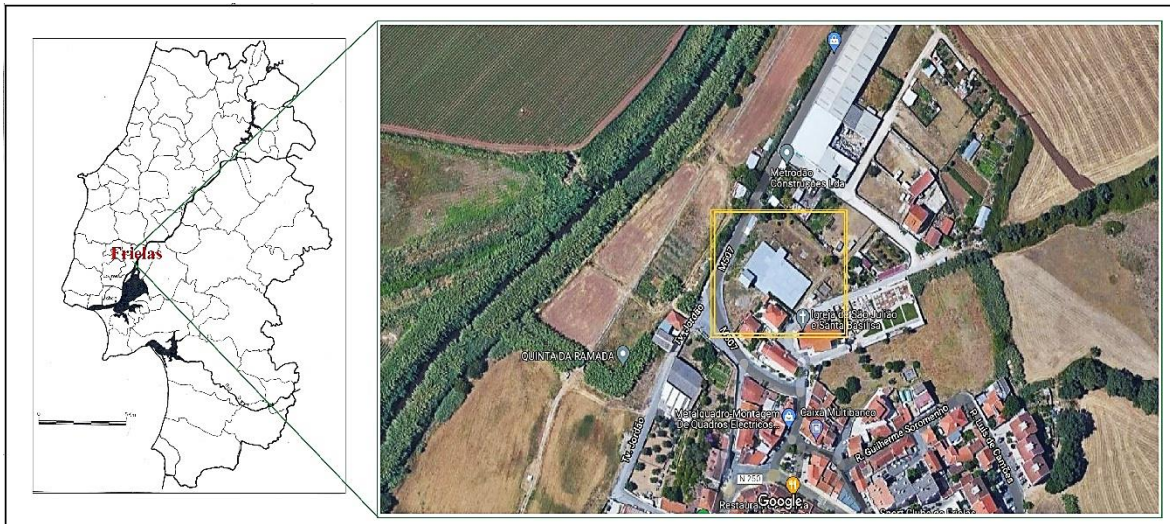


Figure 2. 1- Location of the Roman villa of Frielas in Google map. Yellow square marked the site.

The site has a total area of 3500 m² and the area that is under excavation corresponds to the villa's urban pars which belongs to the end of the 3rd century/beginning of the 4th century AD. There is evidence of previous occupations at the site that corresponds to the high imperial period fit in the 1st/2nd century AD and the archaeological record also reveals that the villa was abandoned at the beginning of the 7th century AD. As a result of its location in the floodplain of Loures, it certainly benefited from the proximity of the river allowing for navigability, water supply, fish activity, salt exploitation, and soil fertility. About 2 km, on the Frielas bridge, the Roman trade route that connected *Olisipo* (Lisbon) to *Conimbriga* (Coimbra) existed. It is possible that there was a secondary access path to Villa de Frielas. This road system would have been complemented by the hydrographic network that at the time, was very relevant for the economy, freight transport, and population mobility. The

section that passed on Frielas bridge corresponds to the milestone found in Frielas, with a probable chronology from the 4th century AD, that can be attributed to Emperor *Magnentio*, who ruled the West between 350/353 AD (Silva, 2001).

The crossing of roads that the bridge of Frielas currently represents may have had correspondence in Roman times, thereby forming a secondary access path to the villa of Frielas (Fig. 2.2). This set of conditions would certainly have had promoted the establishment of this Roman rural property. The Roman society greatly appreciated the rural world, as a result of which many wealthy families owned rural properties which constituted a true pole of economic production. The establishment of *Villa de Frielas* would certainly not be very different from that of the other villas that are already widely known, although the data currently available is incomplete and correspond only to the urban pars of the villa.

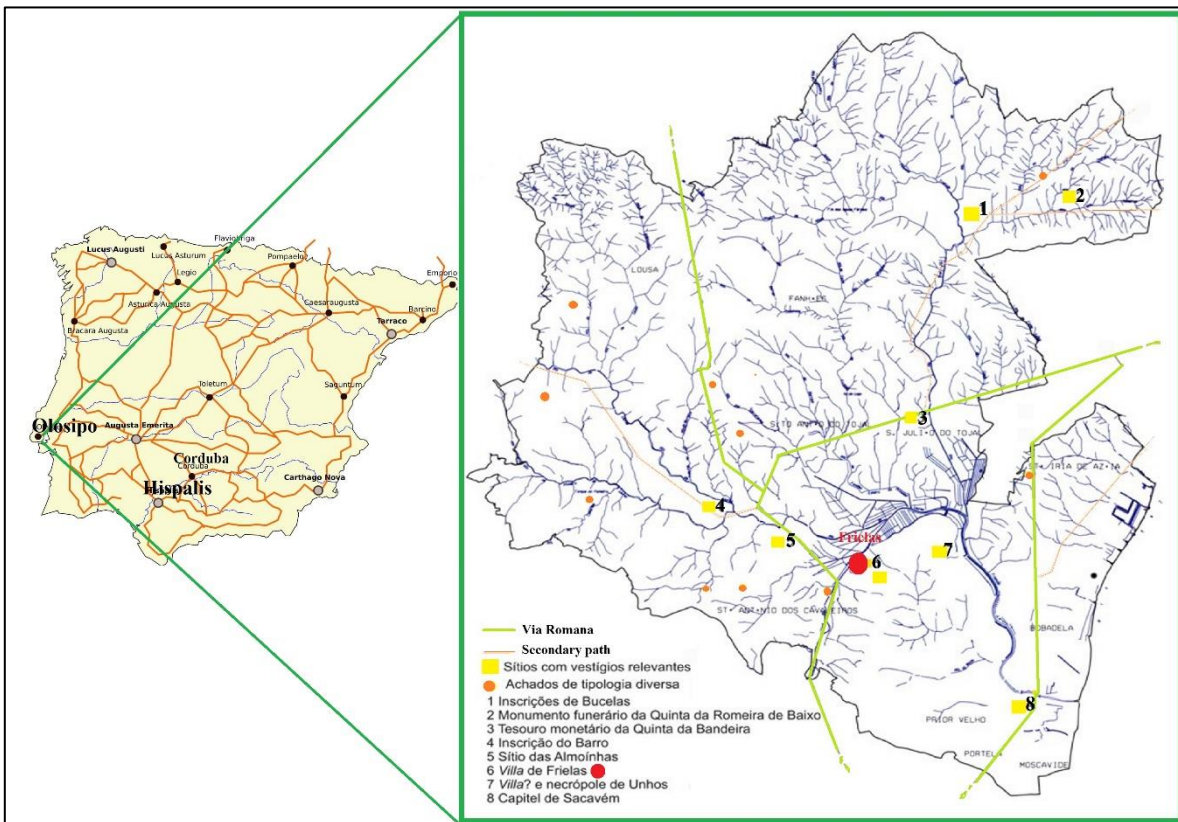


Figure 2. 2- Ancient Roman trade route (left), Roman roads and secondary paths in ancient Lisbon territory (right) (the map adapted from Silva, 2012).

In literature, the concept of the villa has earned different connotations and it is widely discussed by classical and contemporary authors. The classification of the villa is given by its use, and it can be classified, according to Carneiro (2016), as a space of *negotium*, which is determined by its functionality in terms of “agricultural and livestock production cannons of property” (Carneiro, 2016); or as a space of *otium*, which consists of a set of spaces and environments where daily personal life habits take place. The second type of villa was used

not only as a private residence to display the identity of the dominus and his cultural knowledge of the world, but also as a political, social, and economic statement reinforced by the personal relationships of the owner (Carneiro, 2017a; Carneiro, 2014). The villa as a space of *otium* became a tool to show to the world the dominus' power by the celebration of exclusive feasts and gatherings involving people from the same socioeconomic status. These feasts would take place in opulently adorned rooms sometimes with colorful mosaics and water mirrors imitating nature to create astonishing atmospheres (Carneiro, 2014), in which case the villa Romana de Frielas makes no differences.

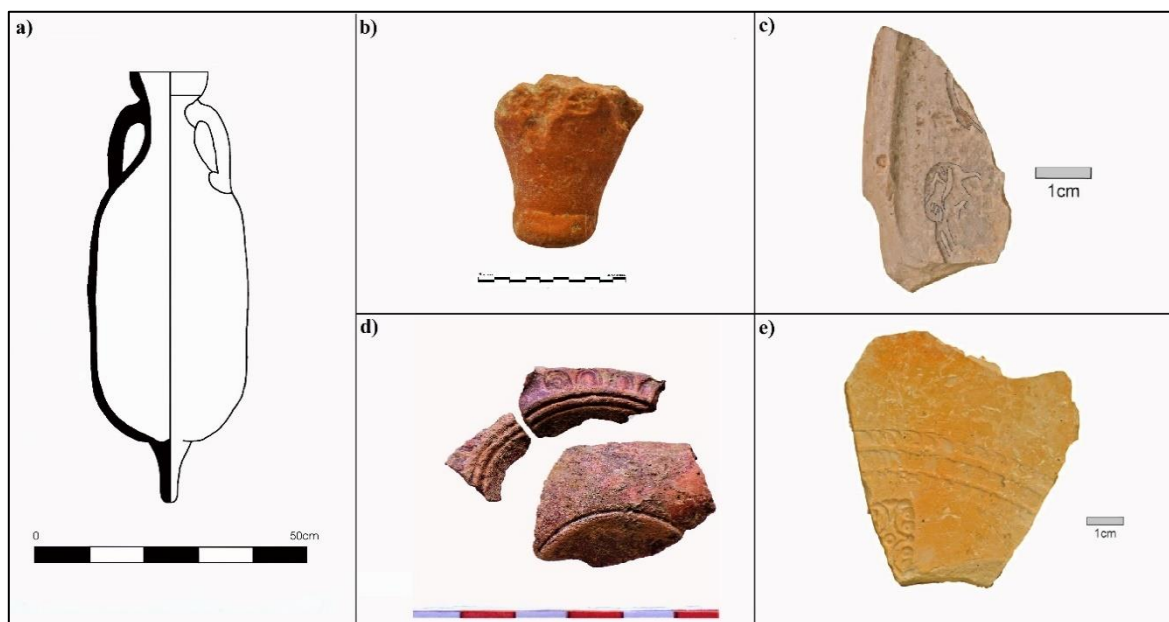


Figure 2. 3- Representative ceramic and amphorae fragments from the Roman villa of Frielas, a) Drawing of Amphorae (Haltern 70), b) Fragments of amphorae (Late roman time), c) decorated ceramic fragments (525-550 AD), d) decorated ceramic fragments, e) ceramic fragments (470-500 AD.). Images were collected from Ana Raquel and (Quaresma, 2017).

The collection of some fragments of figurines and the existence of stored surpluses, a product of intense agricultural production as well as the appearance of some fragments of loom weights was indicative of the practice of weaving, as well as the rearing of woolen cattle. It is quite possible that the establishment of this Roman Villa in Frielas took place in the mid-3rd century AD to the beginning of 4th century AD, which is contemporary to the beginning of roman urban decay, a situation that allowed the development of the great rural property. At a time when difficulties were beginning to plague the Roman Empire, these small rural poles tended to implement systems of self-sufficiency, reducing their dependence on the outside, without giving up certain luxuries (Silva, 2012; Quaresma, 2017). In the case of Frielas, this situation is evident with the mosaic pavements and imports of *terra sigillata*. The various pits that were opened and found to be very disordered are a worthwhile mention. Though initially they may have been used as storage silos; at one point in time, they were filled with household waste. A radiocarbon dating analysis obtained from a sample of coal collected from a ceramic concentration of the pits gives the date of 960±100 BP, with

intervals for 1 sigma, 997-1214 cal AD and for 2 sigma, 888-1281 cal AD, indicative of a very comprehensive period, but already considered to be Medieval (Silva, 2012).

All the above-mentioned facts provide different functionality to the housing space of Villa Romana and although its existence and content are equally important in the study of the continuation of occupation of this site, these facts have made it difficult to interpret the current structures of the Roman period.

2.2 Roman villa of Frielas

Depending on the data currently available, the territory of Loures had a strong occupation in Roman times, namely in Imperial times, with little evidence from the 2nd century A.D. The Frielas villa fits into this chronological panorama, even revealing an extended occupation. Analysis of amphorae material and Terra sigillata results in continuity in the consumption patterns of this villa, since the third quarter of the 1st century A.D. to the beginning of the 5th century AD; following which there appears a set of indications that point to the gradual abandonment of the villa until the beginnings of the 7th century AD. Within the wide period of effective occupation of the villa, two construction phases initial (third quarter of 1st century AD- first quarter of 3rd century AD) and the second phase (first quarter of the 3rd century AD - first quarter of the 5th century AD) have been distinguished.

2.2.1 The initial phase (third quarter of 1st century AD- first quarter of 3rd century AD)

Very few physical traces remain of the first phase indicated by the presence of some sections of a wall found beneath the structures of the next phase and certain archaeological materials. It is very likely to have begun in the third quarter of the 1st century A.D., extending until the middle of the third century AD, during which a restructuring took place of the entire villa - or at least the *pars urban*. Contributing to this chronology are the decorative motifs of the mosaics that point towards the end of the third century AD or the beginning of the fourth century AD. It should also be noted that the architectural elements identified here refer to the mid/late third century A.D. The absence of italic sigillata and scarcity of thin-walled ceramics (some small fragments of the indeterminate form), as well as the weak presence of terra sigillata, and the predominance of the Dressel amphoras are strong indicators that the functioning of the Frielas villa would have started from the third quarter of the 1st century AD (Silva, 2012).

The sections of the remaining walls have small/medium dimension limestone construction connected by earth and insufficient to verify the original plan (Fig. 2.4), therefore it is not possible to acquire more details about the architecture of this first villa. There is a probability that tiled floors may have existed as evidenced from settlement layers made up of dozens of loose tesserae in the mosaics of the later villa which may be the result of the dismantling of the previous floors.

The materials recovered from this phase such as the sigillata and amphoras help characterize this initial phase. In addition to the absence of italic sigillata, there is a weak representation of the productions of *sudgálicas*. The presence of which can be understood by the competition that the Hispanic imports will have provoked throughout the second half of the 1st century AD, as identified from the fragments of bowls with figurative decorations and the marble bowl. Bowls predominate the Hispanic collection by 13.23% (Silva, 2012). Despite the difficulty inherent to the distinction of producing centers, the first macroscopic observation of the various fragments resulted in the predominance of imports from *Andujar* over that of from *Tritium*. This fact cannot be ignored by the presence of a set of olive amphorae, which attest commercial contacts with the Andalusian region since the beginning of the 1st century AD. In the case of some Dressel, produced between the 1st and 3rd centuries AD, remains of fish preparations have been found which would have been an overwhelming majority in amphoras of Lusitanian origin. Another type of Dressel found has a representation of 26.50% and was produced mainly between the 2nd century AD and the beginning of the 3rd century AD corresponding to the first moment of industrial production and pottery of the Tagus and Sado valleys.

2.2.2 Second Phase (First quarter of the 3rd century AD - First quarter of the 5th century AD)

This second phase of occupation of the Frielas villa had undergone a profound architectural reformulation resulting in a U-shaped house, with a wide peristyle of quadrangular plan bounded by a columned portico of which only four attic column bases and an Ionian capital (second half of the 3rd century AD / early 4 AD) remains (Fig. 2.4). This new villa is also characterized by mosaic floors, cladding painted, and marble parietals (Silva, 2012; Quaresma, 2017).

The construction of this new housing space may have devastated the previous structures, maintaining only a few sections under the new floors. It appears to be the golden period of this villa, during which there is an intense economic activity proven by the abundant import of *terra sigillata* and by the homogeneous set of numismatics, associated with a chronology between the second and fourth quarters of the 4th century AD.

Due to the changes that occurred in the production centers new forms of amphora appeared from the last quarter of the 2nd century AD. The first African imports of *Sigillata* begin to arrive in Frielas alongside the decrease in Hispanic production thus characterizing a new phase of occupation of the villa. As in the previous phase, the consumption of fish preparations is also documented by an import from *Bética*, and *Almagro*. There is also the presence of amphoras for transporting olive oil, imported from *Bética*, albeit with a residual character, as is the case with some Dressel amphorae, whose production period includes from the end of the 3rd century AD to 5th century AD (Silva, 2012). Along with the residual character, there is a presence of a North African production, the Late African with a chronology understood between the end of the 3rd century AD and the 4th century AD.

In both moments of occupation, there is a weak representation of the amphoras of olive oil, which may be indicative of the luxury character that these products imported would have in the economic context of the villa. The small number of olive amphorae may presuppose a consumption of olive oil produced on the spot or region, transported in another type of container, with the product imported being reserved for special consumption.

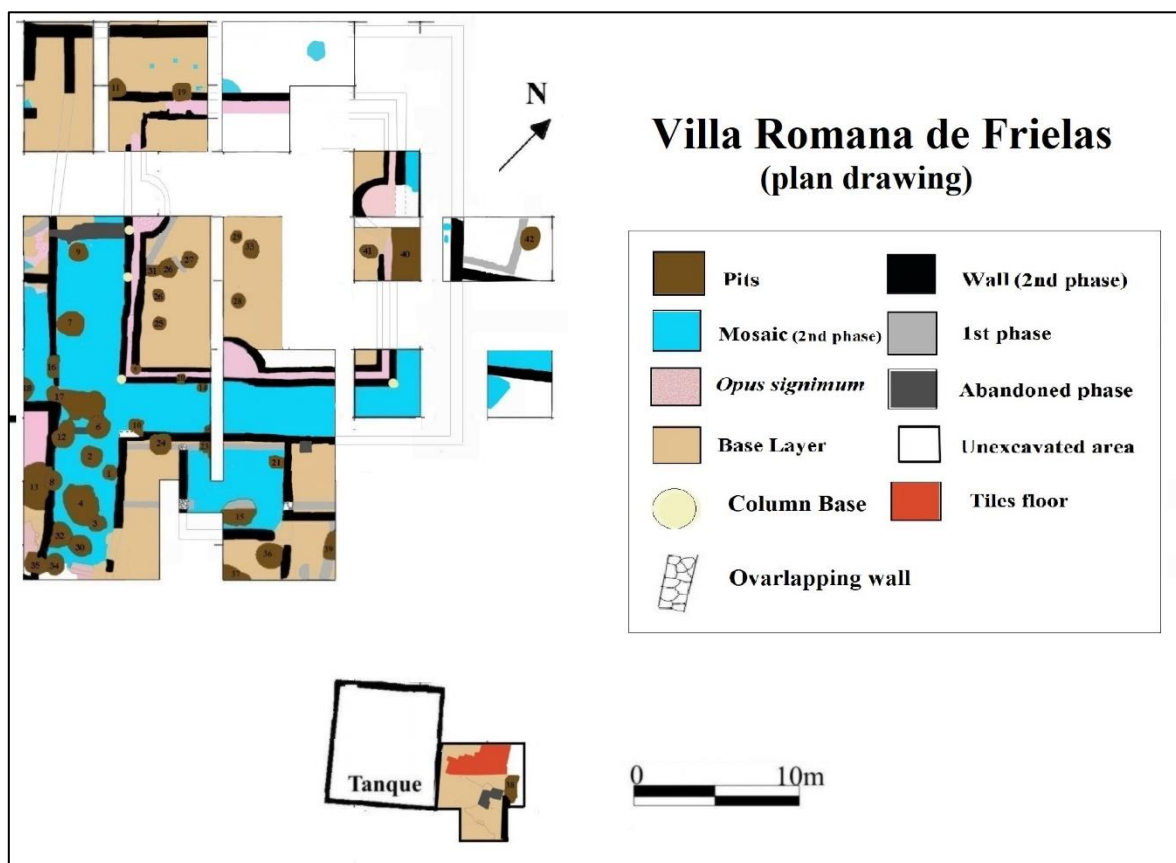


Figure 2. 4- Plan drawing; the Roman villa of Frielas, indicating construction phases. (The drawing adapted from Silva, 2012).

2.2.3 Abandonment phase (Second quarter of the 5th century AD - beginning of the 7th century AD)

From the 5th century AD, it appears that Frielas maintained commercial contacts in the Mediterranean basin, especially at the level of *terra sigillata* and amphorae despite the reduction in imports. Although in a vestigial way, there is the case of two fragments of Late Roman amphorae of olive oil produced in modern Tunisia, between the 4th and 6th centuries were also found. Afterward, the Frielas registration disappeared from the Portuguese productions coinciding with the data that points to the closure of the industrial units in the Tagus and Sado valleys in the first half of the 5th century AD.

Among the imports of *terra sigillata*, two types of ceramic bowls appear wherein the first kind belongs to a chronology between the mid-4th century AD and the first decades of the 6th century AD while the second kind is of smaller dimensions whose productions may have lasted till the 7th century AD. Two fragments of ceramics were found, dating from the mid-5th century AD to the early 6th century AD. Fragments of ceramic bowls were collected on the mosaic floor that lines the access corridor to the peristyle which might be attributed to the 6th century AD to mid-7th century AD. Thereby, it can be assumed a definitive abandonment of the Frielas villa at the beginning of the 7th century AD (Silva 2012). Nevertheless, stratigraphically, the latest contexts with imports belong to 525-550 AD after this chronology, there was no indication of imports, which is disabled the archaeologists from having a correct idea of the 6th, 7th, 8th, and 9th centuries, which is in between the latest imports and the C¹⁴ dating results of the pits (Quaresma, 2017).

The fall in imports is indicative of the decreased incapacity of the owner of the Frielas villa. This hypothesis can be corroborated by the patching of the mosaic floors and reducing the functional space of the house. *Opus signinum* was used for filling gaps in mosaic floors, and sometimes fragments of imbrication were used instead of tesserae (Silva, 2012). Although a prolonged time may have damaged some of these pavements, it is evident that the owner may no longer have had adequate economic support to properly repair the mosaic floors. In the case of the space reduction, it appears that at certain height walls were built on the floors with mosaic, thereby creating closed spaces over what once used to be wider areas. This is visible in the southwestern wing of the peristyle (Fig. 2.4).

2.3 The architecture of the villa

As mentioned above, the villa has two construction phases. The architectural style of the first phase cannot be adequately recorded due to limited structural evidence. This is so as most of the structures of this phase were destroyed during the construction of the second phase. The second phase has better architectural features present. The features of this phase project functionality through the presence of some compartments surrounding the peristyle with portico and mosaic floor passages (Silva, 2000). The abandonment phase has no remarkable architectural features, except some structural remains which could have been unfinished walls or traces of destruction of earlier phases (Fig. 2.4).

2.3.1 Peristyle

The Villa develops around a quadrangular peristyle, which is 17.5 m wide, with an area of about 306 m². It consists of two parallel walls with a water mirror in between them. These walls are made up of irregular-shaped limestone and mortar. The interior wall is 50cm wide and appears to be wider than the exterior (about 37cm) with a parietal coating composed of two layers: the first layer of mortar, applied on the limestone, and a second layer which is pink, probably due to the presence of iron oxide in its constitution. This layer is etched and appears to have been prepared for a final layer, which may have been stucco. The base of the space between the two walls has a concave section, coated with *opus signinum* to function as a waterproofing element (Fig. 2.5). This concave section appears to be continuously uneven for about 1 cm from southeast to northwest and from southwest to northeast, which is probably related to the circulation of water in this space. It should be noted that there are no traces of the water inlet or outlet that has been found in this space to date. Two semi-circles that are equally coated with *opus signinum* are present on the southwest and northeast sides and plucking from the narrower wall. Although symmetrical, they are not centered on the peristyle. The central part of the peristyle appears to have been landscaped as there are no traces of pavements. The portico, about 3m wide, would be covered by a shed, judging by the abundant presence of scattered tiles found, supported by a colonnade that would exist throughout the perimeter of the peristyle of which there are three columns bases left. The floor of the portico was covered with mosaic (Silva, 2000).

2.3.2 Compartments

On the southwest side of the Villa, some compartments were identified (Fig. 2.5) whose functionality is not yet clarified. Although compartment 'd' has only a few traces of the walls, it is possible to conclude that they were all paved with mosaic. The walls that delimit these compartments are composed of irregular limestone and clay, presenting an average width of

60cm. In compartments, 'a', 'b' and 'c', the walls were coated with painted stucco on both sides. The absence of traces of stucco next to compartment 'd', even though a very destroyed space, may lead to consider it less noble or important. However, the application of the various coating layers has some variants: the first layer of mortar, based directly on the limestone presents, in its composition, and at some points, fragments of imbrue or bulge, in an attempt, to regularize the face of the walls. A second thinner layer, on which the stucco would be applied, may or may not have been painted (Fig. 2.5) (Silva, 2000).

It is not possible to completely reconstitute the decorative motifs to the extent that what remains is a large drop of stucco fragments, where the colors red, blue, green, yellow, and white are recognized. In the southeast, a corridor and two possible compartments were identified while the corridor has the floor paved with mosaic, the two compartments have no traces of any type of pavement. The walls that delimit these spaces have the same constitution as the previous ones; as for the cladding, only the wall that delimits the corridor to the northeast has cladding (the southwest boundary of this corridor corresponds to the northeast wall of compartment 'a'). Thus, on the southwest face, and like those described above, some fragments of brick are observed in the first layer of mortar, on which a second thinner layer of the mortar is seen, with no traces of the stucco layer. On the northeast face, although there are no traces of coating mortar, some fragments of tile are seen. To the northwest of the peristyle arises a wall consisting of unequipped limestone and clay, corresponding to the limit of the portico of the peristyle. It should be noted that it is very destroyed (Silva, 2000).

2.3.3 Mosaic

In compartment 'd' appeared the first fragment of mosaic, in situ, of this Villa; with 50.5 x 46.5 cm, the first fragment of the mosaic was found in situ in compartment 'd' with dimensions 50.5x 46.5 cm. It was only connected either to the whiteish part of the wall or to the ornate part with simplified meander and diamonds inscribed. The compartment 'c' had another fragment with the same dimensions as the previous one, but the decorative motif is unclear. In 'b' and 'a', mosaics whose original dimensions may be reconstituted are preserved. In compartment 'b' the mosaic frame is formed by crosses in yellow and the field has a polychrome geometric composition while in 'a' the mosaic has not yet been discovered since it overlaps a thick layer of stucco tipping from the wall.

The mosaic of the corridor presents a field consisting of a geometric composition delimited by a double fillet, black with inscribed squares, filled by a multiple braided and polychrome. These squares are surrounded by isosceles triangles on three of their sides. At the center of the composition, there seems to be a white cross, whose arms occupy the entire width of the corridor. At the end of the 2001 campaign, the square (Fig. 2.5) to the southeast was excavated revealing a part of a mosaic, which represents part of a pitcher, inscribed on a

floral motif. As a reduced area, without any associated structure, it was not possible to identify the functionality of this space. The south-west and south-east corridors (Fig. 2.5) have mosaic with various geometric decorative motifs: while in the former there is a field covered by a checkerboard of bands with white circles (in which several red motifs are inscribed, with yellow and black) tangent to squares and small white circles with inscribed crosses in red and yellow, and in the latter, the field is marked by an orthogonal composition of lines of swastika intricacies with, black, red and yellow, and squares with Solomon (*salomao*) knots inscribed (Silva, 2000).

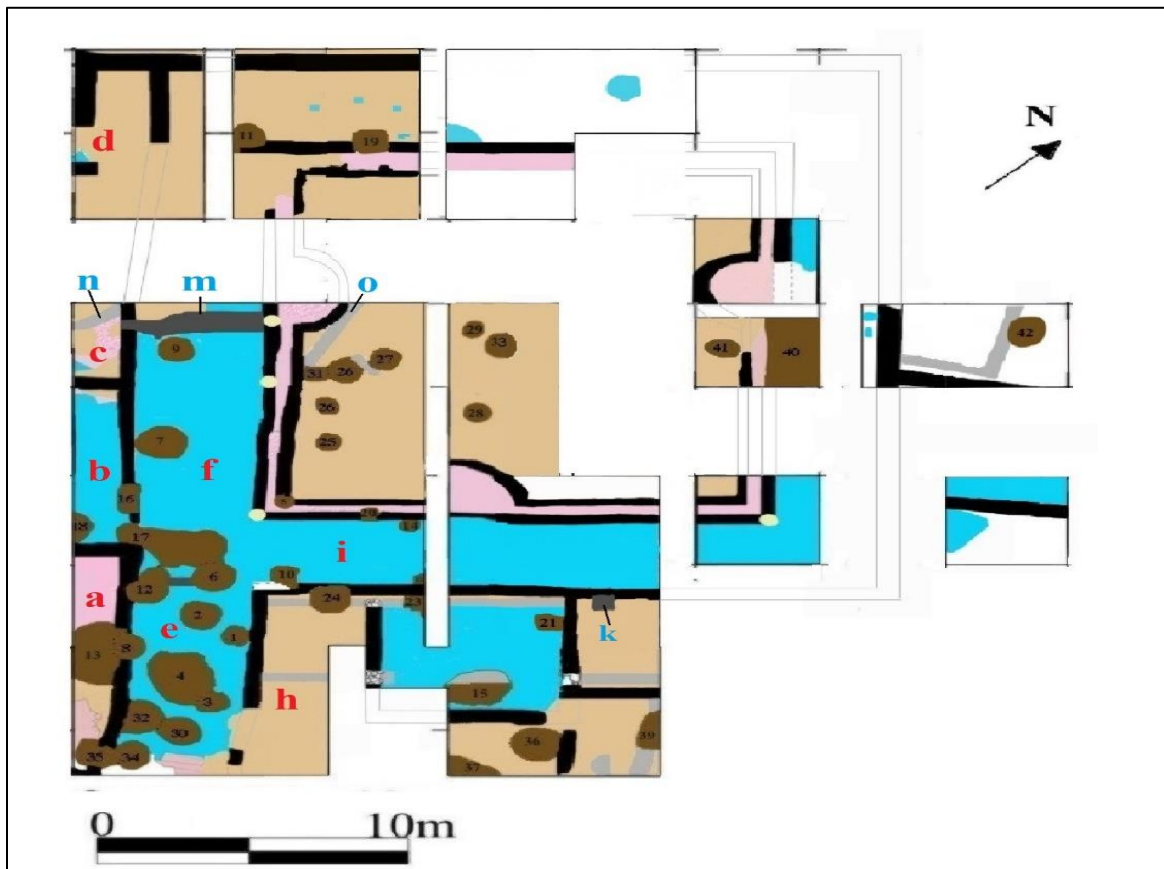


Figure 2. 5- Plan of the villa. (Adopted from Silva, 2000)

2.3.4 Structures

The structures uncovered seem to indicate more than a moment of construction in this Villa. Considering, the structures 'n' and 'o' (Fig-2.5) there are two sections of walls misaligned in relation to the other walls existing in the Villa and in relation to themselves. About 50cm wide, both are made up of irregular limestone and clay, with no traces of parietal coating. The section of the wall is located inside the peristyle, diagonally between the outer wall of the peristyle and semi-circular structure. The continuation of the works may clarify whether it is a structure anterior to the peristyle or a decorative complement inside it. In relation to

the 'n' wall, it was partially overlapped, by the fallen tile that would have made the villa's level of abandonment. If it corresponds to the northwest boundary of compartment 'c' (Fig.2.5), it may have been a space different from the others and with a specific function. Although the laying layer of the mosaic of compartment 'c' ends next to the face of the wall, the possibility of greater antiquity of this structure cannot be excluded which thereby corroborates the hypothesis mentioned above.

The structures 'i', and 'm' (Fig. 2.5), correspond to a remodeling of the original villa plan. The section of wall 'k', about 60cm wide, consisting of irregular limestone, and clay remains, is located partially on the mosaic of the corridor and on the mosaic of *ganizes*, which marked the southeast entrance of the Peristyle. Although it has been mostly destroyed — by the pits opened later — there are still some traces of their continuation to the northeast. When this wall was built, the southeast entrance of the peristyle that was marked by the massive panel of the *ganizes*, would apparently have been deactivated, reducing the width of the portico. The 'm' structure has slightly different characteristics; with a large stain of mortar, involving a few limestones, of very irregular contour, upon which there are traces of the start of a wall, with parietal coating. This structure sits on the mosaic and interrupts the wall that bounded the portico to the southwest. Like structure 'k', it would also 'close' the southwest corridor of the peristyle. Although the wall that overlaps it presents characteristics like the others, it is based on a foundation consisting of the stain of mortar that, when built, cut the tile felling there, assuming a construction after the abandonment of the Villa. (Silva, 2000)

2.3.5 Entrance of the passage

The location of the villa entrance is still in doubt. Given the proximity of the main road connecting *Olisipo* to *Conímbriga*, it is possible that there was a secondary access path to *Villa de Frielas*, which is currently very difficult to identify. It will also not be excluded from river access, although this hypothesis requires archaeological confirmation. In relation to the interior passages, only one was identified: the southeast entrance of the peristyle, marked by a mosaic panel, which presents an orthogonal composition of adjacent *ganizes*, in black and white, limited by a double fillet. This panel would divide the peristyle space from the corridor and the southeast part. Another type of passage marked as doorstep was not identified, the reasons for which may relate to a set of garbage dump pits of household waste (perhaps initially used as silos), that were opened in the Medieval / Modern period and that destroyed structures and mosaics making it difficult to acquire a correct reading of the villa's plan. (Silva, 2000).

2.4 Geological context

Villa Romana de Frielas in the parish of Frielas, municipality of Loures, district of Lisbon, is located in the northern part of the parish, on the right bank of the Póvoa stream (*Ribeira da Póvoa*). In geological terms, it is on the Paleogene (Eocene-Oligocene) lands, with the formation identified as '*Formação do Benfica*' (Φ_{Bf}) and '*Calcário de Alfovelos*' (Φ_{Bf}^a) composed of conglomerates, marls, reddish sandstone, clays, and limestones (Manuppella *et al.*, 2011). It is formed as a track with an orientation of Southwest to the northeast, between *Pontinha*, *Odivelas*, *Póvoa de Santo Adrião*, *Frielas*, and *Loures*. Due to its location, the floodplain of Loures is partly affected by the alluvial of Holocene formation.

Along with the Benfica formation the surroundings of Loures is in the geological formation of '*Complexo Vulcânico de Lisboa*' (CVL- β^1), '*Formação da Bica*' (C^2_{Bi}), '*Formações de Galé e Caneças*' (C^2_{Gc}) and Miocene sequential deposit of M_{B1} (*calcários de Entracampos*), M_{B2} (*Calcários do Casal Vistoso*) and M_{L1} (*Calcários da Musgueira*).

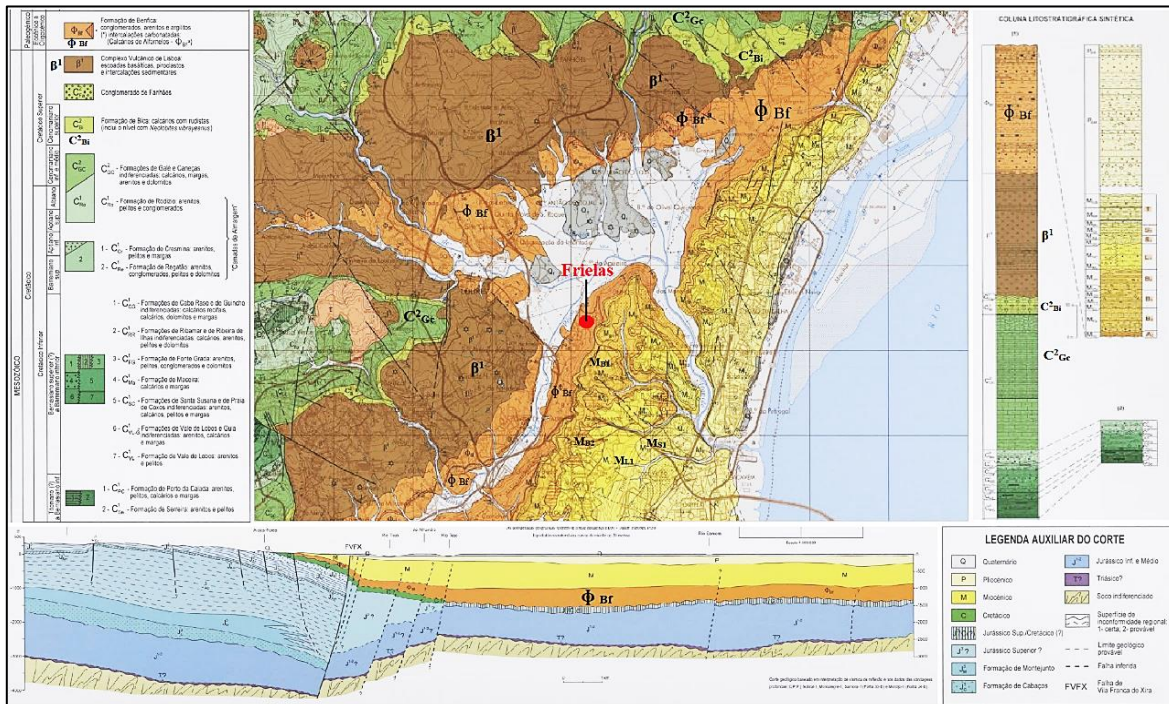


Figure 2. 6- Geological map of Frielas and its surroundings indicating '*Formação de Benfica*' (Φ_{Bf} / red brown), '*Calcário de Alfovelos*' (Φ_{Bf}^a /stripe in red brown), '*Complexo Vulcânico de Lisboa*' (CVL- β^1 /dark brown), '*Formação da Bica*' (C^2_{Bi} /light green), '*Formações da Galé e Caneças*' (C^2_{Gc} /dark green) and sequential deposit of M_{B1} (orange), M_{B2} (stripe in Orange), M_{L1} (yellow), M_{S1} (light yellow). The nomenclature and names used for the various units correspond to those defined in the Explanatory Notice of the Geological Map of Portugal, at a scale of 1:50,000, Folha 34-B, Loures (Manuppella *et al.*, 2011).

According to lithostratigraphic studies of Choffat (1950), Antunes (1967; 1979), Azevêdo (1991), the Benfica formation consists of a succession of continental deposits, reaching about 400 m thick. The sediments concerned can be correlated with the deposits of a Paleogenic stage widely represented on the N and NW edge of the Tagus depression, as well as in the

regions of *Arganil*, *Coimbra*, and *Nazaré*, where there are precise chronological references of various levels of the Eocene (Reis & Cunha, 1989).

The formation of Benfica is based on erosive discontinuity over the Lisbon Volcanic Complex. In some places, it is directly related to the cretaceous period (Albiano, Cenomaniano). The Formation of Benfica constitutes broadband, with orientation SW-NE tilting to Southeast divided the Benfica formation into four layers according to its geological formation, the 1st layer formatted as an inclined stratified layer with an estimated thickness of 80 m and composed of conglomerates, sandstone, quartz, quartzite, schist, shales, and feldspathic clasts, which is originating from the ante-Mesozoic deposit or formatted from Mesozoic detritic deposits were reddish, or whitish marls can be found. The conglomerates occasionally contain rolled clasts of Mesozoic limestones and rolled cretaceous oysters (near *Santo Antão do Tojal*) and cretaceous ostracods (Verdelho).

The 2nd layer is about 10 m thick, consisting of conglomerates and sandstone, with carbonated cement, red-brick color, rosy, and light greenish associated locally and laterally, with horizons of white, nodulous, sometimes pulverulent limestones, *Alfornelos* limestones. They have lacustrine facies and *palustres* (swampy) and have been the target of important pedogenetic and diagenetic actions, in part, corresponding to calculus. In the Loures region, carbonates indicate deposition in small endorheic depressions (Azevêdo, 1991).

The 3rd layer consists of reddish sandstone and lutite with levels of rosy carbonated concretions. It is based on discontinuity over the anterior, marked by the occurrence of conglomerates with silica clasts, quartzite, and quartz and Cenomanian limestones, cemented by white clays at the base passing to red at the top (6 m); limestone clasts are increasingly abundant to the top. This corresponds to a marl deposit, reddish to rosy, with some scattered clasts, and with well-exposed carbonated concretions in the vicinity of Quinta Nova (1 km to N de Loures). The set is around 200 m thick and tilts from 100° to 250° between Azenha Velha and Alfornelos.

The 4th layer consists of conglomerates and coarse sandstones with rolled elements of Jurassic limestones (Limestones of S. Pedro, Shales of Ramalhão) and Cretaceous, basalt, cretaceous sandstones, cemented by reddish clay matrix. The set is covered by conglomerates with large limestone and quartzite clasts, in bodies of metric thickness alternating with red and brown sandstone, with nodular or crusted carbonated horizons (Manuppella *et al.*, 2011).

3 SAMPLES AND METHODOLOGY

.....

3.1 Analytical techniques and methods

3.1.1 Optical Microscopy

The optical microscope can be used to examine the mineralogy of mortar components as well as their textural and spatial interrelationships. This technique can be used to identify aggregate, binder, organic and inorganic additives (including pozzolans), porosity, and other features such as lime lumps, cracking, and secondary mineral formation. For archaeological purposes, optical microscopy can be used to determine the provenance of raw materials manufacturing processes, and the presence of degradation processes (Elsen, 2006; Stuart, 2007).

Optical microscopy is a technique that allows the acquisition of information about the morphological traits and structure of a sample by magnifying things from x2 to x2000 times with resolutions up to 0.2-0.5 μm depending on the apparatus (Stuart, 2007). The premises of optical microscopy are that the visible light interacts with the specimen by passing through the thin sections of the specimen, around 20-30 μm thickness in transmitted-light or polarized-light modes, resulting in a range of color absorptions and pleochroism of the sample through plane-polarized light (PPL), and showing interference colors and birefringence through cross-polarizers (XPL). Anisotropic materials can be distinguished using polarized light microscopy because of their unique optical properties in terms of crystallographic axes and the distinctive interference colors produced by split incident light rays passing through the sample, which show different refractive indices depending on the vibrational plane coordinates (Middendorf *et al.*, 2005a; Stuart, 2007).

3.1.2 X-Ray Diffraction (XRD)

X-Ray Diffraction (XRD) is a technique for determining the atomic arrangement in solids, as well as identifying and mineralogical phases in polycrystalline materials (Goffer 2007; Stuart 2007; Artioli 2010). In the study of mortars, XRD can be used complementary to microscopical techniques and chemical analysis to identify the types of binder (e.g., lime, gypsum) and aggregates (siliceous, calcareous, ceramics) of mortar samples. XRD is the most used technique. This can be accomplished by analyzing the crystalline compounds' characteristic orientation texture, crystallite size distribution, and lattice micro-strain effects, resulting in a semi-quantification of the specimens' mineralogical composition based on the relative intensities provided by the diffraction patterns. (Middendorf *et al.*, 2005a, Artioli, 2010). X-ray powder Diffraction can only contribute to a bulk examination of the carefully

homogenized powders, (Fine fraction and Global fraction) therefore petrographic studies are needed to substantiate the assumptions made by the crystal phases of the diffraction patterns (Groot *et al.*, 1999; Middendorf *et al.*, 2005a).

The impact of x-rays towards a crystalline material causes diffraction, which occurs when "two waves reach the crystal at an angle θ and are diffracted at the same angle by adjacent layers." The waves are in phase when the first wave hits the top layer and the second wave hits the next layer" (Fig-3.1. a) (Stuart, 2007), as indicated by the Bragg's Law equation (4):

$$n\lambda = 2d \sin\theta \quad (4)$$

where ' λ ' corresponds to the wavelength of the incident radiation (in angstrom), ' n ' represents the diffraction order, ' d ' corresponds to the interplanar distance between planes of atoms of the crystal structure and ' θ ' to incident angle – between the incident beam and diffracted X-ray beams (Pollard *et al.*, 2007; Stuart 2007; Artioli, 2010; Bannert 2017s).

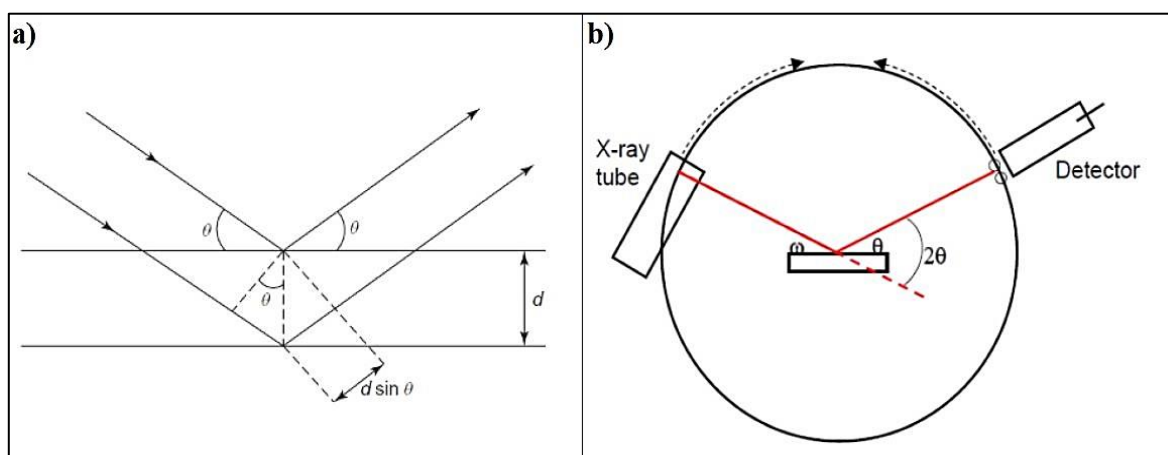


Figure 3. 1- a) Schematic representation of the interference process by waves produced by the ordered arrangement of atoms in a crystal (Stuart, 2007), b) Schematic diagram of an XRD diffractometer setup (Stuart, 2007)

During the XRD analysis, the sample is placed on a holder, a monochromatic X-ray beam is directed at the sample and a detector records the intensities of the diffracted beams (Fig-3.1. b). The diffracted peak profiles were obtained, as a function of the scattering angle 2θ . These peak patterns are characteristic of specific crystalline phases that could be identified by the comparison with standard XRD patterns (Stuart, 2007). A disadvantage of powder XRD comes with the nature of the sample required as a powder, in which the sum of the patterns of the crystalline phases present in the sample may overlap in the diffractogram, thus their individual characterization may represent a complex task (Stuart, 2007).

3.1.3 Thermogravimetric Analysis (TGA)

Thermogravimetric analysis (TGA) is a thermal method for determining a material's weight loss as a function of temperature or time. It can be used to calculate the mass change in material induced by physical changes (e.g., phase transitions) or chemical changes (e.g., chemical decomposition) because each material will show a unique sequence of reactions at various temperatures, TGA data provide characteristic curves for a given substance (Stuart, 2007).

By placing the sample in a crucible within a furnace in a sensitive balance under a controlled temperature program in an inert atmosphere (N₂), the mass losses were tracked during the heating program. The mass change within the measured material during heating is recorded in a thermogram, which is then used to make a relative quantification of the carbonate fraction of the mortars, estimate the composition ratios, and so define the manufacturing technologies. To accomplish a thorough characterization, the data received from the soluble fraction because of acid dissolution, as well as the data gained from granulometric analysis on aggregate composition, will be used to supplement the information provided by TGA.

The first Derivative Thermogravimetric Curve (DTG) concerning temperature allows plotting the most representative changes within the sample during the heating process, with the peaks indicating the maximum mass losses due to the characteristic physical or chemical decomposition of the distinct materials in function of temperature (Middendorf et al, 2005a; Stuart, 2007; Földvári, 2011).

For mortar studies, the main weight loss is expected between 600 and 900°C, confirming the decomposition of calcium carbonate (CaCO₃) into calcium oxide (CaO) and carbon dioxide (CO₂), which is indicative of a calcite composition of the lime-based binder. However, weight losses at lower temperatures can be shown in the ranges of 75-100°C for the dehydration of the lime-based binder; (Middendorf *et al*, 2005a).

The equation (5) is used to calculate the carbonate content in terms of the percentage of calcite.

$$\text{CaCO}_3\% = [\text{P}(\text{CO}_2) \cdot \text{M}(\text{CaCO}_3)]/\text{M}(\text{CO}_2) \quad (5)$$

P (CO₂) is the percentage of mass loss between 600 and 900°C, which corresponds to CaCO₃ breakdown, M(CaCO₃) is the molar mass of calcium carbonate (100.082 gmol⁻¹), and M (CO₂) is the molar mass of carbon dioxide (44.02 gmol⁻¹).

3.1.4 Scanning Electron Microscopy coupled with Energy-Dispersive Spectroscopy (SEM-EDS)

The scanning electron microscope (SEM) is an adaptable technology that is well known in the cultural heritage field. Its applications include elemental analysis, elemental mapping, and image acquisition. It's been useful in the study of ceramic and mortars, helping with the identification of raw materials, manufacturing procedures, or provenance research. The SEM-EDS analyses could be done directly on the objects or as a cross or thin sections (Goffer 2007; Stuart 2007; Artioli 2010).

An electron source (comprising a tungsten filament, a Wehnelt cylinder, and an anode) produces a beam of electrons under vacuum by applying a current to the anode, which emits and accelerates them through the anode towards a specific area of the sample's surface in a raster scan, interacting with the atoms of the surface (Stuart, 2007; Artioli, 2010). This contact generates a variety of signals, which are gathered and amplified by a detector above the sample (Stuart, 2007; Artioli, 2010) and used for various purposes.

Due to the use of accelerated electrons (between 102104 eV, 0.123-0.012 nm wavelength) SEM-EDS can show us a higher magnification image up to x100,000 times (Stuart, 2007), with higher resolution and wider depth of focus, compared to optical microscopy (Stuart, 2007; Artioli, 2010). It can create three-dimensional pictures with detailed morphological information about the substance being studied (Middendorf *et al.*, 2005a; Stuart, 2007). By recording the intensity of the distinctive X-rays of certain elements at each point in a spectrum and tables, and mapping their distribution on the sample's surface, it is possible to identify the qualitative composition of the chemical elements in the sample using an EDS detector and SEM (Middendorf *et al.*, 2005a; Stuart, 2007).

Back-scattered electrons (BSE) are the result of the sample's elastic scattering after the electron beam strikes it, retaining a small fraction of the beam's energy, and they're useful for detecting the contrast of areas with different chemical structures to determine the topography of the surface and their elemental distribution throughout the sample's surface (Stuart, 2007; Artioli, 2010); Secondary electrons (SE) are low-energy electrons (less than 50 eV) emitted from a sample's surface, resulting in an inelastic collision followed by an ionization process, and they produce images that show the characteristics and morphologies of the material (Stuart, 2007; Artioli, 2010). Ionization processes produce X-rays, which are detected by an EDS, allowing chemical elements to be identified and an elemental distribution map of the specified raster region to be created (Stuart, 2007; Artioli, 2010).

3.1.5 Acid attack and Granulometric analysis

The chemical process of attacking mortars with an aqueous solution of hydrochloric acid is used to obtain information about the ratio of the soluble fraction (carbonate binder, salts, and organic compounds) to insoluble residue (non-carbonated aggregates) present in the mortars (Middendorf *et al.*, 2005b). The resulting insoluble residue is utilized to quantify the composition of the various grain fractions and to perform morphological analysis of each type using a stereoscopic microscope. The method developed by Hanna Jedrzejewska (Jedrzejewska, 1960; Jedrzejewska, 2014) for defining the basic aspects to understand the technology used for the historical lime mortars production resides in three properties that can be determined by the acid attack and thermogravimetric analysis. These parameters are the percentage of the “soluble” amount of sample in acid (without CO₂ generation), the amount of sand (the insoluble residue in acid), and the proportion of carbonates (measured by TGA-DTG) (Jedrzejewska, 2014; Borsoi *et al.*, 2019). The soluble fraction will be expressed as a percentage and calculated using the equation (6).

$$\text{Soluble fraction (\%)} = 100 - \Sigma (\text{Insoluble residue (\%)} + \text{Carbonates (\%)}) \quad (6)$$

According to Middendorf *et al.*, (2005b), mineralogical and petrographic microscopic analysis of the samples should be undertaken before chemical analysis to determine whether the aggregates can dissolve in acid or if the binder has hydraulic properties to accomplish the desired element separation.

The insoluble residues are then utilized to obtain the aggregate grading curve, which is used to determine the main grain fraction present on each sample. This, along with the binder to aggregate ratio, is a key step in the characterization and reconstruction of historical mortars (Middendorf *et al.*, 2005b).

3.2 Sampling

A total of eighteen mortar samples and two soil samples were collected from the Roman villa of Frielas, to understand the construction phases, structures, and functional representation. Samples were carefully collected using a hammer and chisel with the clear objective of causing no harm or destruction to the archaeological site. The archaeologists and conservators in charge of the site were present at the time of the sample collection.

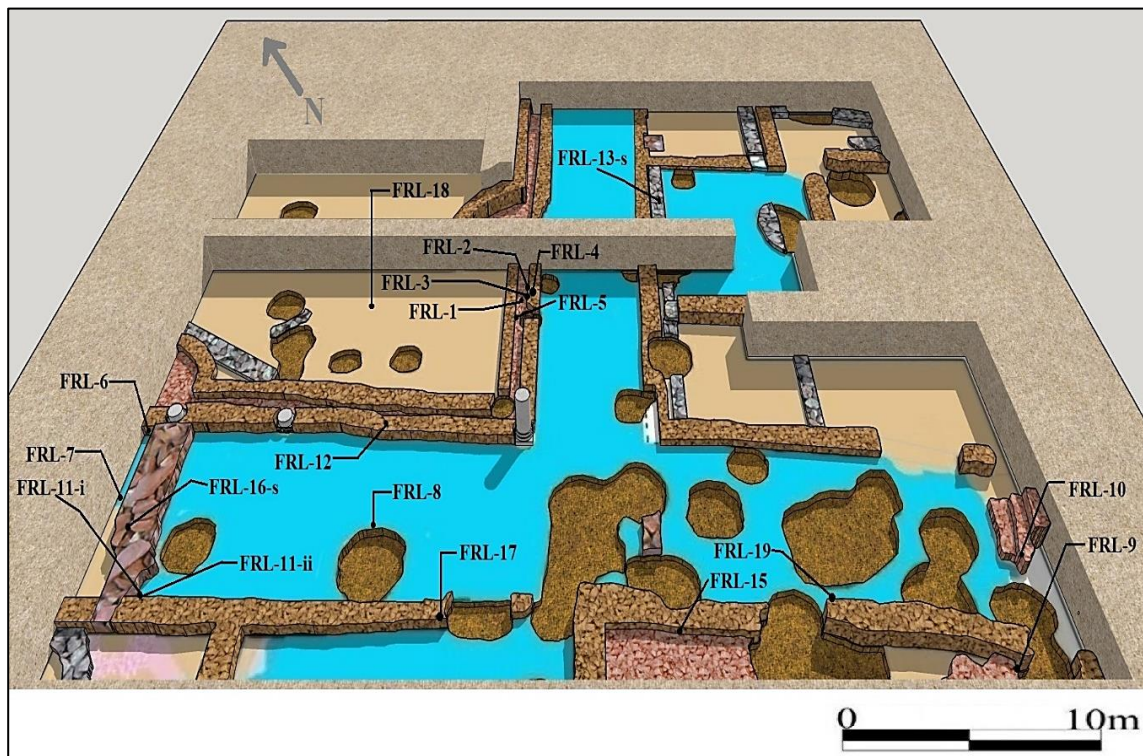


Figure 3. 2- Scheme showing the location of the sample collected from the Roman villa of Frielas.

Samples were collected in plastic bags representing the name of the site with the 'FRL' tag, documented, and labeled according to the pointing location and functions of the structure, and photo documentation as well. All the mortar samples were collected from the 2nd phase of the villa (Fig-3.2), as the other phases have no traces or availability of mortar according to the archaeological record. The first five samples were collected from the bottom surface of the water channel of the peristyle, (FRL-1) and the sidewall of the water channel (FRL-2, FRL-3, FRL-4, and FRL-5). Two samples were from the embedded column wall of the peristyle (FRL-6 and FRL-12). A single sample (FRL-18) was collected from the detachment of the wall with mural painting located on the inside of the peristyle square.

The peristyle is surrounded by a mosaic floor which has evidence of destructions from the abandonment phase. The west-facing wall of the peristyle is parallel to the mural painting wall of the villa and connected by an irregular wall (abandonment destruction). One sample

was collected from the overlapping mosaic floor layer (FRL-7) which is connected to the irregular wall. And another sample was collected from the mosaic floor (FRL-8).

From the inner side of the mural painting wall, two samples were collected (FRL-11-i, FRL-11-ii), which were attached with some crumbly dried soil. The other two samples from the wall detachment were collected during the excavation of 2001 (FRL-17) and 2007 (FRL-19). From the outer side of the same wall (west-facing), one more sample (FRL-15) was collected. And at the end of this wall towards the southeast corner two more samples were collected from the filler of the floor (FRL-9) and staircase (FRL-10) (Fig-3.3). Samples were collected from between the joining stones of the wall structure of 1st phase (FRL-13-s). Samples were also collected from the abandonment destruction wall (FRL-16-s).

During the cleaning process, some samples were discovered to have stratigraphic layers, in which case they were labeled with 'U' (upper layer) and 'D' (lower layer). A total of four mortar samples had the same stratigraphic layer (FRL- 6U-D, FRL-8U-D, FRL-10U-D, and FRL-19U-D). Two samples were further sub numbered due to the presence of parallel layers within the sample corresponding to the difference in texture or position (FRL-7_i, FRL-7_ii, FRL-11_i, and FRL-11_ii). Two samples with the painted surface were also collected (FRL-17 and FRL-18). The general description of all samples is presented in Tab. 3.1.

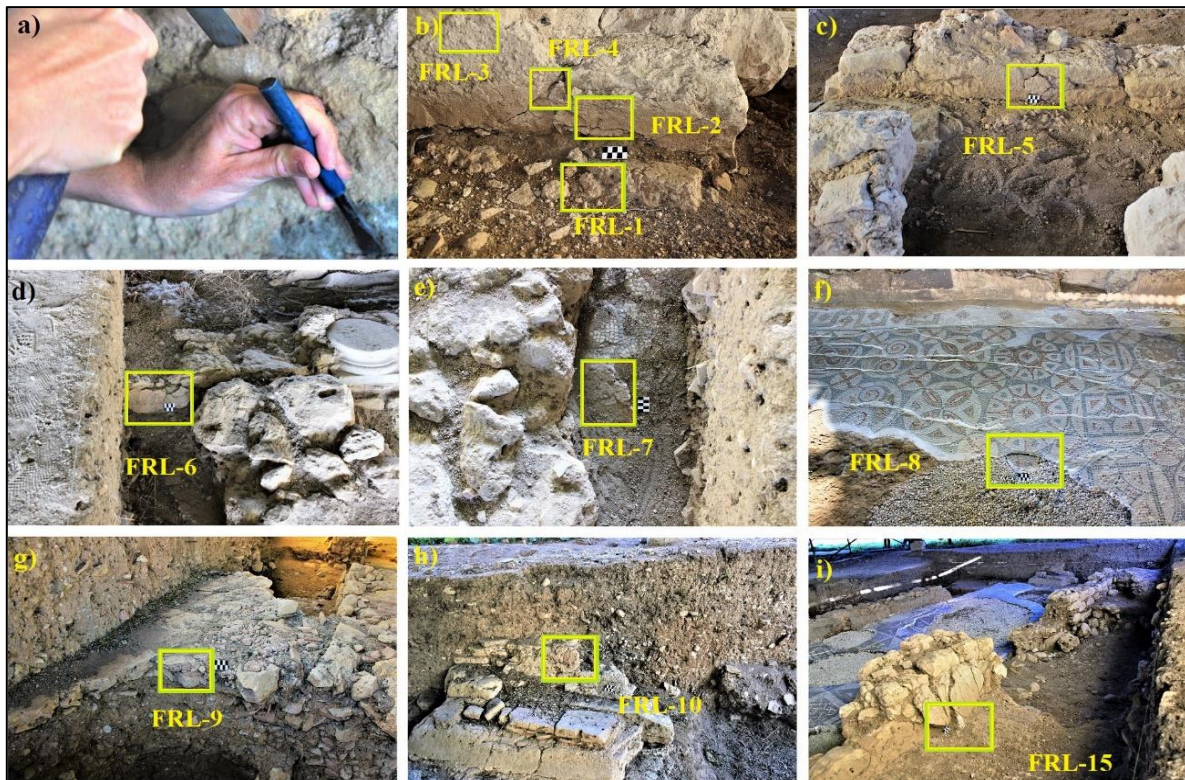


Figure 3. 3- Sample collection from the Roman villa of Frielas, a) carefully using hammer and chisel, b) water channel sidewall, c) parallel wall of water channel, d) peristyle wall, e) overlapping floor, f) mosaic floor, g) filler mortar, h) stairs, i) compartment wall (opposite side of the mural painting).

Table 3. 1- Mortar and soil samples from the Roman Villa of Frielas

Sample	Structure	Function	Layers	Location	Phase/ period
FRL-1	Water channel floor	Render	No	L-12	2 nd phase/3 rd -5 th century AD
FRL-2	Water channel side wall	Render	No	L-12	
FRL-3	Water channel side wall	Render	No	L-12	
FRL-4	Water channel sidewall	Filler	No	L-12	
FRL-5	Water channel Side wall	Render	No	L-12	
FRL-6	Peristyle wall	Render	Stratigraphic layer	J-11	
FRL-7-i	Floor (Overlapping mosaic floor)	Filler	No	J-11	
FRL-7-ii	Floor (Overlapping mosaic floor)	Filler	No	J-11	
FRL-8	Floor (Mosaic)	Floor	Stratigraphic layer	K-10	
FRL-9	Floor	Filler	No	O-10	
FRL-10	Stairs	Filler	No	O-10	
FRL-11-i	Wall (Mural painting)	Render	No	J-10	
FRL-11-ii	Wall (Mural painting)	Render	No	J-10	
FRL-12	Peristyle wall	Filler	No	L-11	
FRL-15	Side wall	Render	No	M-10	
FRL-17	Detached wall fragment	Render (Mural painting)	Painting layer	L10-A/B	
FRL-18	Detached wall fragment	Render (Mural painting)	Painting layer	K13-A/B	
FRL-19	Detached wall fragment	Decorative	Stratigraphic layer	N10-A	
FRL-13-s	Wall	Soil	No	M-13	1 st phase/ 1 st - 3 rd AD
FRL-16-s	Wall	Soil	No	J-10	Abandonment phase/ 5 th -7 th AD

3.3 Sample preparation

Before initiating any processual preparations, the samples were left to dry at 40° C in a ventilated oven overnight. The process was repeated twice for some samples to get effective drying. After that, all the dried samples were cleaned using a chisel, scalpel, and brush to remove unwanted dirt, biological habitation. Once the samples were sufficiently cleaned and dried, they were observed and recorded for their macroscopic characteristics such as color, texture, identical stratigraphy, type of aggregates, and additives. Finally, all the samples were photographed with scale (centimeter) using a high-definition camera as a part of the documentation process.

For initiating the preparation procedure, samples were treated by the following steps in correlation with the desired analytical techniques. Based on the relations between sample preparation and the type of analytical techniques, 3 main groups of preparation are discussed in the following section 3.3.1, 3.3.2 and 3.3.3. The diagram (Fig. 3.4) represents the sample preparation for each analytical technique.

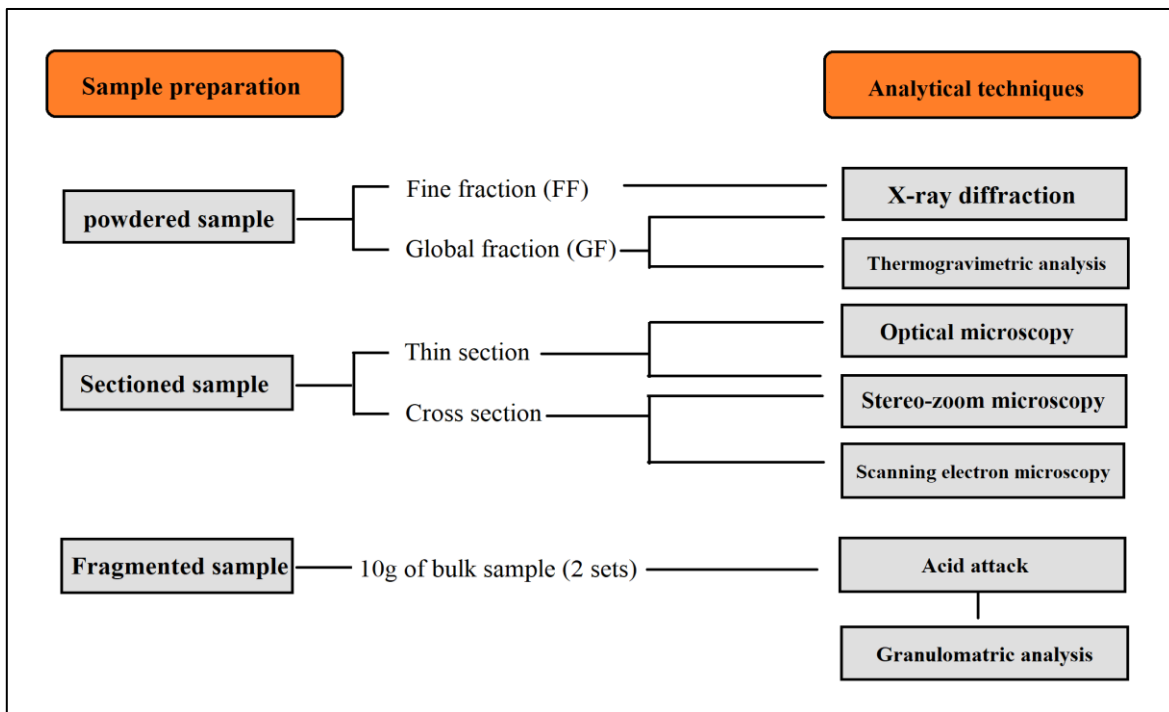


Figure 3. 4- Sample preparation diagram.

Among all the samples, four samples appear to have clear identical stratigraphy (FRL-6, FRL-8, FRL-10, and FRL-19). To follow the preparation procedure, the stratigraphic layer was divided carefully with a rubber hammer and chisel. They were labeled with ‘U’ (upper layer) and ‘D’ (lower layer) accordingly with the sample name.

3.3.1 Powdered sample

To perform the thermogravimetric analysis (TGA) and x-ray diffraction (XRD) analysis, powdered samples were employed. Two different powders were prepared following different procedures. For TGA, only global fraction (GF) and for XRD both global and fine fraction (FF) were needed. Global fraction represents the bulk sample while the fine fraction, containing particles smaller than 0.063 mm has a higher probability of binder enrichment.

Following the procedure, 10g of representative sample was separated using a rubber hammer and chisel, and the fragmented sample was grounded by hand in a mortar and pestle grinder bowl made of agate in order to disaggregate them into fine fractions (Fig-3.5. a). Later, each sample was grounded into a PM 100 Planetary ball mill machine (Retsch) for 10 minutes at 500 rpm (with 3 balls of < 1 cm Ø) to obtain the finer powder (Fig-3.5). In some cases, the process was repeated to dispose of all the grains such as quartz or hard ceramic fragments to obtain a homogeneous powder. For the fine fractions (FF), each sample was gently disaggregated without breaking apart the aggregates and then sieved with a stainless-steel test sieve (ASTM E11, 100mm x 40mm, Retsch) with a mesh size of 63 µm and the powder was collected to perform the powder XRD analysis.

Samples containing chromatic layers (FRL-17, FRL-18) were prepared after removing the pigmented layer carefully from the surface of the mortar, using a scalpel and brush. The samples with the stratigraphic layer (FRL-6, FRL-8, FRL-10, and FRL-19) were separated into sub-samples with the help of a mallet hammer and chisel, and in some cases, the Discoplan-TS diamond disk was required to cut with. After separation, they were powdered separately as an upper layer (U) and lower layer (D). Due to insufficient samples, it was not possible to collect fine fraction powder for some samples (FRL-1, FRL-4, FRL-11-ii, FRL-17, FRL-19-U). Both GF and FF powder were used for the mineralogical characterization by XRD to cross-check the minerals and binder enrich properties in the mortar. For the TGA analysis, an amount of 25-30 mg of global fraction (GF) powder was used.



Figure 3. 5- Tools used for the preparation of the powdered samples: a) Disaggregation by mortar and pestle, b) Powdering equipment PM 100 Planetary Ball Mill (Retsch), c) Agate grinding jar and grinding balls

3.3.2 Sectioned sample

Two types of sectioned samples were prepared: polished sections (cross-section) for stereo-zoom microscopy and SEM-EDS analytical techniques, and thin sections for petrographic microscopy. Thin sections were obtained from the polished sections using TS method developed by Struers (Struers, 2014).

For the polished section, a representative part of the cleaned sample was separated using a rubber mallet hammer and chisel, and in some cases, the discoplan-TS machine was required to cut. All the collected pieces were kept in an oven at 40° C overnight to eliminate moisture and placed in a circular plastic mounting cup (2 cm diameter). In the case of the larger pieces, a plastic container was used. All the samples were then positioned in the desired orientation and labeled before being embedded in the mixer of resin. 25 parts of Struers EpoFix resin with 3 parts of Struers EpoFix hardener by weight ratio was used. Then, the resin-embedded polished section was left for 12-16 hours to dry at room temperature. After hardening, they were dismantled from the plastic container and cut in the discoplan-TS. For getting effective flat and smooth surface they were later sanded and polished by hand using respectively P# 220, P#P 320, P# 600, P# 800, and P# 1000 silicon carbide paper (Fig-3.6. k).

For the preparation of thin sections, glass slides were unpolished for better attachment with the sample surface using the Discoplan-TS polishing part to achieve the thickness of 1.15mm. Afterward, glass slides and polished sections were thoroughly cleaned with acetone and placed into a hot-plate at 50° C temperature for 6-10 minutes. Meanwhile, a mixture of 2 g of Buehler Epoxy Resin and 0.9 g Buehler Epoxy Hardener was prepared and applied on polished sections which were then mounted on the unpolished surfaces of the glass slides for the purpose of gluing. After gluing, they were left overnight under pressure in System-Adele press for hardening and better attachment. Then, the glued samples were cleaned with a scalpel and acetone to remove the excessive resins. Later, they were cut using the Discoplan-TS cut-off part. And finally, the thin section was polished by hand, using P# 600, P# 800, P# 1000, P#1200, and P#2400 silicon carbide paper until the samples showed the first order birefringent color of Michel-levy chart under the optical microscopy.

After acquiring a thin section from the elaborated polished section, the polished section was sanded and polished again following the same procedure, described before to expose the mortar surface. No coating or further preparation of the sectioned sample was needed to do the SEM-EDS analysis.

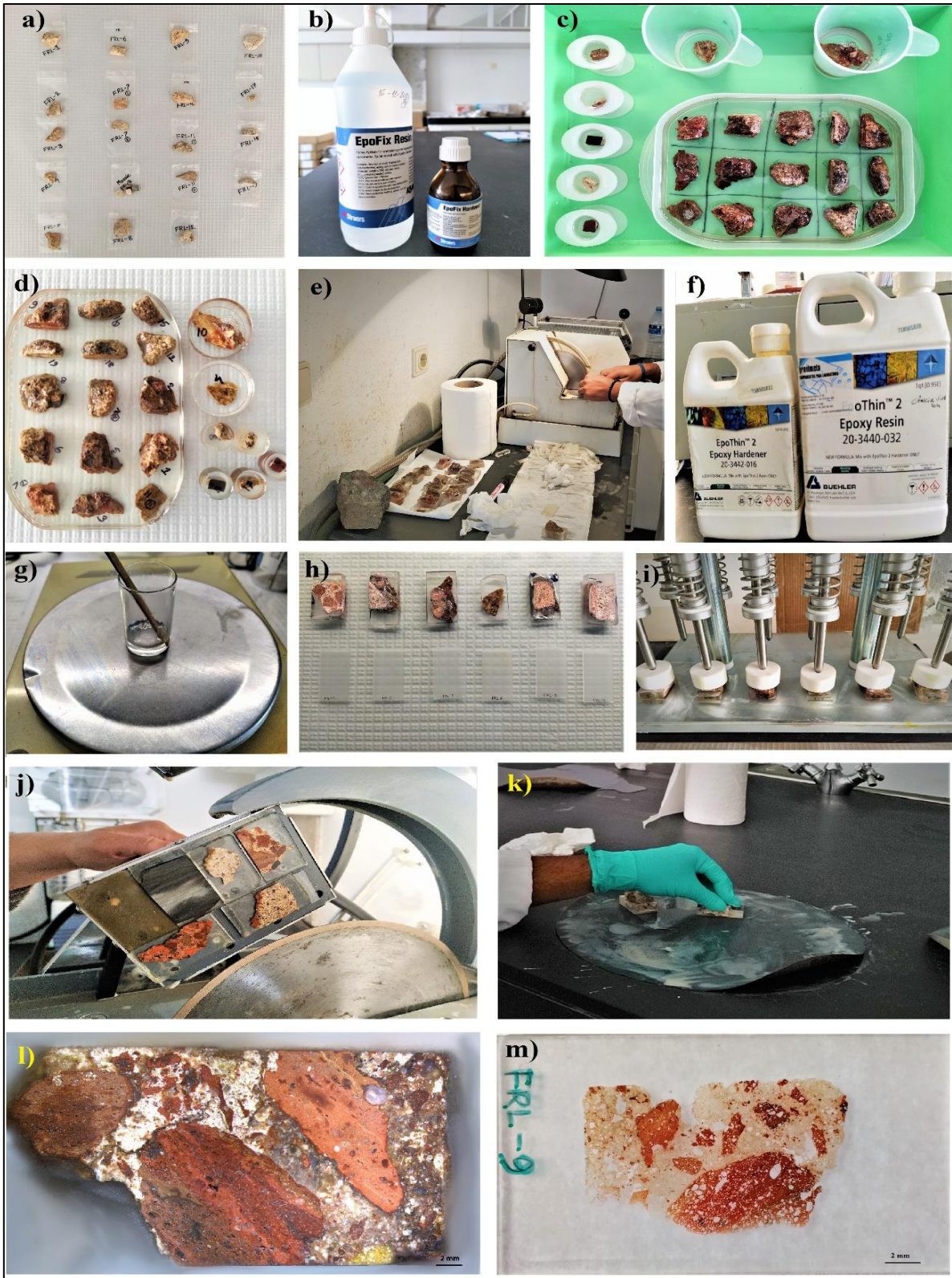


Figure 3. 6- Thin section and polished section preparation: (a) selected part of samples, (b) Struers EpoFix resin and hardener (c) Sample in resin solution, (d) hardened sample (e) cutting by discoplan-TS, (f-h) Buehler Epoxy Resin for gluing, (i-j) System Abele press Cutting out the thin sections under vacuum using a Logitech CS10 Thin Section Cut Off Saw (k) polishing thin section by hand on silicon carbide paper (l) Results of FRL-9, polished section (m) and thin section.

3.3.3 Fragmented Sample

For acid attack and granulometric analysis, about 20g of a fragmented portion of the sample were required from the sample to perform these techniques. The selection of the fragmented portion was chosen carefully after the disintegration of the sample in a smaller fraction by using a mallet hammer. To minimize experimental error two sets of 10g fractions were acquired for the analysis. The initial weight was recorded and later compared with the final weight acquired after the acid attack. Both sets of fragments were first subjected to acid attack then granulometric analysis. The analysis was done in duplicate, and the results were measured as average values.

The samples which have stratigraphic layers (FRL-6, FRL-8, FRL-10, FRL-19) were separated and prepared individually for each layer. Samples containing painting layers were also prepared after removing the paint layer from the mortar surface. In some cases, due to insufficient sample, only one set of 10g fragmented samples were collected (FRL-4, FRL-11-ii, and FRL-19-U) and for sample FRL-17, no acid attack and granulometric analysis were conducted.

3.4 Experimental Conditions

3.4.1 Optical Microscopy

Optical microscopy was used to determine the mineralogical and morphological characteristics of the samples, specifically to identify the light reflection within aggregates in terms of the size, shape, color, and texture. This kind of information can help to determine the provenance of the raw materials, by correlating the mineralogical patterns of the samples with the geological data (Elsen, 2006). This observation was made with a Leica- DM2500 P, Modular Polarization Microscope, using the objectives of 2.5, 5, 10x, and 20x, under plane-polarized light (PPL) and cross-polarized light (XPL). And the images were taken with a Leica- MC-170 HD digital camera.

3.4.2 Stereo-Zoom Microscopy

Stereo-zoom microscopy was used for all the prepared polished sectioned samples to make a preliminary observation, in order to identify the types of aggregates, morphology, inclusion (ceramics, fibers, organic or inorganic additives) and to define the stratigraphic layers and colors. For this observation Leica-M205-C Stereoscopic Microscope was used and the images were taken with a Leica DFC-295 digital camera.

3.4.3 X-Ray Diffraction (XRD)

X-ray Diffraction (XRD) was used to analyze both global fraction (GF) and fine fraction (FF) in order to identify the mineralogical composition and the crystalline phases of the samples. Global fraction represents the bulk sample, and the fine fraction represents more of the binder.

A Bruker D8 Discover X-ray Diffractometer was used with a Cu-K α X-ray generator working at 40 kV voltage and current at 40 mA. The diffractograms were obtained at a 2θ , scanning between an angular range from 3° to 75° with a velocity of 0,05° per second measuring time by an LYNXEYE linear detector. The standard polymer sample holders containing approximately 1 g of powdered samples were used for the analysis and the DIFFRAC. SUITE EVA software was used to identify the mineral phases with the Powder Diffraction Files of the International Centre for Diffraction Data (ICDD PDF)-2. The results obtained from XRD analysis were used as complementary with the results from OM and SEM-EDS analysis.

3.4.4 Thermogravimetric Analysis (TGA-DTG)

Thermogravimetric analysis (TGA-DTG) was performed in the powder global fraction (GF) of the samples to quantify the amount of binder with carbonate composition by measuring the weight losses within the samples. In this technique, the unique patterns of the weight losses are used as a result of their physical and chemical changes throughout a heating process (Stuart, 2007).

For this analysis, a platinum crucible containing approximately 25-30 mg of GF powder of the sample was placed inside the furnace, where the mass of the crucible was measured with a sensitive balance. Then the furnace is heated under a controlled temperature in an inert atmosphere, and the changes in the sample mass due to decomposition were recorded in a thermogram. As a result, a TGA curve was plotted with the sample mass (%) as a function of temperature. Also, the derivative technique, the DTG curve was obtained from the initial thermal curve, which allowed to capture the specific temperatures in high accuracy in which the characteristic changes occur (Földvári, 2011).

The samples were analyzed in a Simultaneous Thermal Analyzer STA 449-F3 Jupiter by NETZSCH, in an inert atmosphere of Nitrogen (Air Liquide Alpha-gas compressed N₂) with a flow rate of 70 mL/min. The heating program was set at a linear velocity with a constant increase rate of 10°C/min starting from 40°C and until reaching 1000°C. The quantitative analysis in the selected temperature ranges was performed by using Proteus software. The results of the thermogravimetric analysis were used complementary to the results obtained from the acid attack.

3.4.5 Scanning Electron Microscopy – Energy Dispersive X-ray Spectrometry (SEM-EDS)

Scanning Electron Microscopy coupled with Energy Dispersive X-ray spectrometry (SEM-EDS) was used for elemental analysis, elemental mapping, and image acquisition of the mortar sample. Experimentation was carried out on the prepared polished section and no coating was applied on the sample before the analysis due to their non-conductive properties.

A Hitachi S-3700N (Hitachi High Technologies, Berlin, Germany) Scanning Electron Microscope coupled with a Bruker XFlash-5010 (Bruker Corp, Billerica, Mass. USA) Silicon Drift Deflector (SDD) Energy Dispersive X-ray Spectrometer was used to perform the micro-analysis of the samples. The analysis was carried out under variable pressure, operated with an accelerating voltage of 20 kV and a chamber pressure of 40 Pa. The spectra for the chemical analysis were plotted on an energy scale of 0-20 keV with a spectral resolution of 129 eV at Mn K α . Data were obtained in the form of elemental distribution maps, point and multipoint analysis processed with Esprit 1.9 software. The SEM images were captured in backscattered (BSE) mode, for obtaining information about the textural features of the samples.

3.4.6 Acid Attack and Granulometric Analysis.

Acid attack analysis was carried out to determine the ratio between soluble fraction and insoluble residue of the mortar samples. To perform the experiment, an aqueous solution of hydrochloric acid (HCl), with a concentration of 1:3 (v/v) was prepared (Fig. 3.7.a). The analysis was carried out in duplicate for each set of samples prepared according to the procedure as explained in section (3.3.3 Fragmented sample). All sets were weighted and recorded for the comparison of the initial and the final weights. The experimentation was carried out by slowly adding 120 mL of the solution into a 250mL beaker containing 10 g of fragmented sample. After the release of CO₂, the beaker was put on a hot plate and the mixture was heated up to boiling temperature and left for 10 more minutes while stirring (Fig. 3.7.b). The mixture was then cooled down by adding distilled water. After it reached room temperature, it was filtered under vacuum using a Büchner funnel and VWR grade 413 qualitative filter paper (Fig. 3.7.e). During this process, the insoluble residues were washed at least twice with distilled water. After the filtration, they were left in the oven for at least 48 h at around 60°C to ensure the moisture is completely removed. The dry insoluble residues were once again weighed and recorded. The initial and the final values were plotted (Appedix-8.7) for the determination of the soluble fraction: insoluble residue ratio for each set of samples.

The granulometric analysis was carried out to determine the particle size distribution of the insoluble residue in each sample that is representing the siliceous aggregates. It was performed on the resultants of the acid attack by sieving them through stainless steel test sieves ASTM E11 with a diameter of 100 mm x 40 mm by RETSCH. The sieves used for the analysis had mesh sizes of 4, 2, 1, 0.500, 0.250, 0.125, and 0.063 mm. To capture the granulometric distributions of the samples, the insoluble residue obtained by each sieve was weighed and recorded. After that, each fraction was observed under a Leica M205 C Stereoscopic Microscope and photographed by a Leica DFC 295 digital camera. The results were presented in plots and diagrams. The data was used as complementary to the results achieved by the thermogravimetric analysis. Together they were used to determine the production of the historical mortars of the Villa Roman do Frielas according to the method introduced by Hanna Jedrzejewska (Jedrzejewska, 1960) as described in (Section 3.1.5 Acid attack and granulometric Analysis)

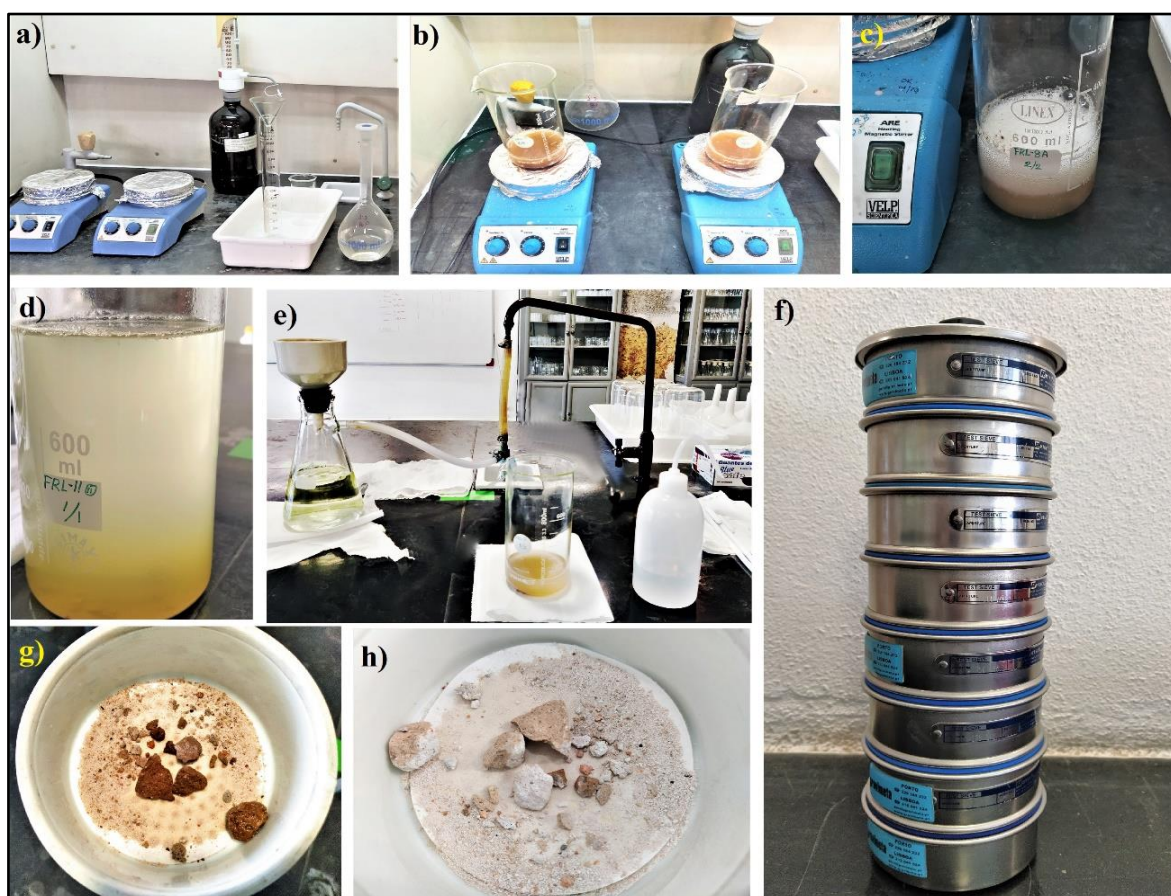


Figure 3. 7-Experimentation of the analysis: a) Preparation of HCl aqueous solution, b) Heating up the sample in HCl aqueous solution on hot plate up to boiling temperature, c) Cooling down the solution, d) Adding water to the solution, e) Filtration under vacuum using a Büchner funnel, g) Filtered wet sample using filter paper, h) Dried sample, f) Sieving using ASTM E11 test sieves.

4 RESULTS

.....

All the results are based on analytical techniques that were used to characterize (or study) the historical mortars from the Roman villa of Frielas in terms of raw materials, production technology, manufacturing recipes, and provenance. It compiles data from stereo-microscopy evaluations, mineralogical characterizations by Optical Microscopy, X-Ray Diffraction (XRD), compositional and elemental characterizations Thermogravimetric Analysis (TGA-DTG), Scanning Electron Microscopy coupled with Energy Dispersive X-Ray Spectrometry (SEM-EDS), Acid Attack, and Granulometric Analysis.

4.1 Preliminary Observation

Visual and preliminary observations of the samples which was made with an unaided eye helped to make an initial assessment in order to identify stratigraphic layers, colors, textures, strength, major features (lime nodules, cracks, lithic fragments, etc.) and to categorize them according to their certain similarities and differentiations. It provides an overall idea about the mortar samples which would then help proceed towards further evaluation. As a processual methodology, all samples were photographed and documented during observation. Based on their similarities and distinctive properties, functionality, and construction phases, samples were divided into preliminary representative groups.

According to the visual inspection, the colors of the samples were mainly whitish, brownish, and reddish except the samples FRL-6 and FRL-19 whose upper layers were pink (FRL-6-U) and white (FRL-19-U) in color respectively. The reddish samples (FRL-1, FRL-2, FRL-3, FRL-5, FRL-7-i, FRL-9, and FRL-10) were collected from the peristyle water channel wall, stairs, and compartment floor filler predominantly consisted of ceramics. The whitish samples were mainly filler (FRL-4, FRL-12), floors (FRL-7-ii, FRL-8) and render (FRL-6-D) mortars. Samples collected from the compartment sidewall (mural painting wall) were observed to be brownish (FRL-11-i, FRL-11-ii, FRL-15, FRL-17, FRL-19) meanwhile, the sample FRL-18, which was collected from the other detached wall fragment, also appears to have a similar color.

The samples FRL-17 and FRL-18 were observed to have chromatic layers with dark brown and brown thin pigmented layers respectively (Fig-4.1). The case of FRL-19 which was collected from the compartment wall appears to be a decorative sample with curves in a whitish layer. For all the samples with stratigraphic layers, it was observed that the upper layers were more binder rich with smaller siliceous aggregates than the lower part. Sample FRL-8 contains tesserae (Black, red, and white) in a whitish binder matrix as the upper layer (FRL-8-U).

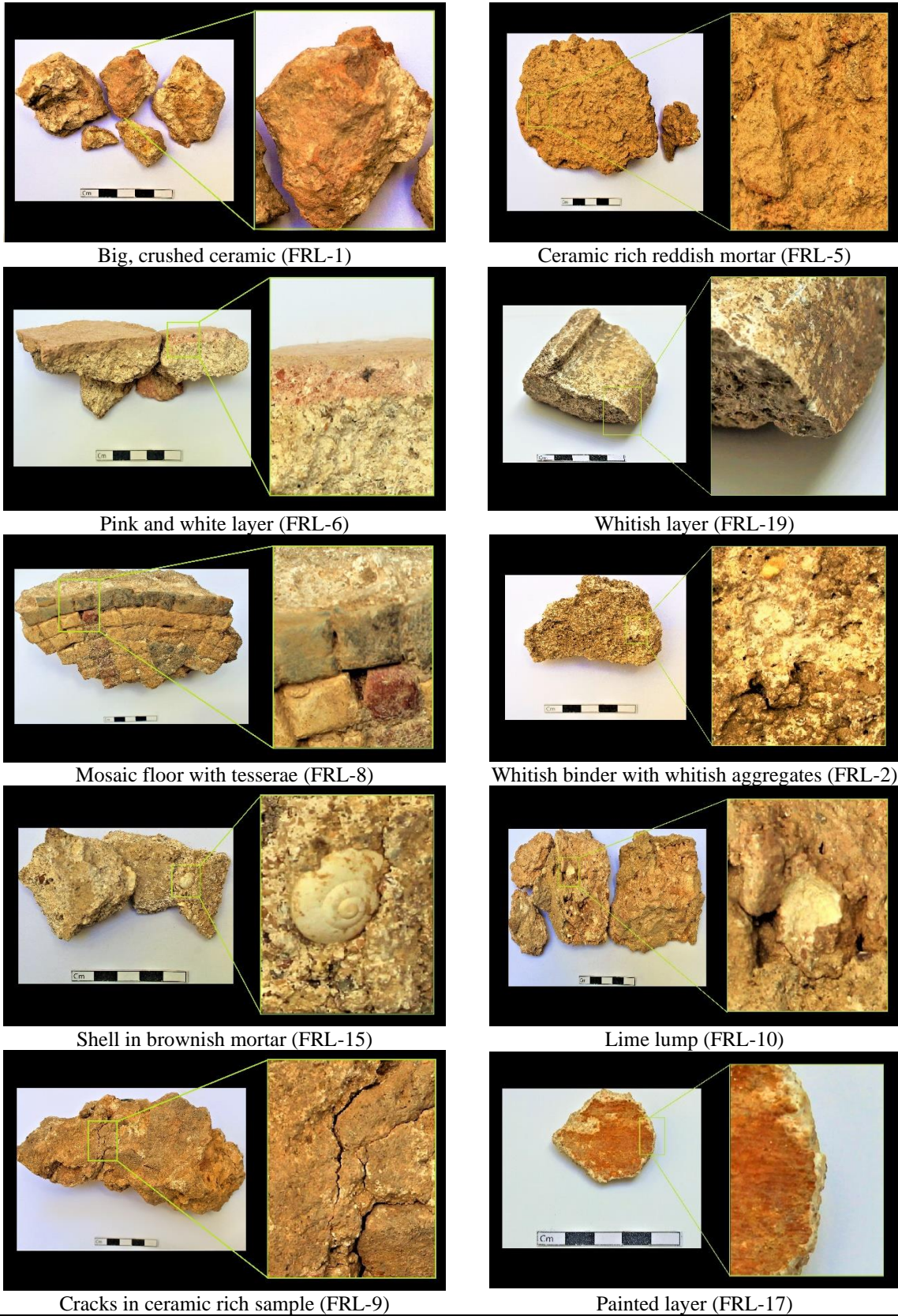


Figure 4. 1- Visual observation and Photographic documentation of representative mortar samples.

The resistance of the samples was also observed during the disaggregation, wherein it was noticed that all the samples with crushed ceramics or ceramic fragments as aggregates were stronger in terms of mechanical strength (Tab-4.1). The whitish samples which contain siliceous aggregates in the binder-rich matrix were mostly with medium mechanical strength and in some cases fragile as well (FRL-4, FRL-12). The samples in brownish color (including samples with paint) were mainly weak in strength and fragile (FRL-15, FRL-17, FRL-18)

It was observed that some of the samples have visible cracks (FRL-1, FRL-3) and lime nodules (FRL-4, FRL-10, FRL-12) while some samples were found with shell or fragments of a shell (FRL-15, FRL-17) and black lithics as aggregates (FRL-1, FRL-18, FRL-19). The samples that contain ceramics were with large-sized (20-30mm) crushed ceramics (FRL-1, FRL-7-i, FRL-9, FRL-10) and medium-sized (10-20mm) crushed ceramics (FRL-3 and FRL-5).

Table 4. 1- General features of mortar samples obtained by visual observation

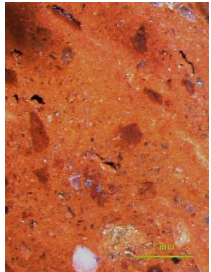
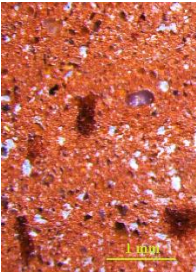

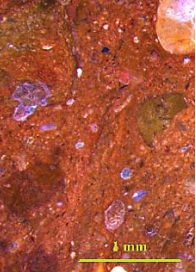
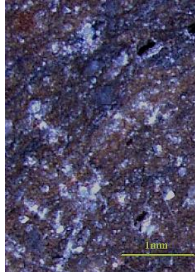
Sample	Layers	Mechanical Strength	Binder color	Aggregates	Thickness/cm	Description
FRL-1	No	Strong	White	Ceramics, coarse sand	2-3	Cracks
FRL-2	No	Strong	White	Ceramics, coarse sand	1.5	Ceramics, coarse sand
FRL-3	No	Strong	Reddish	Ceramics	1	Cracks,
FRL-4	No	Mild strong	White	White sand	2	Lime nodules,
FRL-5	No	Strong	Reddish	Ceramics	2-3	Crushed ceramics
FRL-6	Yes	Mild strong	Pinkish	Fine ceramics and sand.	0.5	Similar size aggregates
			White		2	
FRL-7-i	No	Strong	White	Ceramics and sand	2-3	Crushed ceramics
FRL-7-ii	No	Mild strong	White	White sand	2-3	Similar size aggregates
FRL-8	Yes	Mild strong	White	White sand	1.5	Fine cracks,
			White		4	
FRL-9	No	Strong	Reddish	Ceramics	5	Cracks,
FRL-10	No	Strong	Yellowish	Ceramics	1	Lime nodules,
			Reddish		1.5	
FRL-11-i	No	Fragile	Brownish	Brown sand	0.7	Lithic fragments
FRL-11-ii	No	Fragile	Brownish	Brown sand	0.5	Lithic fragments
FRL-12	No	Mild strong	White	White sand	3	Lime nodules,
FRL-15	No	Fragile	Brownish	Brown sand and shell	2	Shell fragments
FRL-17	Painting layer	Fragile	Brownish	Brown sand and shell	1	Shell fragments
FRL-18	Painting layer	Fragile	Brownish	Brown sand	1.5	Black lithics fragments
FRL-19	Yes	Mild strong	White	Brown sand	0.8	Black lithics fragments
			Brownish		4	

4.2 Stereo-zoom microscopy

After visual and preliminary observation, stereo-zoom microscopy was used to make the assessment more supportive and effective. Stereo-zoom microscopic analysis was conducted with the polished sectioned (cross-section) specimen to understand the binder and aggregate characteristics. Additional information was obtained from the insoluble residue (see section 3.1.5) of the samples regarding aggregates observing grain size and shape.

The most abundant aggregates were ceramics fragments and siliceous grains (quartz and feldspar), with different sizes and proportions throughout the samples. Though it must be noted that some samples were found with shell fragments (FRL-15, FRL-17, and FRL-18) and some samples were with black and brown lithic fragments (FRL-1, FRL-19). The hydraulic structure (water channel) and the others *opus signinum* samples were analyzed in order to make a general observation of the ceramic-rich samples. There were several kinds of ceramics as aggregates in the ceramic-rich samples. Five types of ceramics were distinguished and classified by their color (orange, red, brown, dark brown, and black), composition, size, porosity, and inclusion (Tab-4.2).

Table-4.2- Types of ceramics fragments found in samples.

Orange	Red	Brown	Dark Brown	Black
				
<p>Compact composition, random siliceous inclusions in a fine clay matrix. Light color, poorly sorted.</p>	<p>Coarse grain, high proportion of inclusion, porous and well sorted.</p>	<p>Medium to small siliceous inclusions, random grains, poorly sorted. Light color.</p>	<p>Big and small siliceous inclusions with random grains, poorly sorted. Deep color. Compact.</p>	<p>Porous, coarse grain, high proportion of inclusion, very dark color and well sorted.</p>

The frequency of various types of ceramic fragments found within the samples, and it was observed that dark brown and red ceramics was predominated the samples (Tab-4.1), particularly those containing large, crushed ceramics (more than 20mm) associated with *opus*

signinum. In samples FRL-3 and FRL-5, orange and red ceramics were abundant with traces of black ceramics (Fig-4.2). FRL-6, the Upper pinkish layer, was another sample that contained ceramic fragments smaller than 4mm and in red color.

Table 4. 3- Distribution frequency of ceramic fragment types found in samples.

Sample	Orange	Red	Brown	Dark brown	Black
FRL-1	-	-	++	++	
FRL-2			-	+	
FRL-3	++	+	-	-	-
FRL-5	++	++	+	-	-
FRL-6-U		++	-	-	
FRL-7-i		+		+	
FRL-9	+	+		+	
FRL-10-D		+	+	+	

*Most frequent ++ + - least frequent.
axis

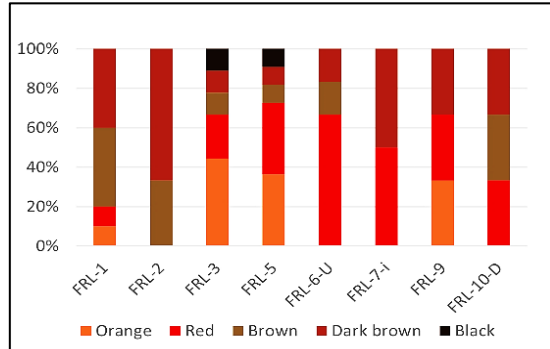


Figure 4. 2- Type of ceramics found in each Sample. 'Y' showing visually estimated volume.

For most of the samples, the binder was mainly white in color. Some samples appear to have cracks (FRL-1, FRL-2, FRL-3, FRL-4, FRL-8, and FRL-12), and small-sized rounded lime lumps (FRL-2, FRL-8-U, FRL-10-D, FRL-11-i, FRL-11-ii, FRL-18) which might be an indication of water shortage in the lime slaking process, during the conversion of calcium oxide (CaO) into calcium hydroxide, Ca(OH)₂ (Elsen, 2006; Adriano *et al.*, 2009; Cardoso *et al.*, 2014).

The sample FRL-6 appears to have a pink layer (0.5cm) on the upper part containing mainly small fragments of ceramics as aggregates and within the binder, resulting in a smooth pinkish color whilst the lower layer contains siliceous aggregates in a whitish binder. The sample FRL-8 contains tesserae (1cm³, black, white, and red in color) on the binder-rich white matrix with a small number of siliceous aggregates in the upper layer (1.5 cm) (Tab-4.5). Meanwhile, the lower layer is rich and compact with siliceous (white, yellow, and brown in color) aggregates with a low amount of the binder portion.

In the case of the sample FRL-10 (collected from the staircase), there appears a thin yellowish layer of about 5 mm (upper layer), containing yellowish homogeneous aggregates in a yellowish binder, which seems to be a finishing layer (*intonaco*) on the surface of the lower layer. In the lower layer there is a predominance of ceramic fragments as medium and small size aggregates. Random-sized lime lumps can also be seen in the lower layer of the sample (Tab-4.4). As a decorative fragment of the wall, sample FRL-19, contains two identical layers; the upper layer containing very thin white paint on the surface of whitish binder rich matrix where the aggregates are small, angular, and sub-angular shaped white, milky, and random reddish color grains and in the lower layer (FRL-19-D) different colors of aggregates are visible, especially black, and brown.

Table 4. 4- General aspect of the samples under stereo zoom microscope.

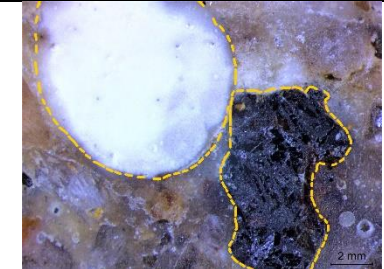


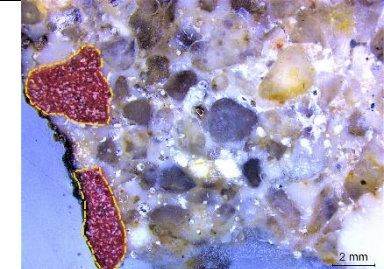
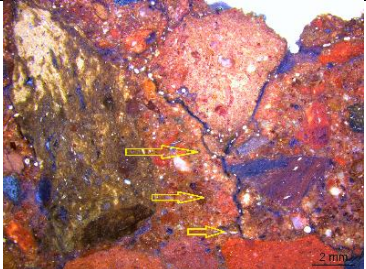
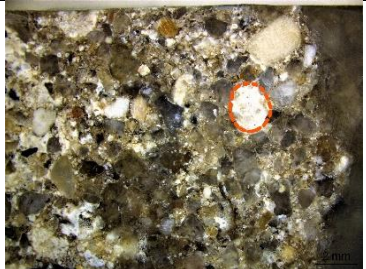


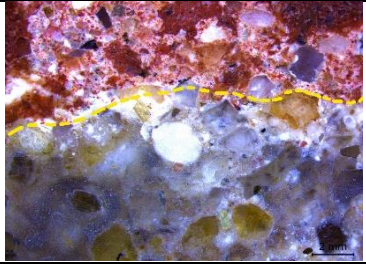
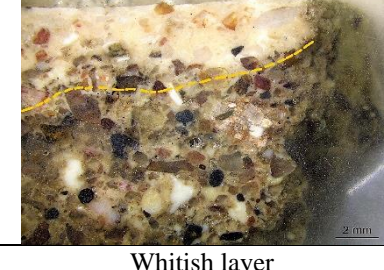
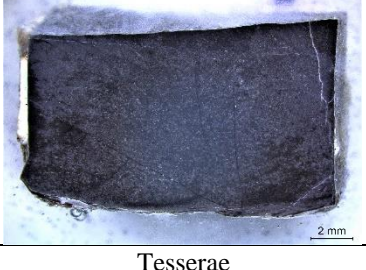


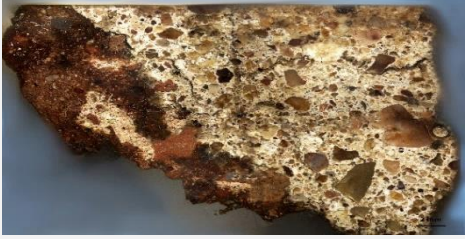

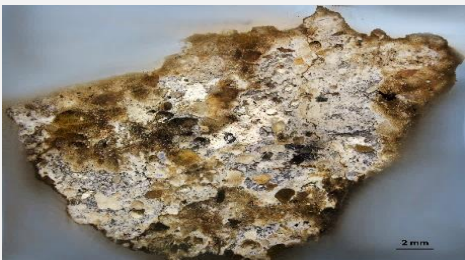



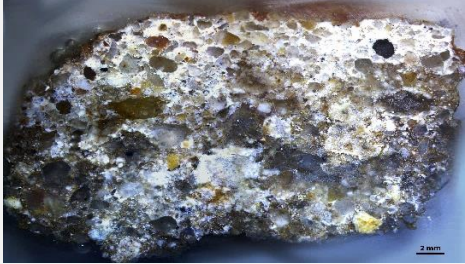
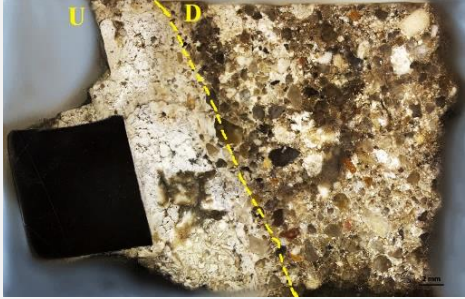

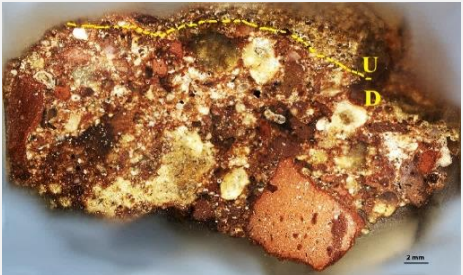


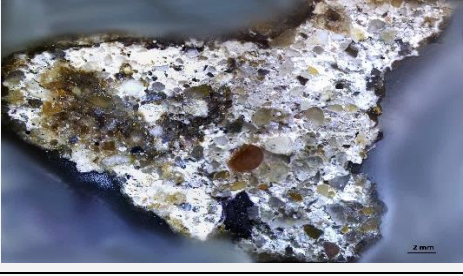


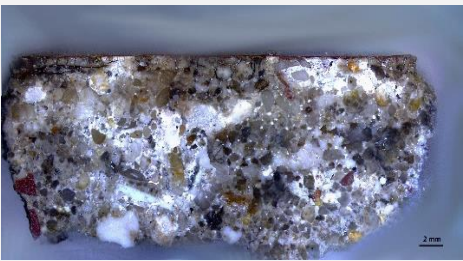
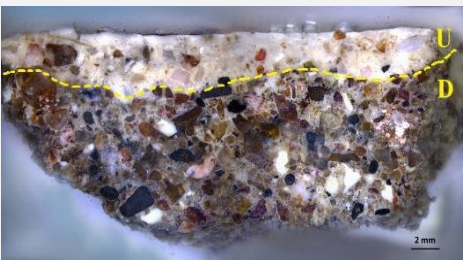
		
Milky quartz-black aggregates	Siliceous aggregates	Ceramic fragments
		
Lithic fragments	Cracks in binder	Rounded lime lump
		
Lime nodules	Shell fragments	Layered mortar
		
Whitish layer	Tesserae	Painting layer

Table 4. 5- Preliminary assessment and microscopic observations.

Sample	Structure	Color	Description	Polished Section
FRL-1	Render mortar from water channel bottom surface.	Reddish Brown	Big crushed ceramic aggregates, 4mm-20mm long, different colors, and shapes. Sub-rounded dark aggregates. Cracks in the binder.	
FRL-2	Render mortar from water channel sidewall.	Whitish Brown	Cracks in the binder, few big ceramic fragments with sub-angular and sub-rounded aggregates in the binder. Black, gray, and brownish aggregates. Lime lump is present.	
FRL-3	Render mortar from water channel sidewall.	Reddish Orange	Cracks in binder, very compact medium size crushed ceramic aggregates. Angular and sub-angular few black and brown aggregates are present. Some lithic fragments are visible.	
FRL-4	Filler mortar from water channel sidewall	Whitish Gray	Fine cracks in binder with on average homogeneous white and grayish aggregates in small size and shape. Very fragile composition in lime-rich binder.	
FRL-5	Render mortar from water channel sidewall	Reddish orange	Very compact small and medium size crushed ceramic aggregates. Angular and sub-angular black and brown aggregates are visible. Lithic fragments are also visible.	

FRL-6	Render mortar from the peristyle wall	Reddish Pink	Upper layer (U), mostly reddish fragments of small-sized ceramics mixed with binder, few other whitish aggregates also visible.	
		Whitish Gray	(D) Few Sub-angular ceramics and other random-sized aggregates in a whitish matrix can be visible.	
FRL-7 (i)	Filler mortar from overlapped mosaic floor	Reddish Brown	Big crushed ceramic aggregates, 4mm-20mm long, different colors, and shapes. Sub-angular brownish aggregates. Fine Ceramics fragments mixed with binder.	
FRL-7 (ii)	Filler mortar from overlapped mosaic floor	Whitish Gray	Mostly white and brownish small and medium-size aggregates, Few black sub-rounded aggregates in a different size. Medium strength of binder composition.	
FRL-8	Mosaic Floor	White	Upper layer (U) containing tesserae. Mainly whitish binder with small amount of similar size aggregates. Lime lumps and fine cracks are visible. Nearly fragile.	
		Whitish Gray	(D) Small and medium size of whitish and brownish aggregates. Fragile and nearly crumbly.	
FRL-9	Filler mortar from compartment floor	Reddish Brown	Big crushed ceramic aggregates, 4mm-20mm long, different colors, and shapes. Sub-angular reddish ceramic fragments are visible in the whitish binder.	

FRL-10	Render mortar from stair	Yellowish Brown	Upper layer (U), fine yellowish color aggregates mixed with the binder. Mostly small size and shape.	
		Reddish Brown	(D) Small and medium-size ceramic aggregates, Small random shape lime lumps are present.	
FRL-11 (i)	Render mortar from mural painting wall	Whitish Gray	Random size aggregates in the whitish binder, with brown-yellowish, and few black grains. Random size lime nodules are present.	
FRL-11 (ii)	Render mortar from mural painting wall	Whitish Gray	Small and similar size brown, yellow and reddish aggregates in a whitish binder, few black grains also visible, rounded lime lumps are present.	
FRL-12	Filler mortar from peristyle wall	Whitish Gray	Very crumbly and fragile. Fine cracks in binder with on average homogeneous white and grayish aggregates in small size and shape.	
FRL-15	Render mortar from compartment wall	Brownish Gray	Small and random size aggregates, mostly black, red, whitish, and brownish in color, shell fragments are present, very crumbly.	

FRL-17	Render mortar from mural painting wall	Brownish Gray	Containing dark brown painting layer. Small but random size aggregates, whitish, brown, and black aggregates are visible.	
FRL-18	Render mortar from mural painting wall	Brownish Gray	Containing brown painting layer. Small and random size aggregates, mostly black, red, and brownish in color. Shell fragments are present. Lime lumps are present. Crumbly or fragile.	
FRL-19	Decorative mortar from compartment wall (Mural painting wall)	White	The upper layer (U) is mainly binder with homogeneous whitish aggregates. Similar size and shape of whitish and very few reddish grains.	
		Brownish Gray	The lower layer (D) with small and random size angular and sub-angular aggregates, mostly whitish, black, red, and brownish in color.	

4.3 Petrographic Analysis

The petrographic microscope can be used to understand the spatial distribution of components including the structure and texture of mortars by means of thin sections. This further helps to understand the bonding, the kind of binder, and aggregate and can also throw light on the application and hardening process of the mortar as well as offer preliminary data on the use of additives and admixtures within the mortar (Middendorf *et al.* 2005a).

Most of the samples displayed a similar mineralogical character based on their aggregate composition. The main minerals abundant in all samples were quartz and feldspars (K-feldspar and plagioclase) in angular and sub-angular form. Although quartz grains have been mainly observed as single grains, in a few cases it was present as part of lithic fragments such as quartzite or associated with feldspars as granitic grains (Tab-4.6). Besides, within the ceramic-rich sample quartz can be seen as inclusions. In ceramic-rich samples, micas (muscovite and biotite) can be seen within the ceramic inclusions as well as in the binder.

The basaltic grains were mostly rounded and sub-angular shaped which were found in samples FRL-15, FRL-17, FRL-19, and FRL-1. In some cases, alteration of olivine with the presence of iron-oxide can be seen in association with basaltic grain or vitreous texture grain.

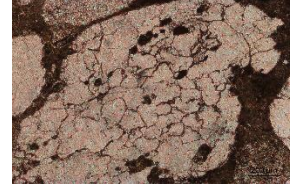
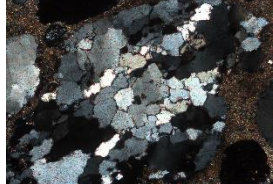

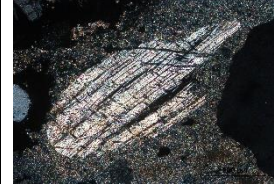
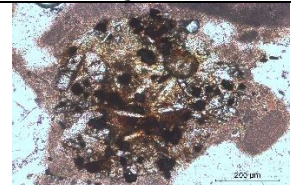
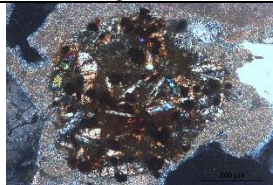
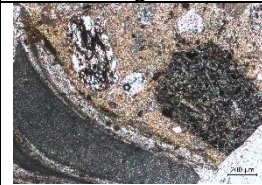
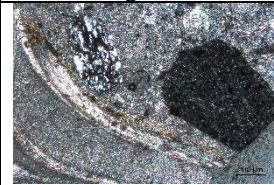
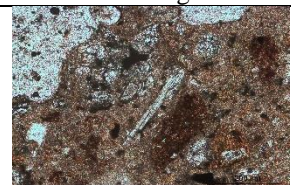
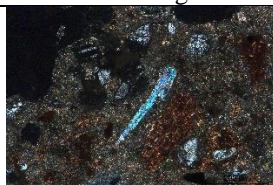
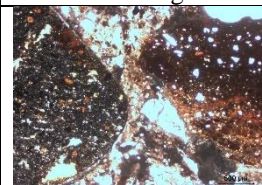
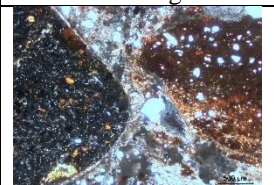
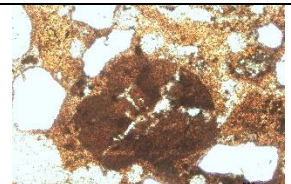
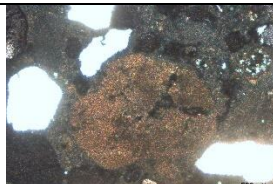
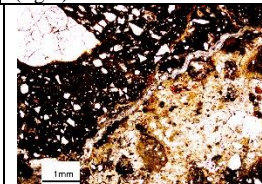
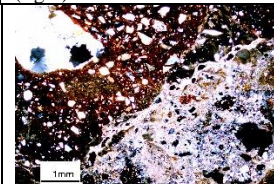
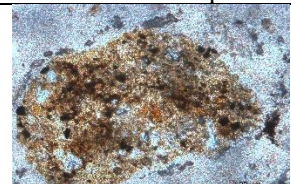
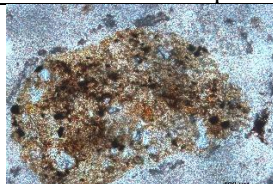
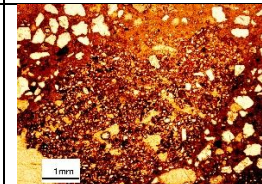
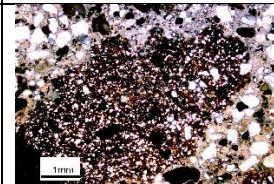

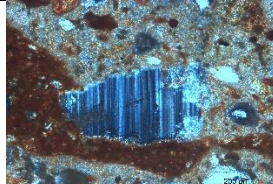
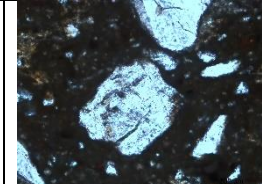
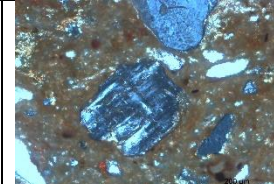
Table 4. 6- Representative petrographic images of the general composition of mortars.

<p>XPL FRL-18 General distribution, angular and sub-angular aggregates. Presence of quartz, feldspar, and quartzite.</p>	<p>PPL FRL-12 Aggregates distribution in lime rich binder. Predominance of quartz and feldspar.</p>	<p>XPL FRL-19 Transition between layers. Lime rich paint (top), lime rich binder with limestone and crushed lime fragments. Quartz, feldspar, and shell as aggregates (bottom).</p>
<p>XPL FRL-17 Painting layer (top), lime binder and smaller siliceous aggregates. Shell fragments, basaltic grain, (right), lime lumps (left bottom)</p>	<p>PPL FRL-4 Lime rich binder, Predominance of quartz and quartzite. Small angular and sub-angular shape.</p>	<p>XPL FRL-3 Angular shaped ceramic fragments alongside with fine cracks. Finer ceramic dust in lime binder.</p>

Some samples appear to be abundant with shell fragments and calcitic bio-clasts such as samples FRL-11-i, FRL-11-ii, FRL-15, FRL-17, and FRL-19. In the case of lithic grains, sandstone was observed in ceramic-rich samples (FRL-1, FRL-3, and FRL-5) although, it could be hard to distinguish sandstone from ceramic fragments as aggregates in a binder matrix. The presence of angular and sub-angular limestone fragments was observed within the samples.

Lime lumps were observed in some samples (FRL-2, FRL-8-U, FRL-10, FRL-11-ii, and FRL-18) which is confirm by the stereo-zoom observation. Cracks in the binder were observed mainly in the samples with ceramics. The most abundant cracks were noticed surrounding the ceramic fragments or voids and in certain cases, carbonated recrystallizations are visible in the cracks. Also, within the binder, it was possible to observe carbonated grains which were not easily distinguishable as they share a similar composition with the binder itself. But in some cases, they are well defined in a very clear angular shape similar to fragments of limestones. Such inclusions give the binder a continuous and homogenous appearance.

Table 4.7 - Representative petrographic images of the minerals observed under XPL (cross polarized light) and PPL (plane-polarized light).

			
PPL Quartzite	XPL Quartzite	PPL Plagioclase	XPL Plagioclase
			
PPL Basaltic grain	XPL Basaltic grain	PPL Shell fragment	XPL Shell fragment
			
PPL Muscovite	XPL Muscovite	PPL-ceramic fragment (right)	XPL-Ceramic fragment (right)
			
PPL Lime lump	XPL Lime lump	PPL Cracks	XPL Cracks
			
PPL Limestone	XPL Limestone	PPL Sandstone	XPL Sandstone
			
PPL Plagioclase	XPL Plagioclase	PPL Microcline	XPL Microcline

The lighter colored layers (Upper layer) of the samples with whitish stratigraphy such as FRL-19-U appear to be more enriched with more carbonated and few siliceous aggregates. The binder was more continuous in upper layers, whereas the lower layers of the sample were composed of dark lithic (sandstone, basaltic grains) aggregates which were mostly smaller in size (1-0.5 mm) and had less amount of binder.

Table 4. 8- Results of Petrographic observation of the studied sample from the Roman villa of Frielas

Sample	Quartz	Quartzite	Feldspar	Basalt	Sandstone	Limestone	Mica	shell	Ceramics
FRL-1	++	+	+	+	+	+	+		+++
FRL-2	++	+	++		+	+			+
FRL-3	+		+		+	+	++		+++
FRL-4	+++	+	++						
FRL-5	++		++		+	+	+		+++
FRL-6	++	+	+						+
FRL-7i	+		+						+++
FRL-7ii	+++	+	+						
FRL-8	+++	+	+						
FRL-9	+						+		+++
FRL-10	+					+			+++
FRL-11i	++	+	+			+			+
FRL-11ii	++	+	+		+	+		+	+
FRL-12	+++	+	++						
FRL-15	++	+	+	+		+		+	
FRL-17	++	+	+	+		+		+	
FRL-18	++	+	+			+			
FRL-19	++	+	+	+		+			

+++ abundant, ++ major, + minor

4.4 X-ray Diffraction (XRD)

X-ray diffraction (XRD) analysis can be used in addition to chemical and microscopical analysis to identify the mineralogical composition of mortar samples. The mineral composition of the samples was determined by using global fraction and fine fraction. The samples with stratigraphic layers were analyzed separately for each layer and the samples with painting layers were also analyzed after the paint layer had been removed.

The result of the global fraction reveals the predominance of quartz and its presence as the main constituent in all the samples (Tab-4.9). Quartz appears to be rich in the samples with ceramics as it is present in both the binder and the ceramic inclusions. Depending on the semi-quantified data of crystalline phases of the samples, FRL-2, FRL-6-D, FRL-7-ii, FRL-8-D, FRL-11-ii, and FRL-12 had the highest amount of quartz while, samples FRL-5, FRL-6-U, FRL-8-U, FRL-9, FRL-15, FRL-17, FRL-19-U, and FRL-19-D had the lowest amount of quartz (Tab-4.9). Samples with the stratigraphic layers clearly depict that the lower layer

contains more quartz than the upper layer. Along with the quartz, all samples have an abundance of K-feldspar (orthoclase and microcline) while microcline was more abundant when compared to orthoclase which is present in minor amounts. Sample FRL-7-ii has the presence of albite (Na-plagioclase) while other samples only have it in trace amounts.

In the case of calcite, samples with whitish stratigraphic layers (FRL-8-U, and FRL-19-U) have a predominance of calcite over the quartz and feldspar, and there is a limited presence of calcite in the rest of the samples. Other minor or trace minerals found in the samples were anorthite (FRL-9 and FRL-19-U), ferrosilite, augite, hematite, and muscovite. Muscovite was mainly present in the ceramic-rich samples (FRL-1, FRL-3, FRL-5, FRL-7-i, FRL-9, and FRL-10-D) and occasionally traces of biotite were only associated with ceramic rich samples.

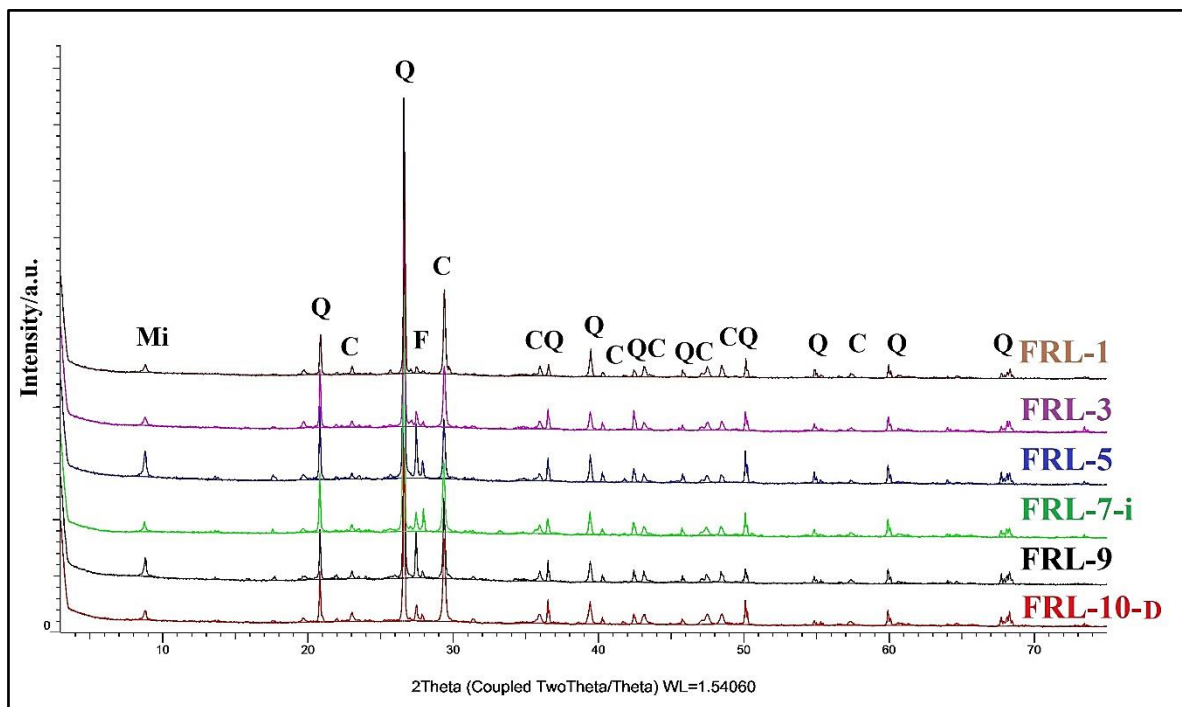


Figure 4. 3- XRD patterns (Global fraction) of ceramic rich samples (Group-A), (Q-quartz, C-calcite, F-feldspar, and Mi-mica).

Samples with the traces of ferrosilite, augite, and hematite revealed brownish color with black rounded grains when observed in stereo-zoom microscopy and basaltic grains were noticed in petrographic observations. It may probably indicate that the basaltic grains were associated with these minerals.

Considering the results from petrographic analysis and stereo-zoom observation, the results obtained from XRD analysis similarly indicates the main three group of samples according to their mineral crystalline phases detection. In the first group (Group-A), ceramic-rich samples were found with traces of micas (Muscovite and biotite) (Fig.4.3), while the second group (Group-B) have only a predominance of quartz, feldspar, and calcite (Fig-4.4).

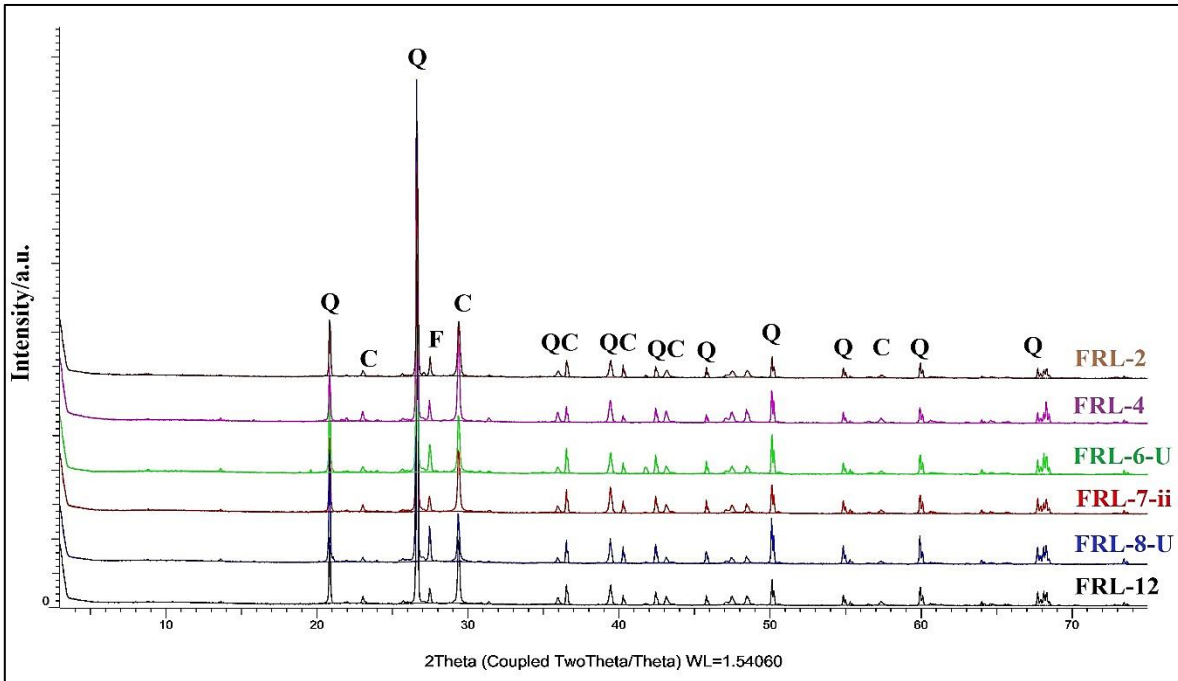


Figure 4. 4- XRD patterns (Global fraction) of ceramic rich samples (Group-B), (Q-quartz, C-calcite, F-feldspar)

The third group (Group-C) can be differentiated by the presence of augite, ferrosilite, and hematite (Fig. 4.5) which could be associated with basaltic lithic fragments. In addition, this group also contains shell fragments. The rest of the samples are sub-samples as the upper layer, which can be considered as another group (Group-D) due to their abundance of calcite and quartz, moreover as their functionality.

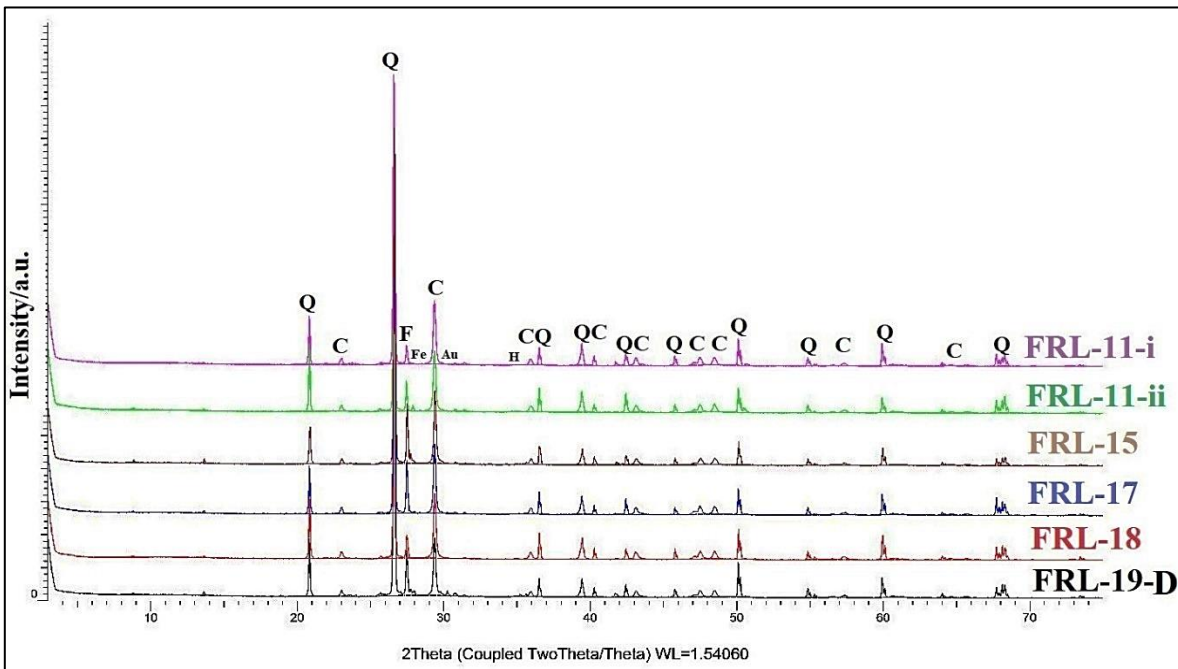


Figure 4. 5- XRD patterns (Global fraction) of basaltic and shell fragment rich samples, (Group-C), (Q-quartz, C-calcite, F-feldspar- ferrosilite, Au-augite, and H-hematite)

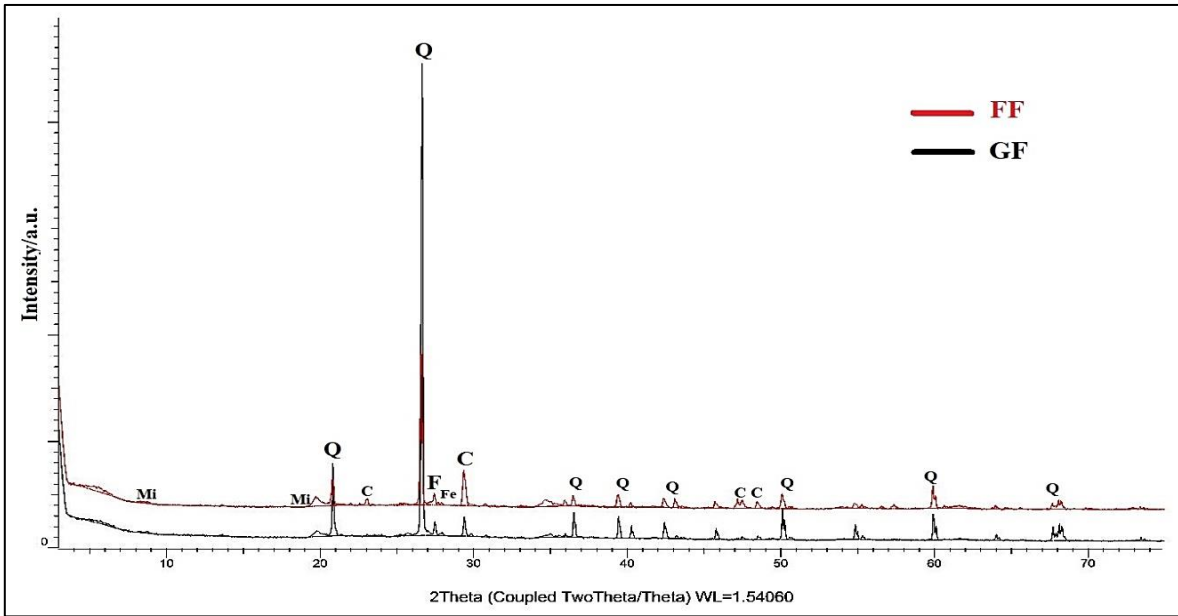


Figure 4. 6-XRD patterns of soil sample-FRL-13-s, (1st phase) (Q-quartz, C-calcite, F-feldspar, Mi- mica, and Fe-ferrosilite).

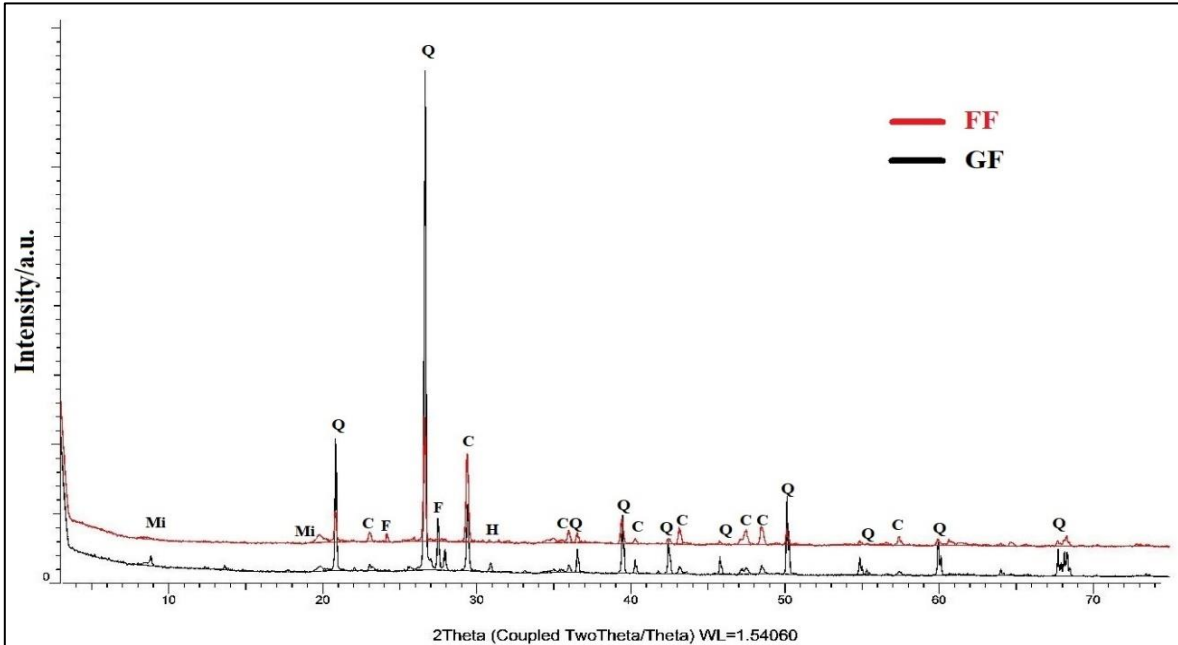


Figure 4. 7- XRD patterns of soil sample-FRL-16-s (abandonment phase) (Q-quartz, C-calcite, F-feldspar, Mi- mica, and He- hematite).

Soil samples from the first construction phase (FRL-13-s) and abandonment phase (FRL-16-s), were analyzed in global fraction and fine fraction (< 100 mm sieved) powder in order to identify the clay minerals or any probability of mortar indication that can be used in the building materials for these two phases. Results showed that FRL-13-s (Fig. 4.6) and FRL-

16-s (Fig. 4.7) have a predominance of quartz, and traces of calcite. In addition, both samples were found with the trace of muscovite and feldspar.

Also, the fine fraction (0.063mm sieved fraction, rich in binder) analysis of all the mortar samples was similar to the global fraction diffractograms and could not provide any additional information.

Table 4. 9- Mineralogical composition of the global fractions of mortars assessed by XRD.

Sample	Quartz	Calcite	K-Feldspar		Plag-Feldspar		Ferrosilite	Augite	Hematite	Mica	
			Microcline	Orthoclase	Albite	Anorthite				Muscovite	Biotite
FRL-1	+++	++	+		T			T	T	+	T
FRL-2	++++	+	++		T						
FRL-3	+++	+	++		T					+	T
FRL-4	+++	++	++		T	+				T	
FRL-5	++	+	++		+					+	+
FRL-6-U	++	+	+++	+	T					T	
FRL-6-D	++++	+	++	+	T					T	
FRL-7-i	+++	+	++		++				T	+	
FRL-7-ii	++++	+	++		T					T	
FRL-8-U	++	+++	++		T						
FRL-8-D	++++	+	++		T						
FRL-9	++	+	++	+	T	T				+	
FRL-10-U	+++	+	++	+	T					T	
FRL-10-D	+++	++	++	+	+		+	T	T	+	
FRL-11-i	+++	+	++	+			T	T			
FRL-11-ii	++++	+	++		T		T	T		T	
FRL-12	++++	+	++	T						T	
FRL-15	++	+	+++	+			T	T	T	T	
FRL-17	++	+	++	+	T		T	T		T	
FRL-18	+++	+	++	+			T	T		T	
FRL-19-U	++	+++	+		T	T					
FRL-19-D	++	+	++	+	T		T	T		T	

++++ Predominant, +++ abundant, ++ major, + minor, T- trace

4.5 Thermogravimetric Analysis (TGA)

Thermogravimetric analysis is a technique that is carried out on the global fraction (GF) powders of the sample that helps to determine the mortar composition by measuring the mass changes throughout a heating process, in an inert atmosphere. The thermogravimetric curve (TG) was used to determine the percentages of the most significant mass losses during the heating process.

The temperature ranges were set as 40-120°C, 120-200°C, 200-600°C, and 600-900°C according to significant mass losses. The weight loss at 40-120°C is attributed to the physically adsorbed water. 120-200°C is attributed to the loss of crystallization water, while 200-600°C can be related to structurally bonded water (dihydroxylation). And 600-900°C is related to the characteristic mass loss range, for the decomposition of calcium carbonate (CaCO₃) to calcium oxide (CaO) and carbon dioxide (CO₂) (equation 1) (Leone *et al.*, 2016; Ponce-Antone *et al.*, 2020). Mass losses in deferent temperature ranges were recorded (Tab. 4.10) in order to elaborate binder to aggregate ratio based on the amount of CaCO₃ present in the sample.

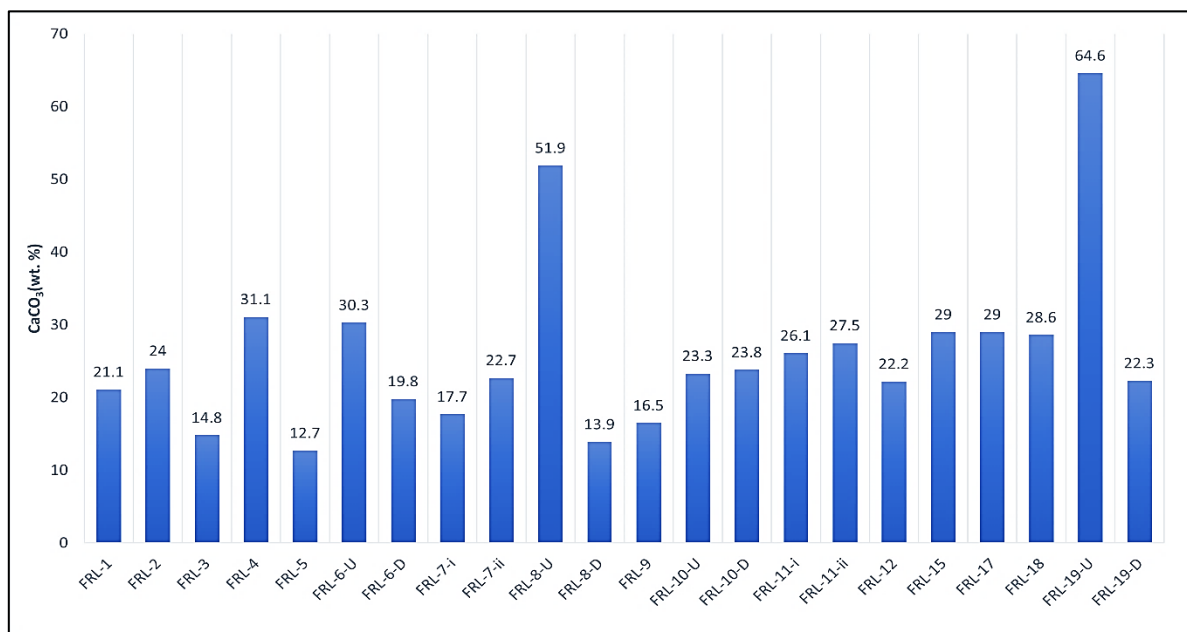
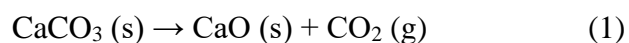


Figure 4. 8-Calculated percentage of CaCO₃ in the samples of Roman Villa of Frielas from TGA results.

The calculated percentage of calcium carbonate as a function of the mass losses in the temperature range between 600-900°C, recorded from the thermogram (Appendix-8.7) showed that the CaCO₃ amount (Fig. 4.8) varies from 12.7% (FRL-5) to 64.6% (FRL-19-U). The samples with ceramics (Fig- 4.9) contain calcium carbonates minimum amount of 12.7 % to a maximum of 23.8% (Group-A) while the samples rich in quartz, are containing CaCO₃ from 19.8% to 31.1% (Group-B).

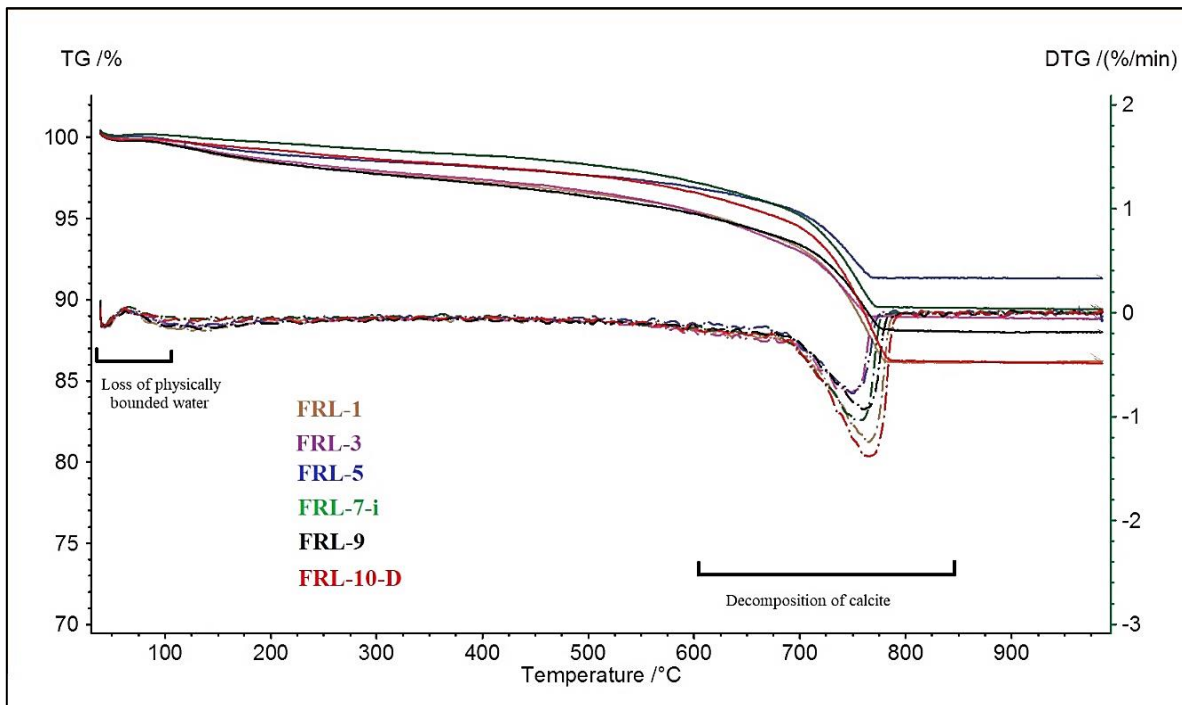


Figure 4. 9-TG/DTG curves of ceramic rich (group-A) samples FRL-1 (brown), FRL-3 (purple), FRL-5 (blue) and FRL-7-i (green), FRL- 9 (black) and FRL-10-D (red). continuous curves representing TG and dashed curves representing DTG data.

The samples with shell and basalt fragments are containing the amount of CaCO₃ from 22.3% to 29% (Group-C). The amount of CaCO₃ due to the presence of other calcium carbonate sources, besides binder in the mortar such as shell fragments, limestone, or any other organic/inorganic calcium carbonates. Due to this reason, the samples with the whitish upper layers, that contain limestone and crushed lime in the binder (confirmed by petrographic observation) show higher amounts of CaCO₃ (Fig-4.10) about 23.3% to a maximum of 64.6% (Group-D). All these percentages were used to estimate binder to aggregate ratios used for the elaboration of each mortar, assuming that the amount of CaCO₃ present in the sample represents the binder composition, and the rest of the mass comprises the aggregates.

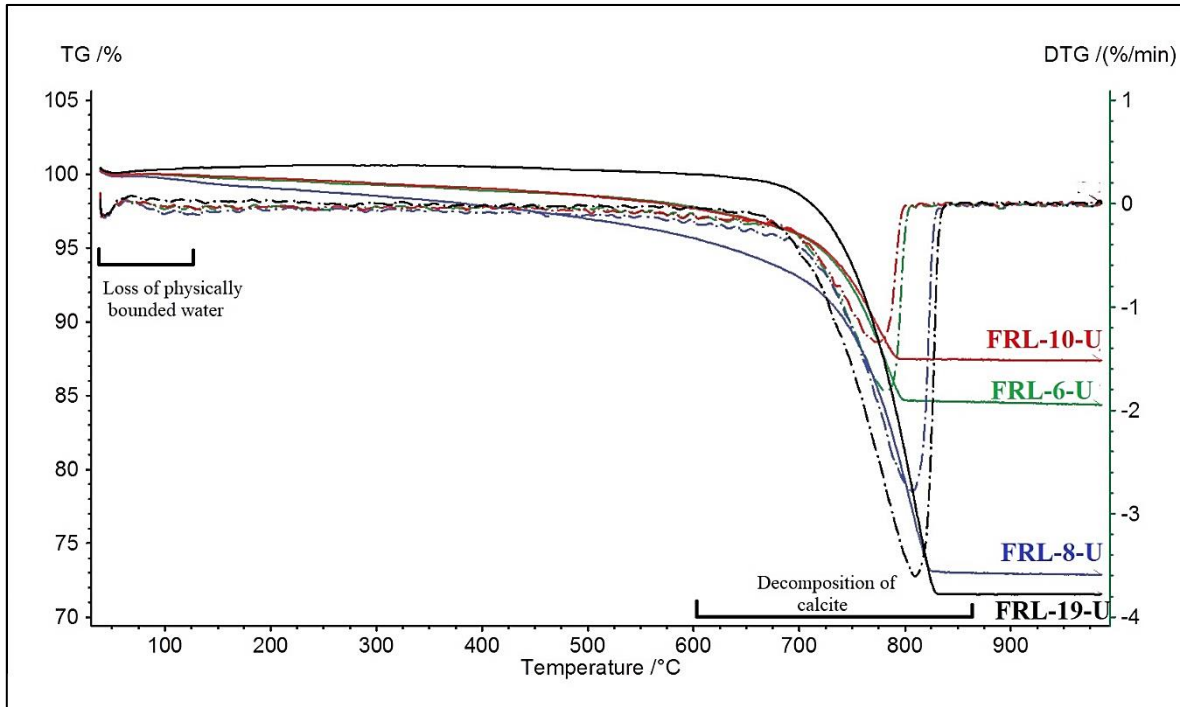


Figure 4. 10-TG/DTG curves of binder-rich upper layers (Group-D) samples FRL-6-U (green), FRL-8-U (blue), FRL-10-U (red), and FRL-19-U (black), continuous curves representing TG and dashed curve representing DTG data.

The other temperature ranges, 40-120°C, showing the mass losses percentage of 0.01 % to 0.87%, while in the range of 120-200°C showing mass losses percentage of 0.01%. to 0.95%. And at the temperature range between 200-600°C, in this range mass losses are as a percentage of minimum 0.57% (FRL-19-U) to maximum 3.38% (FRL-8-U).

Based on the calculated calcium carbonates content, the resulting ratio of binder to aggregates of the ceramic-rich samples varies from 1:3 to 1:7, quartz-rich samples 1:2 to 1:6, and samples containing shell and basalt fragments have a binder to aggerates ratio between 1:2 to 1:3. For the binder to reach upper layers, ratios are 1:1 to 1:3 (Tab-4.10).

The soil samples from the first construction phase (FRL-13-s) and abandonment phase (FRL-16-s) were analyzed in TGA, in order to determine their amount of calcite. In that case, FRL-13-s, the thermogram (Fig-4.11) showing decomposition of clay minerals corresponding to the DTG peaks in between 200-600°C, and decomposition of calcium carbonates in the range of 600-900°C, which is calculated calcium carbonate in an amount of 5.7 % while FRL-16-s have 12.1 % (Fig-4.12).

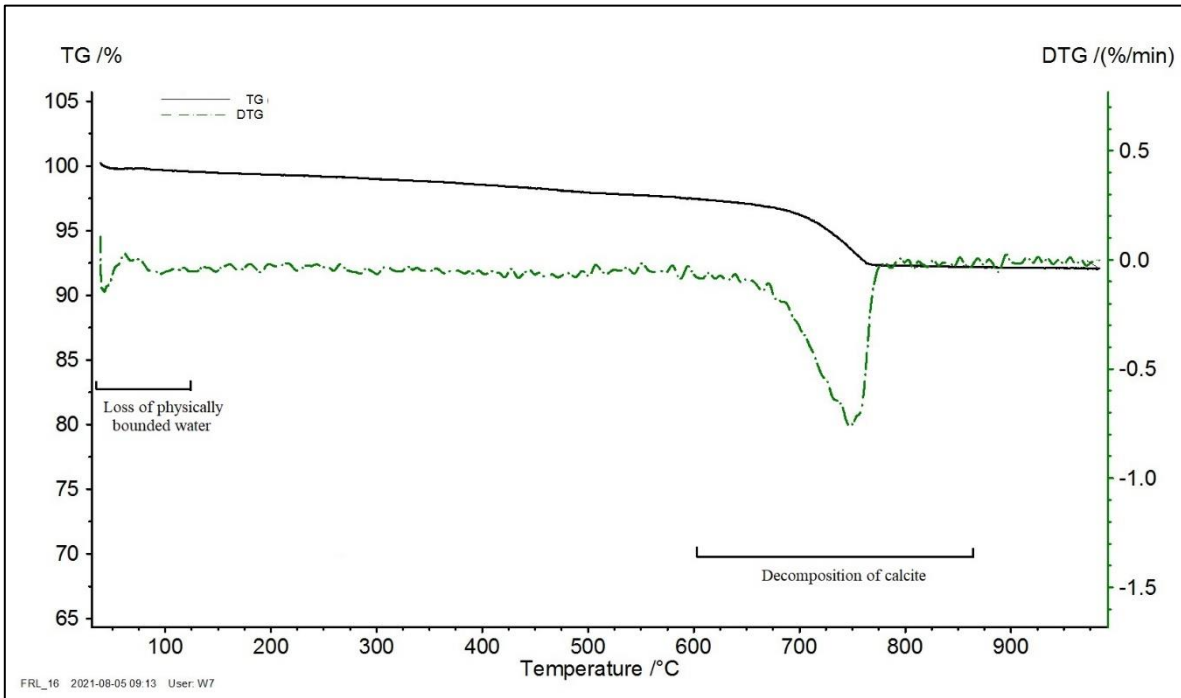
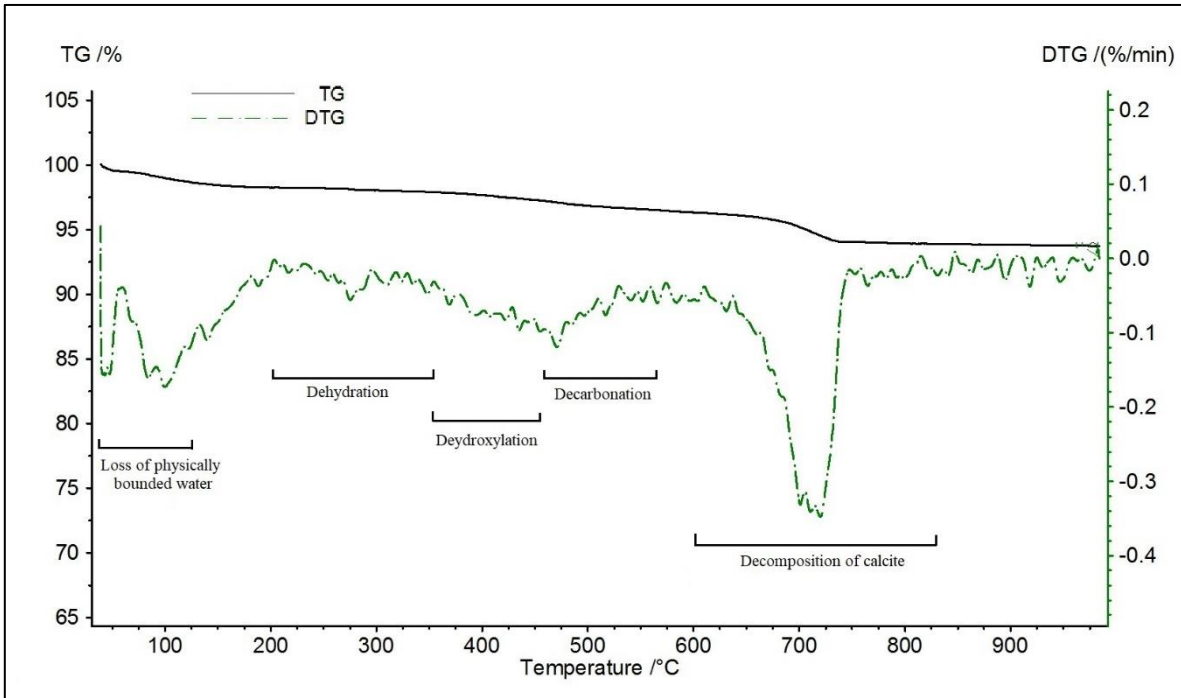


Table 4. 10- TGA results. Record of the mass loss percentages during structurally bound water loss, decomposition of CO₂, CaCO₃ percentage and estimated binder to aggregate ratio.

Sample ID	Mass losses (wt.%) 40-120°C ¹	Mass losses (wt.%) 120-200°C ¹	Mass losses (wt.%) 200-600°C ¹	Mass losses (wt.%) 600-900°C ¹	Calculated CaCO ₃ (wt.%) ²	Binder to aggregate ratio
FRL-1	0.87	0.95	2.96	9.31	21.1	1:4
FRL-2	0.43	0.29	2.02	10.60	24	1:3
FRL-3	0.72	0.82	3.20	6.55	14.8	1:6
FRL-4	0.35	0.25	1.81	13.72	31.1	1:2
FRL-5	0.65	0.66	2.08	5.60	12.7	1:7
FRL-6-U	0.36	0.28	1.79	13.27	30.3	1:2
FRL-6-D	0.06	0.02	1.17	8.72	19.8	1:4
FRL-7-i	0.31	0.36	2.43	7.79	17.7	1:5
FRL-7-ii	0.01	0.05	0.89	10.0	22.7	1:3
FRL-8-U	0.59	0.53	3.38	22.70	51.9	1:1
FRL-8-D	0.08	0.01	1.25	6.12	13.9	1:6
FRL-9	0.78	0.89	3.18	7.30	16.5	1:5
FRL-10-U	0.29	0.23	2.04	10.26	23.3	1:3
FRL-10-D	0.46	0.47	2.62	10.47	23.8	1:3
FRL-11-i	0.17	0.10	2.15	11.52	26.1	1:3
FRL-11-ii	0.16	0.08	1.68	12.11	27.5	1:3
FRL-12	0.27	0.17	1.42	9.77	22.2	1:3
FRL-15	0.01	0.07	0.63	12.79	29	1:2
FRL-17	0.17	0.07	1.24	12.76	29	1:2
FRL-18	0.00	0.10	0.71	12.60	28.6	1:3
FRL-19-U	0.05	0.16	0.57	28.42	64.6	2:1
FRL-19-D	0.17	0.04	1.21	9.81	22.3	1:3

1 Obtained from thermograms (Appendix-8.7)

2 Calculated with the equation (5) for CaCO₃ percentage estimation.

4.6 Scanning electron microscopy with Energy dispersive X-ray spectroscopy (SEM-EDS)

In order to determine the chemical compositions by elemental analysis and textural features regarding binder and aggregates, SEM-EDS analysis was carried out on polished sections. Elemental mapping, imaging, multi-point, and point analysis were applied to obtain information about the samples.

All the samples revealed similar compositions for binders whereas the aggregate compositions are slightly different in sample inclusions. In the form of aggregates were identified mainly quartz, feldspar, and ceramics which corroborates the results obtained from other techniques such as XRD and petrographic analysis. The presence of silicon and oxygen are corresponding to quartz while feldspar has been detected with the presence of aluminum and silicon, in association with either potassium that forms alkali feldspar, or sodium that forms plagioclase feldspar. Also, ceramic fragments were detected by their siliceous inclusions (e.g., quartz and feldspars) in an aluminum-potassium matrix according to clay mineral properties.

Based on the major aggregates identified, the samples are divided as previously grouped. The samples with the ceramic fragments (group-A), samples with a high amount of quartz and feldspar (Group-B), and the samples with shell and basaltic rock fragments (Group-C), rest of the samples are sub-samples as upper layers belong to the group-D.

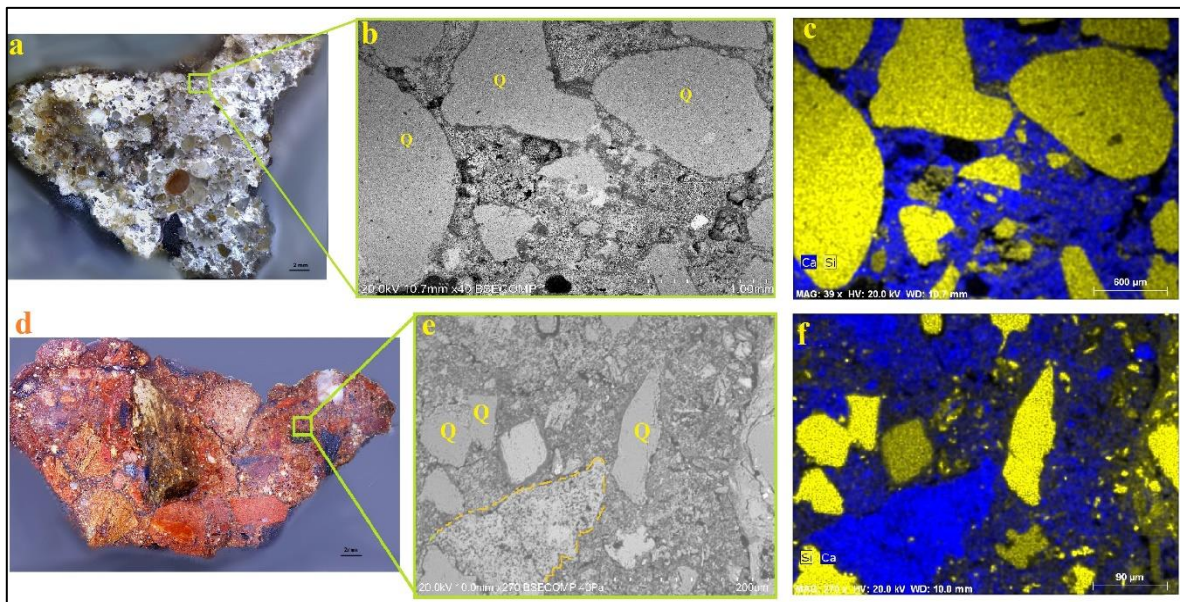


Figure 4. 13-Siliceous aggregates. a) sample-FRL-12 (group-B), b) sub-angular shape aggregates in BSE image of FRL-12, c) Blue=Ca, yellow=Si, the elemental map showing Si-rich quartz in Ca-rich binder, d) Sample-FRL-3 (group-A), e) BSE image indicating crushed lime and angular shape aggregates, f) elemental image showing Ca-rich angular lime fragment and Si-rich quartz as aggregates.

Overall, all the samples were found with sub-angular shaped quartz and feldspar (Fig-4.13.c). Though the ceramic rich samples have different sizes and shapes of ceramic fragments. The rest of the samples (group C) have additions of shell fragments, noticed by the presence of calcium and carbon. This group also contains rounded shape basaltic grains that are confirmed by the petrographic and stereo-zoom observation.

Angular shape Ca-rich fragments were detected in some samples, nevertheless, the absence of inclusion and very angular shape can be an indication of crushed solid lime fragments (Fig-4.13. f). In decorative mortar samples (FRL-19-U) similar kinds of fragments were also observed in the upper whitish layer, which can be an intentional use of crushed lime to make the layer more whitish, meanwhile, in ceramic rich samples, it can be an exception or possible presence of a lime nodule. Samples with shell fragments were identified due to their shape and elemental composition and the presence of Ca is the indication of calcium-rich organic materials (Fig-4.21) or shell (calcium carbonate) itself.

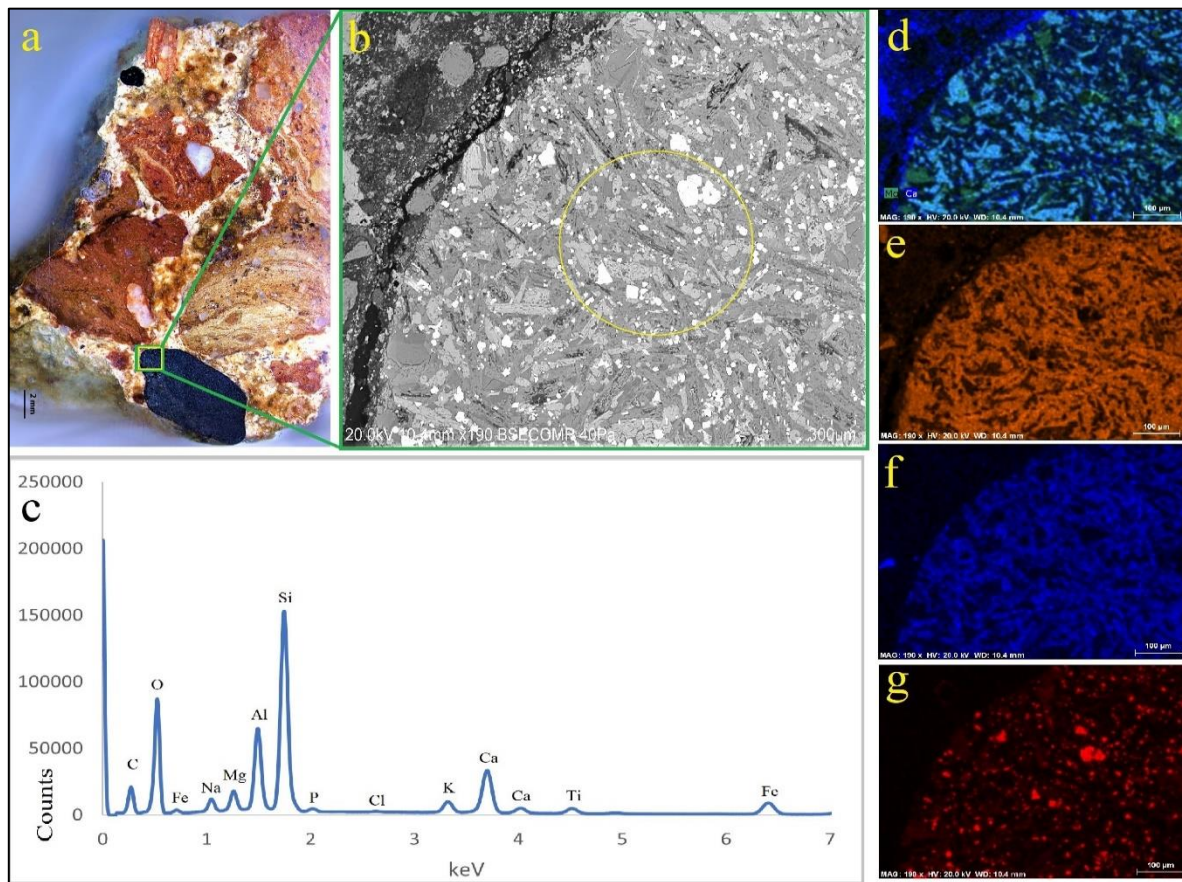


Figure 4. 14-Basaltic rock fragment, a) Sample-FRL-1 with rounded basaltic rock fragment, b) BSE image of basaltic rock fragments, c) multi-point analysis spectrum of the spot marked in 'b' image, d) elemental image of green=Mg, blue=Ca, e) orange=Al, f) blue=Na, g) red=Fe.

Regarding aggregates observed in all the samples, basaltic rock grains were found in the sample group (Group-C). The samples with basaltic rock fragments appear with minerals (Fig-4.15) that can be associated with olivine and pyroxene which was further confirmed with the help of other techniques such as XRD and petrographic analysis.

Basalt is a dark volcanic rock with mainly, pyroxene, plagioclase, and is high in iron and magnesium. They have fine-grained textures. They can also be porphyritic, containing olivine, augite, or plagioclase phenocrysts. The elemental analysis shows similar compositional elements and textural characteristics for the basaltic rock fragments.

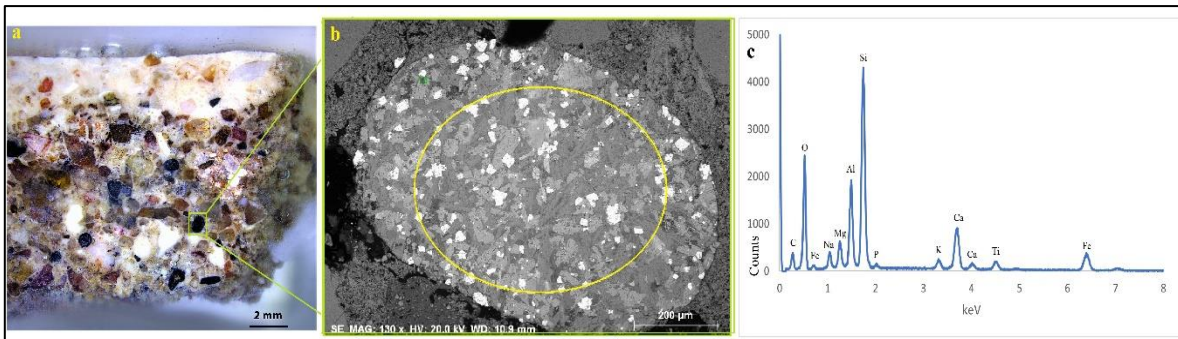


Figure 4. 15-basaltic grain as aggregates, a) Sample-FRL-19 (group-C), b) rounded basaltic grain in BSE image, c) multi-point analysis spectrum of the spot marked in image 'b'.

The presence of Mg and Fe with other elements associated with Si, Ca and Al, is indicative of mafic minerals and plagioclase, respectively. The rounded shape of this kind of aggregates is almost similar in the sample group containing basaltic fragments. Their morphological characteristics indicate their significant transportation from their source of origin.

Samples with stratigraphic layer show Ca-rich binder in upper and the lower layer is composed with quartz and feldspar aggregates also in a calcitic lime binder. For sample FRL-19-U, showed a few random-sized quartz and feldspar as aggregates and there is a predominance of limestone or crushed solid lime that gave the layer a whitish appearance whereas the lower layer is composed with quartz, shell, and basaltic rock fragments as aggregates (Fig. 4.16.g). The sample with tesserae from the mosaic floor, FRL-8 (Fig. 4.17), revealed Ca-rich square stone blocks (black and white) in the upper layer which is associated with fine texture indicating limestone blocks while ceramic blocks may have been used for the red color tesserae.

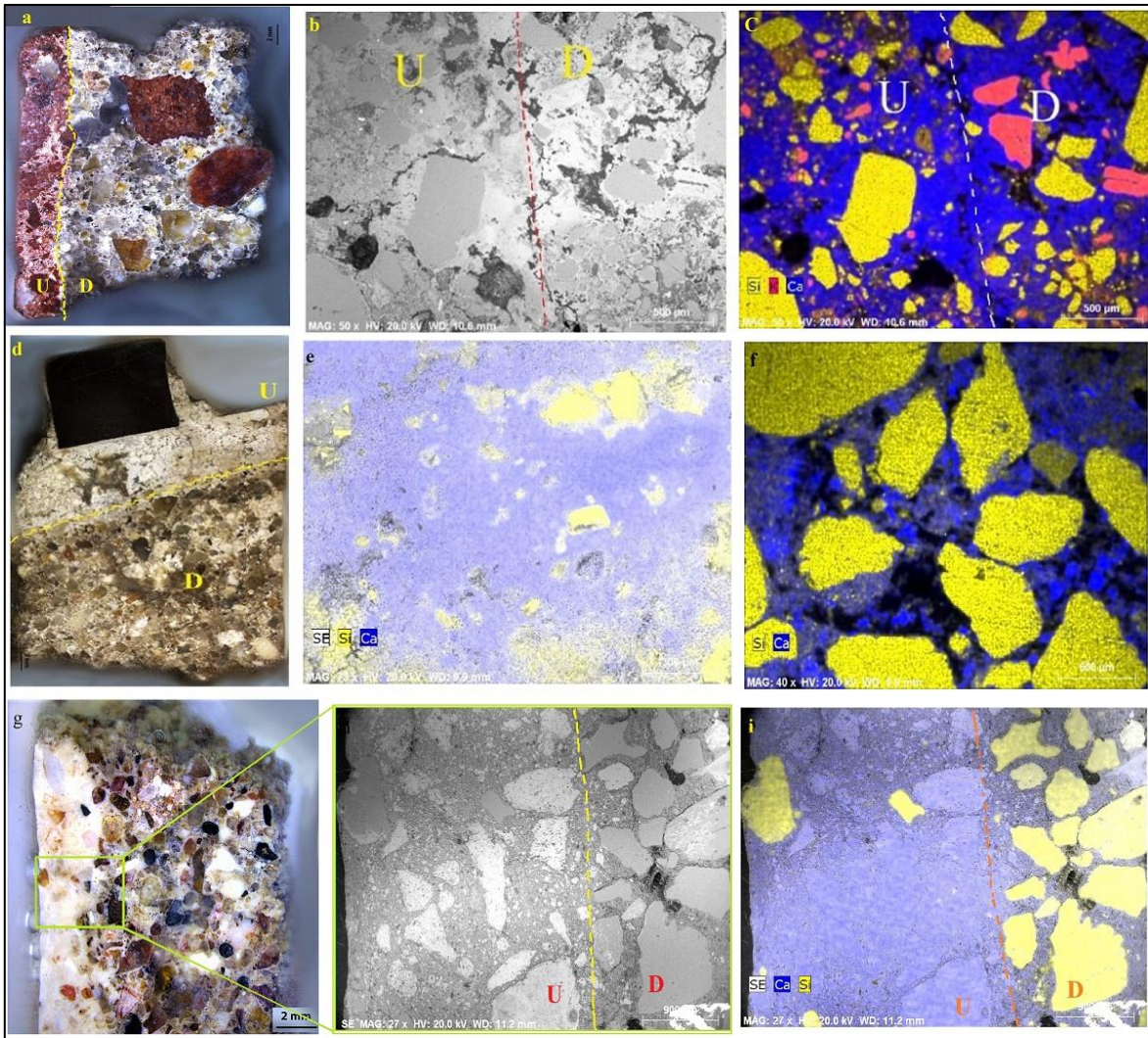


Figure 4. 16-stratified layers, a) FRL-6-U&D, b) BSE image showing Upper and lower layer, c) elemental mapping indicating blue=Ca, yellow=Si, binder, and aggregates in both layers, d) FRL-8-U&D,(mosaic floor), e) binder (blue=Ca) rich upper layer-FRL-8, f) blue-Ca, yellow=Si, angular- subangular quartz in the lime binder (lower layer-FRL-8), g) decorative sample FRL-19-U &D, h) BSE image, i) elemental image showing upper and lower layer and aggregates distribution.

The elemental images showed that the upper layer had a Ca-rich lime binder in presence of siliceous aggregates which implies that the tesserae blocks were bedded (in bedding layer) in the lime-rich matrix (4.16). While the lower layer (nucleus) showed Si-rich angular and sub-angular particles and in association with K and Al which is indicative for feldspar as aggregates in this layer (4.16.f). The sample FRL-6 (Fig. 4.16.a) has a similar result with quartz and feldspar as aggregates in both layers meanwhile presence of ceramic fragments in the upper reddish layer (Fig. 4.16.c) was confirmed by means of other techniques. Elemental analysis revealed the presence of K, Al, and Fe which could be related to ceramics while Si with K and Al indicates quartz and feldspar respectively.

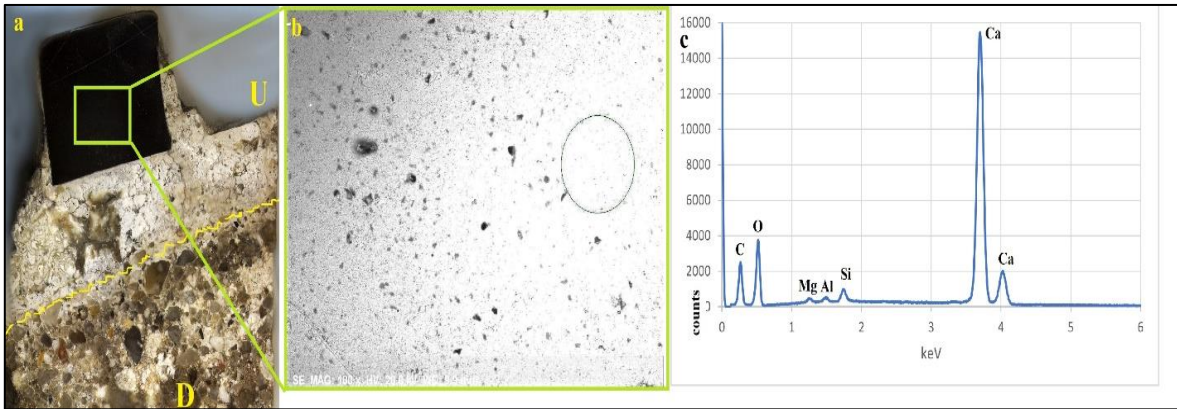


Figure 4. 17- FRL-8 U & D layer, Tesserae composition, a) FRL-8, Mosaic floor, tesserae, b) multi-point analysis on tesserae, c) spectrum of the spot marked on image 'b', the composition of tesserae, Ca, Si, Mg, and Al.

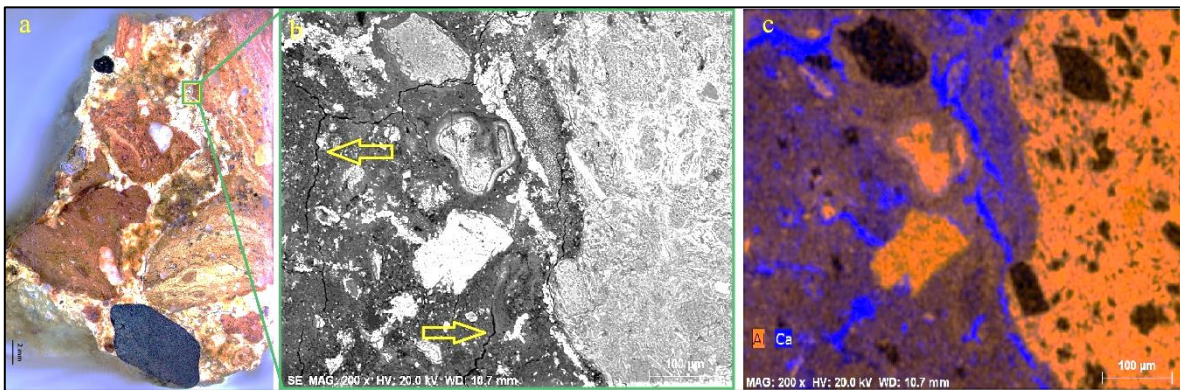


Figure 4. 18-Ceramic rich sample with cracks. a) sample-FRL-1 (group-A), b) arrows indicating cracks in the binder alongside the ceramic fragments in BSE image, c) elemental image- blue=Ca, orange=Al.

The samples with ceramics show evidence of cracks (Fig-4.18. b) in the binder. Cracks developed alongside the ceramic fragments and sometimes within the binder matrix. Though, in some cases, these cracks are seen concentrated in carbon (Fig-4.19.c) which can be the resin from polished section preparation as there is no significant zoning, boundary marks, or pozzolanic reaction observed.

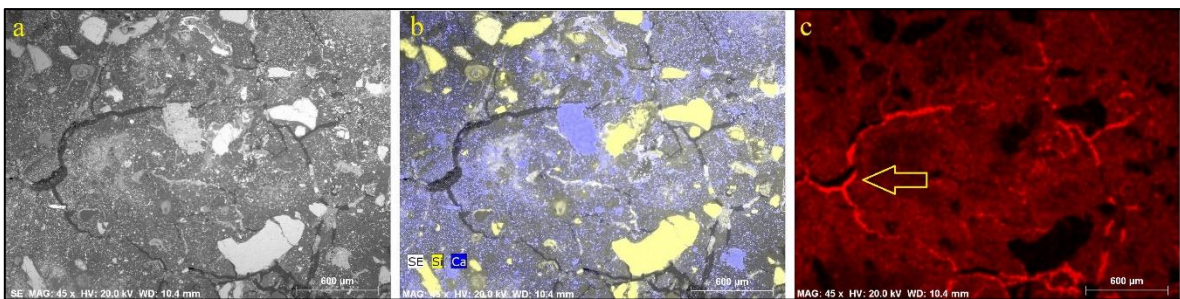


Figure 4. 19-Cracks in the binder. a) BSE image of sample FRL-8-U, b) blue-Ca, yellow-Si showing cracks in the binder and Si rich quartz as aggregates, c) Arrow indicating cracks in the elemental image, red=C.

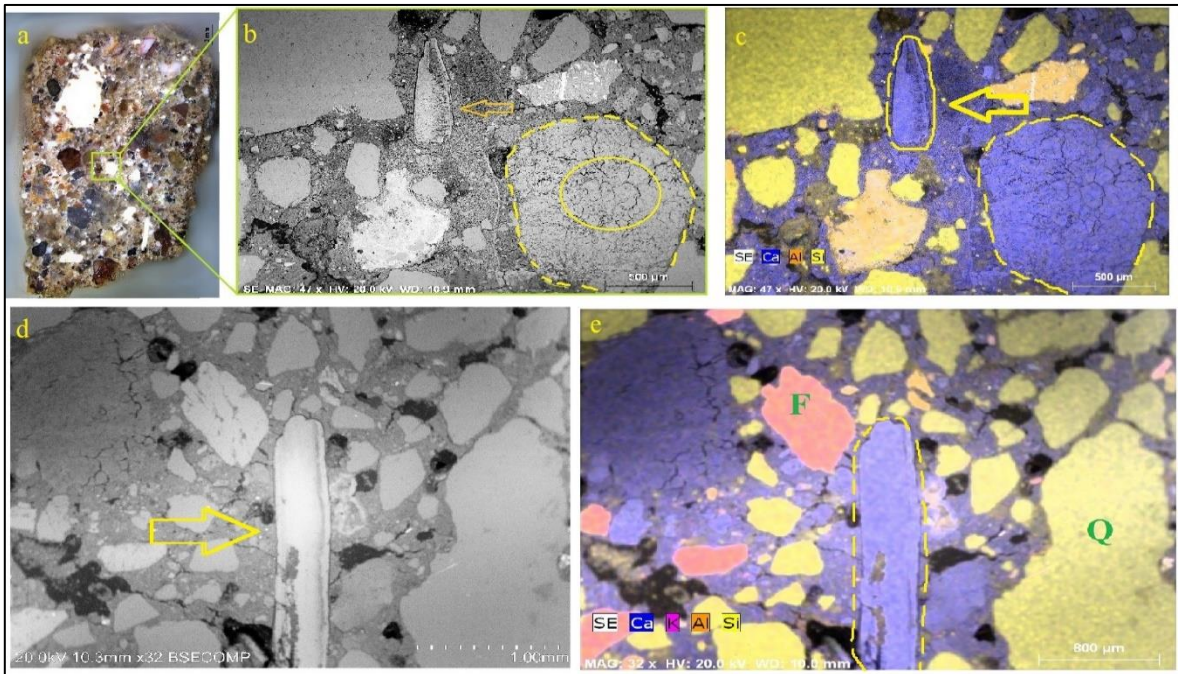


Figure 4. 20-Lime lumps, and shell fragments, a) sample-FRL-15 (group-C), b) BSE image showing rounded lime lumps and shell fragment, e) blue=Ca, yellow=Si, orange=Al, the arrow indicating Ca-rich shell fragment a rounded lime lump, d) linear shape shell fragment, e) Ca, Al, Si, and pink=K, the elemental image showing Ca-rich shell fragments, sub-angular and poorly rounded quartz, and feldspar.

Lime lumps were also present, especially in samples with shell and basaltic rock fragments (Fig-4.20.c). Lime lump must have been generated as a result of lack of water in the lime slaking process when the mortar was being prepared. In which case, the lime lump can give access to the pure lime composition. It can also provide information about the production technology, raw materials, and sometimes even provenance. Multipoint and point analysis were performed to identify the lime lump composition of the samples; the result demonstrates that the lime lump is mainly composed of Ca, C and O (Fig-4.21).

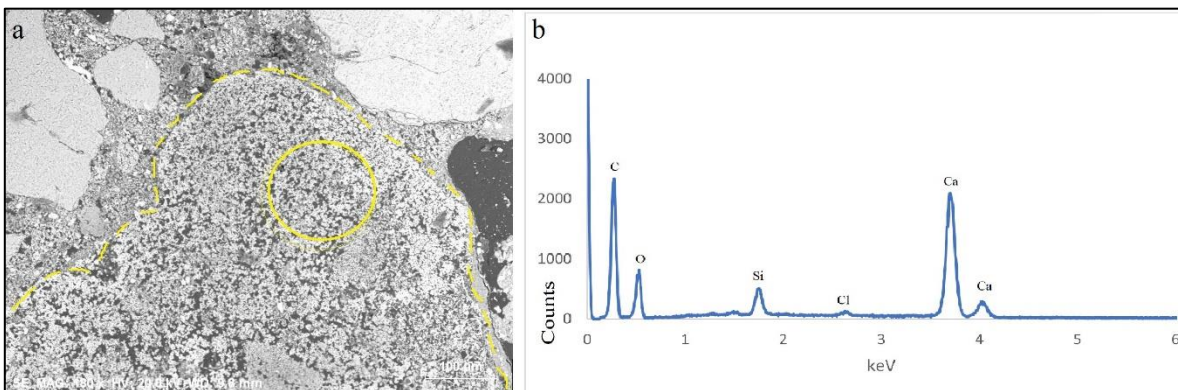


Figure 4. 21-Lime lump, FRL-17 (group-C) a) yellow line indicating lime lump, b) multi-point analysis spectrum of the spot marked in image 'a'.

All the samples show a similar composition to the binder (Fig-4.22). The point and multipoint analysis revealed that the binder was mainly composed of Ca which is indicative of lime binder. A high amount of Ca in the binder composition with a very low percentage of Mg was noted. The presence of other elements such as K, Al, and Si, and Na may be influence from aggregates, or even it could be corresponding to a reduced detrital component of the limestone.

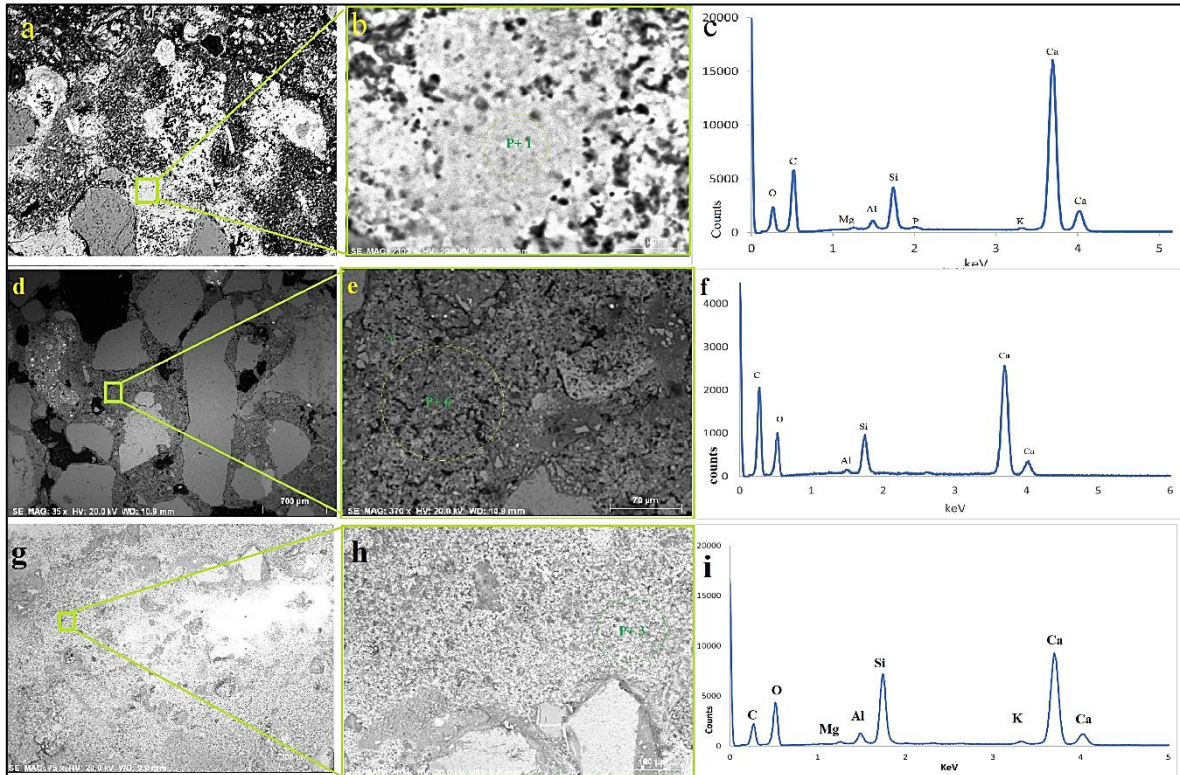


Figure 4. 22 -Binder composition, a) mapping in FRL-1 (group-1), b) point analysis in binder c) spectrum shows binder composition of spot marked in image 'b', d) mapping on FRL-19-D (group-C), e) multi-point analysis in the binder, f) spectrum shows binder composition of spot marked in image 'e', g) areal map on FRL-8-U (group-B), h) point analysis on the binder, i) spectrum shows binder composition with the presence of Ca with Mg, Al, Si, and K.

Samples with chromatic layer were observed to identify any preparatory layer between the paint and mortar surface as well as the pigment composition. Sample FRL-17 and FRL-18 had dark brown and brown color pigmentation. Sample FRL-17 and FRL-18 did not show any identical preparatory layer beneath the chromatic layer though it contained Ca-rich aggregates and binder. The area analysis of the chromatic layer (Fig-4.23) has the presence of Fe with other elements such as Si, Al, Ca, O, C, P, S, K, and Cl. The presence of Fe in the pigmentation indicates that the composition might be made up of red iron oxide pigments, most likely red ochre, combined with lime. Sample FRL-18 showed a similar composition of the chromatic layer with the presence of Fe with Si, Ca, Al, Mg, O, C and Cl. The presence of iron can be an indication of iron hydroxides (combined with lime) which would explain the brown color.

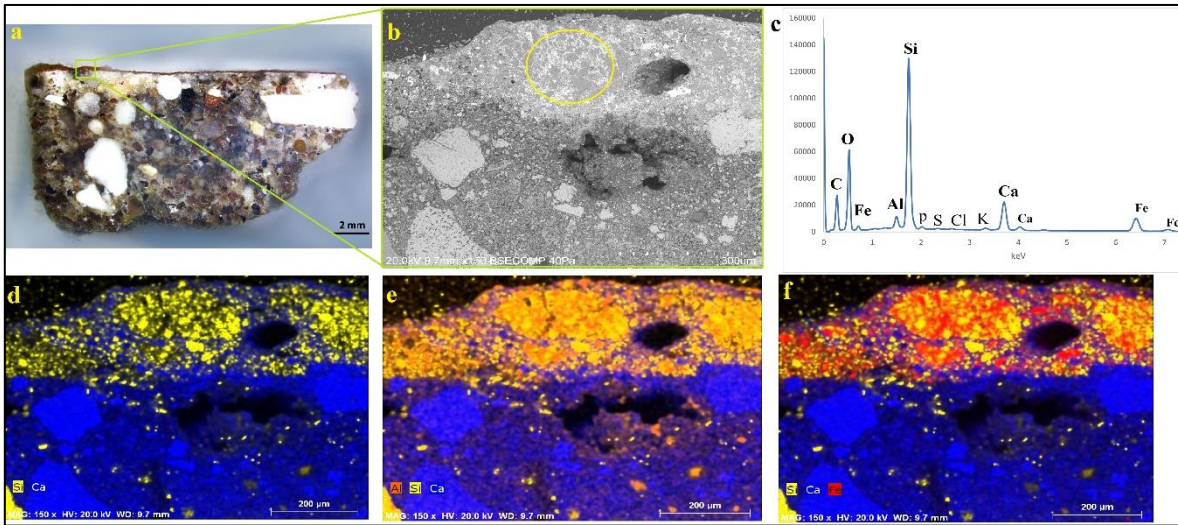


Figure 4. 23-Sample with chromatic layer, a) sample- FRL-17, with chromatic layer, b) BSE image on a pigmented layer, c) multi-point analysis spectrum of spot marked in image 'b', d) elemental mapping, yellow=Si, blue=Ca, e) elemental image of pigmented layer, orange= Al, f) map showing elements yellow=Si, blue=Ca, red=Fe.

4.7 Acid attack and Granulometric analysis

Acid attack analysis was performed for the determination of the soluble fraction and insoluble residue. The soluble fraction can contain the binder, soluble salts, organic materials, and carbonated aggregates, whereas the insoluble residue contains the siliceous aggregates (Silva *et al.*, 2006, Cardoso *et al.* 2014). The obtained results of the soluble fraction can be used to understand the calcium carbonate proportion and can be compared with the calcite decomposition ratio from the TGA-DTG result. While the insoluble residue can be used to determine the grain size distribution (weight %) which represents the siliceous aggregates within the samples.

For the determination of the soluble fraction and insoluble residue, samples were in 10 g of duplicate sets. Wherein an aqueous solution of hydrochloric acid (1:3) was used to carry out the analysis. In the case of certain samples (FRL-4, FRL-11-ii, and FRL-19-U), the analysis was carried out only once and was unperformed for sample FRL-17 as there were no sufficient materials. The analytical data of duplicated samples in mean values is described in appendix-8.6 and the calculated average of the soluble and insoluble fraction ratio is shown in Figure-4.24. The percentages of the soluble fractions of the samples range from 18.35% (FRL-1) to 76.60% (FRL-19-U) whereas the insoluble residues vary between 23.30% (FRL-19-U) to 81.35% (FRL-1).

During the acid attack analysis, samples were analyzed (qualitative) based on their reaction with an aqueous solution of hydrochloric acid before the heating process. Samples that showed long reactions are FRL-2, FRL-6-U, FRL-8-U, FRL-7-ii, and FRL-19-U show similarities related to whitish binder with higher proportions of carbonates. On the other hand, samples that showed short reactions are FRL-15, FRL-18, and FRL-19-D which indicate similar characteristics based on their shell fragments and limestone inclusion in the mortar which is confirmed during thin-section and polished section observation. Similar small and quick reactions were observed in other samples as well.

Samples with white stratigraphic layers (FRL-8, and FRL-19) indicate a higher percentage of soluble fraction in the upper layers meanwhile insoluble residues are comparatively low. On the other hand, lower layers of the mentioned samples have a high percentage of insoluble residues and a low percentage of soluble fractions. Whereas the sample FRL-6 and FRL-10 with pinkish and yellowish layers respectively have a higher percentage of insoluble residues and a lower percentage of soluble fraction.

In general, the samples with shell fragments, observed in the petrographic and stereo-zoom analysis showed the percentage of soluble fraction mainly below 35% which could be related not only to the calcitic binder but also due to the dissolution of other calcium carbonate sources inside the samples (e.g., shell fragments, limestone, Ca-rich organic residue). The ceramic-rich samples have the soluble fraction range lower (in average below 25%) than the insoluble residue (in average above 70%) which could be the result of big ceramic fragments as aggregate proportions which were observed in polished section and thin sections.

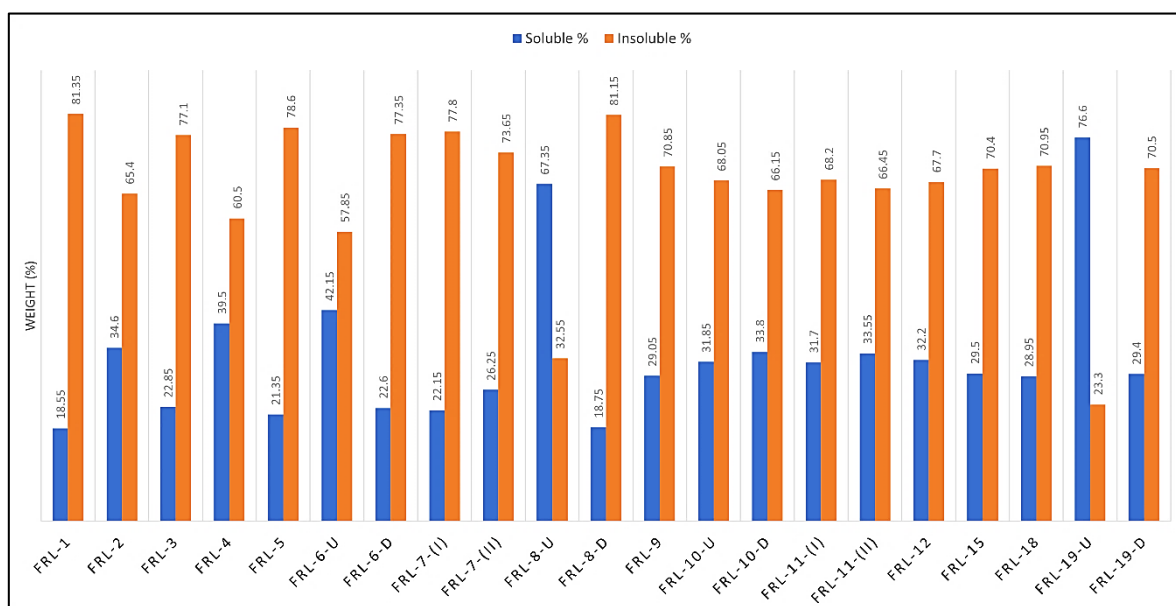


Figure 4. 24- Calculated weight (%) of soluble and insoluble residue obtained by Acid attack analysis. Sample-FRL-17 is not in the chart, due to insufficient materials, there were no acid attack analysis for this sample.

After the acid attack analysis, the main objective of the insoluble residue was to be employed in conducting the granulometric analysis. The insoluble residue was dried overnight at 60°C in an oven to remove all the moisture following which it is then sieved in mesh sizes ranging from >4 mm to <0.063 mm to classify the aggregates into fine gravel (> 4 mm) to silt and clays (< 1/16 mm) textural groups according to Wentworth (1922).

The insoluble residue of samples FRL-8-D, FRL-12, FRL-18, FRL-19-D did not show the fraction greater than 4 mm in their single test, but they appeared in the second duplicate test. This may occur either due to the absence of representativeness of the samples or because the big fraction can be fragments of carbonates that dissolved in the dissolution of acid. Though for more effective data both tests' results were calculated and plotted as average and shown in Fig-4.25.

The sample with ceramic fragments has a predominance of fraction greater than 4 mm among all the samples, categorized as fine gravel group by Wentworth (1922) whilst the second most abundant fraction corresponds to the very coarse sand (1-0.5mm), and the third most abundant fraction is coarse sand (2-1mm) among the samples. The less abundant fractions are very fine gravel (4-2mm), medium sand (0.5-0.25mm) and fine sand (0.25-0.120mm). In general, all the samples have the lowest number of silts and clay (<0.063mm) and some samples have no fractions greater than very fine gravel (4-2mm).

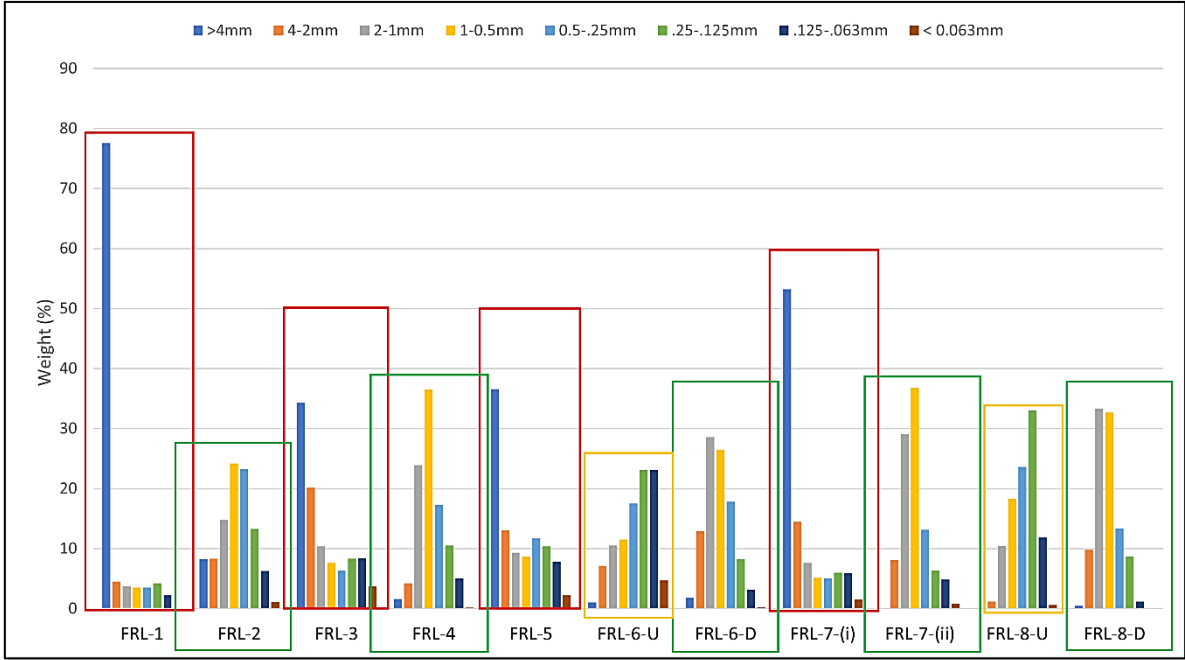


Figure 4. 25.a-Grain size distribution from average mean values in weight percentage. Ceramic rich sample (Group-A) marked in red, quartz rich samples (Group-B) marked in green. Group-C marked as purple, and group-D marked as orange box.

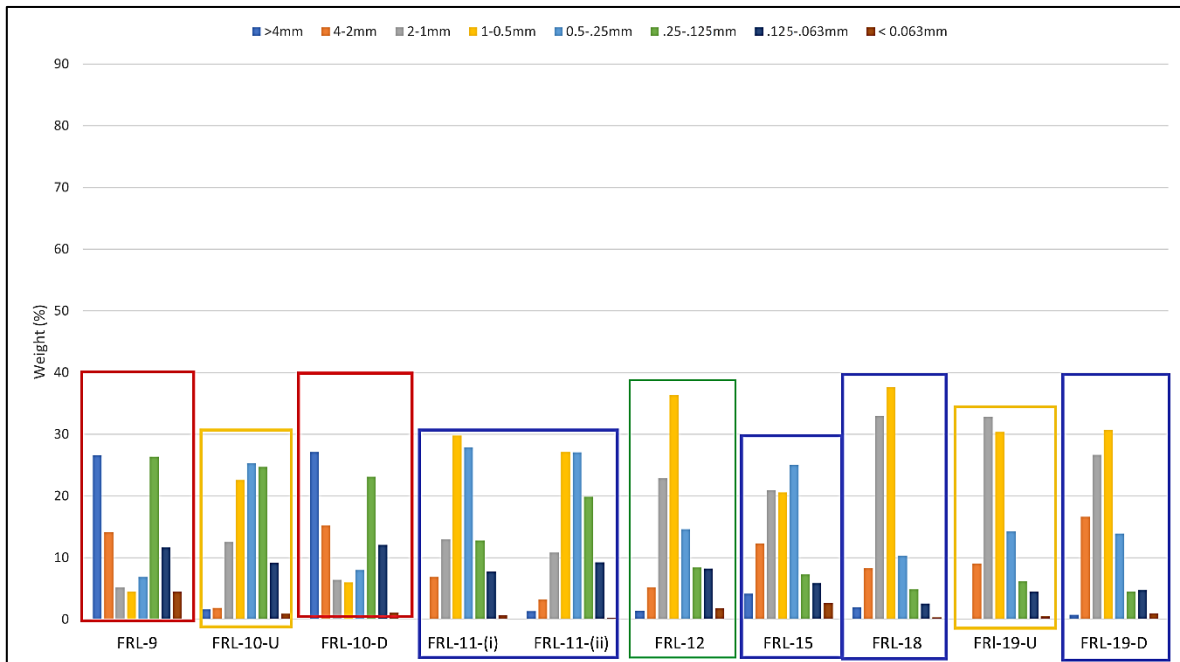


Figure 4. 25.b- Grain size distribution from average mean values in weight percentage. Ceramic rich sample (Group-A) marked in red, quartz rich samples (Group-B) marked in green. Group-C marked as purple, and group-D marked as orange box.

As previously grouped, samples were marked with color box in grain size distribution graph (Fig-25), where it can be observed that the group-A (ceramic rich samples) are showing in general predominance of grain size in 4-2mm to greater than 4mm. Sample FRL-9 (filler) and FRL-10 (stair) have similar grain size distribution as 0.25-0.125mm to >4mm. Sample FRL-3 and FRL-5 also showing similarity containing grain sizes 4-2mm to >4mm. Group-B, samples with abundance in siliceous aggregates are showing major grain sizes in 1-0.5mm to 2-1mm which almost similar with the samples with shell and basaltic rock fragments as named group-C. And the upper layers of stratified samples as group D, showing predominance of grain sizes in 0.125-0.063mm to 0.25-0.125mm.

The mean values of the insoluble residues were also analyzed, using the GRADISTAT statistics software (version-9.1) developed by Dr. Simon J. Blott (2010) to determine sieving error resulting from the sieving process mode, which shows the predominant fractions, sorting, and physical description of the specific textural group (Tab-4.11). The particle size and textural groups in the software is used according to Udden J.A. (1914) and Wentworth, C.K. (1922) who generated a triangular 'Gravel: Mud: Sand' diagram that identified the samples within the respective textural group.

The results from the GRADISTAT software (Tab-4.11) showed four different textural groups among the samples that are gravel (FRL-1), gravelly sand (FRL-2, FRL-4, FRL-6-U, FRL-6-D, FRL-7-ii, FRL-8-D, FRL-11-i, FRL-11-ii, FRL-12, FRL-15, FRL-18, and FRL-19-D) sandy gravel (FRL-3, FRL-5, FRL-7-i, FRL-9, and FRL-10-D) and slightly gravelly sand (FRL-8-U & FRL-10-U). Depending on the predominance of the fraction among all the samples it can be opined that there are two modes wherein ceramic rich samples are in bimodal mode while all other samples are in unimodal mode.

Table 4. 11- Description of the insoluble residue analyzed by GRADISTAT software.

Sample*	Mode	Major fraction		Sorting	Textural Group
FRL-1	Bimodal	>4mm	(77.6%)	Very Well Sorted	Gravel
FRL-2	Unimodal	1-0.5mm	(24.2%)	Poorly Sorted	Gravelly Sand
FRL-3	Bimodal	4mm	(34.3%)	Poorly Sorted	Sandy Gravel
FRL-4	Unimodal	1-0.5mm	(36.5%)	Poorly Sorted	Gravelly Sand
FRL-5	Bimodal	4mm	(36.6%)	Poorly Sorted	Sandy Gravel
FRL-6-U	Unimodal	0.125-0.063 mm	(23.2%)	Poorly Sorted	Gravelly Sand
FRL-6-D	Unimodal	2-1mm	(28.5%)	Poorly Sorted	Gravelly Sand
FRL-7-i	Bimodal	4mm	(53.2%)	Poorly Sorted	Sandy Gravel
FRL-7-ii	Unimodal	1-0.5mm	(36.8%)	Poorly Sorted	Gravelly Sand
FRL-8-U	Unimodal	.25-.125mm	(33.0%)	Poorly Sorted	Slightly Gravelly Sand
FRL-8-D	Unimodal	2-1mm	(33.3%)	Poorly Sorted	Gravelly Sand
FRL-9	Bimodal	4mm	(26.6%)	Poorly Sorted	Sandy Gravel
FRL-10-U	Unimodal	0.5-0.25mm	(25.3%)	Poorly Sorted	Slightly Gravelly Sand
FRL-10-D	Bimodal	4mm	(27.1%)	Poorly Sorted	Sandy Gravel
FRL-11-i	Unimodal	1-0.5mm	(29.8%)	Poorly Sorted	Gravelly Sand
FRL-11-ii	Unimodal	1-0.5mm	(27.1%)	Poorly Sorted	Gravelly Sand
FRL-12	Unimodal	1-0.5mm	(36.3%)	Poorly Sorted	Gravelly Sand
FRL-15	Bimodal	0.5-.25mm	(25.0%)	Poorly Sorted	Gravelly Sand
FRL-18	Unimodal	1-0.5mm	(37.6%)	Poorly Sorted	Gravelly Sand
FRL-19-U	Unimodal	2-1 mm	(32.9%)	Poorly Sorted	Gravelly Sand
FRL-19-D	Bimodal	1-0.5mm	(30.7%)	Poorly Sorted	Gravelly Sand

*The colors indicate the groups- group-A(red), group-B(green), group-C (purple), group-D (upper layers in orange)

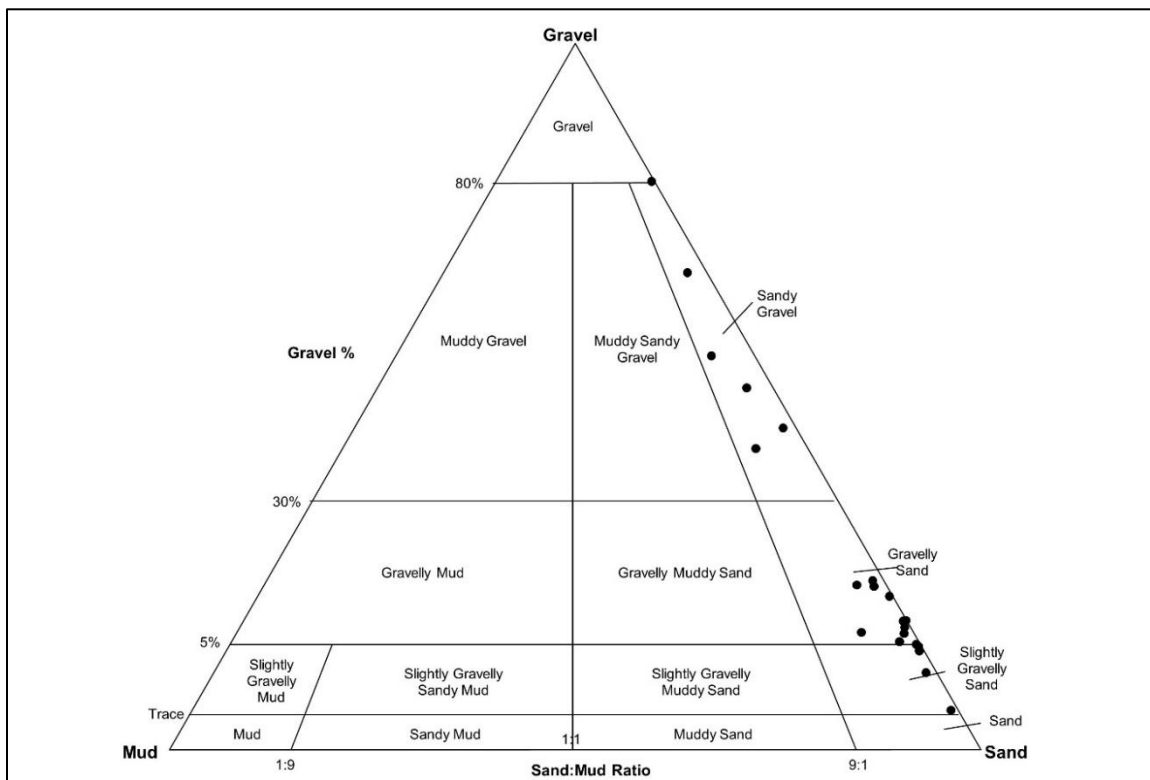


Figure 4. 26 - Gravel: Mud: Sand diagram obtained from the GRADISTAT software.

Almost all the samples were poorly sorted while FRL-1, is very well sorted. In the triangular diagram of Gravel: Mud: Sand (Fig. 4.26). The samples without ceramics were plotted in the gravelly sand zone whereas, sandy gravel zone showing samples with ceramic fragments except for FRL-1 which was almost in the gravel region. And sample FRL-8-U and FRL-10-U appeared in the slightly gravelly sand zone.

After the acid attack analysis, the remaining insoluble fractions were observed and determined under the stereo zoom microscopy to identify their morphological and mineralogical characteristics. In general observation, three different types of residues were found in accordance with their statistics and visual investigation, the first group (Fig-4.27) was the one with ceramic rich samples from the water channel or *opus signinum* structure. In this group, ceramic fragments were prevalent and most of the sizes were greater than 4 mm, and mainly angular to sub-angular shaped which is indicative of the fact it was crushed or intentionally prepared for aggerates. Meanwhile white quartz and more finer ceramics fragments were also present. For sample FRL-1 and FRL-5, yellowish and reddish sandstone can be seen whilst some sample contains black colored (4-2 mm) basaltic rock fragments that is almost in rounded shape.



Figure 4. 27-Ceramic rich samples representative to group A

The second group is mainly with quartz rich whitish samples (Fig. 4.28), that contains transparent quartz (hyaline), smoked quartz (grey), as dominant mineral. And the third group (Fig. 4.29) was the one with the brownish color, dominated by transparent quartz (hyaline), white quartz (milky) and very few amount of citrus quartz (reddish) followed by other rock fragments like basaltic, and granitoid rocks. The size and shape of the quartz, feldspar, and very small amount of quartzite, and possibly sandstones found in samples are mainly appear in the range of 1-0.5 mm and 2-1 mm, while the shapes were angular to sub-angular. The angular and sub-angular morphology of these particles may be indicative of their short distance transportation through the river flow from the original outcrops.









<p style="text-align: center;">FRL-12</p>		
	>4mm	4-2mm
		
2-1mm	1-0.5 mm	0.5-.25mm
		
0.25-.125mm	0.125-0.063 mm	<0.063mm

Figure 4. 28- Representative grain distribution images of quartz rich samples, group-B









<p style="text-align: center;">FRL-19-D</p>		
	<p>>4mm</p>	<p>4-2mm</p>
		
<p>2-1mm</p>	<p>1-0.5 mm</p>	<p>0.5-.25mm</p>
		
<p>0.25-.125mm</p>	<p>0.125-0.063 mm</p>	<p><0.063mm</p>

Figure 4. 29- Representative grain distribution image of group-C, sample with shell and basaltic rock fragments

5 DISCUSSION

.....

The mortars from the Roman villa of Frielas were analyzed by employing a multi-analytical approach to determine and characterize the separate components, namely binder, aggregates, and additives. The results obtained regarding the assessment were compared and confirmed by complementary techniques. The samples chosen from the different construction phases, functionality, and structures were compared to find out similarities and differentiation. To make a correlation with the chronological sequence of the site, the results were discussed as evidence of manufacturing techniques, production technologies, and possible raw materials provenance. The information was analyzed to understand if historic recipes from ancient Roman treatises as described by Vitruvius, were followed in the manufacturing process, or if traditional formulae were adjusted and adapted to meet a specific demand or due to resource constraints.

Considering the characteristics, aggregates type and composition samples were divided into three main groups as ceramic-rich reddish mortar (group-A), quartz-rich whitish mortar (group-B), and shell and basaltic brown mortar (group-C) to be able to discuss their variation and composition concerning their functions and periods. All the samples from different groups were from the 2nd construction phase of the villa (3rd century AD to 5th century AD) according to the archaeological context. Nevertheless, the samples were divided into groups according to their characteristics, and to make the discussion easier the upper layer of the stratigraphic layers were separated into a different group (group D) whilst most of the samples are rendered mortar. Though according to the functionality sample FRL-1, FRL-3, FRL-5 from group-A belongs to the water channel structure, and in group-B, FRL-2 and FRL-4 also belong to the water channel structure or hydraulic structure.

Table 5. 1-Division or groups of samples for the result discussion.

	Groups	Render	Floor	Filler
Ceramic rich reddish mortar	A	FRL-1 FRL-3 FRL-5 FRL-10D		FRL-7-i FRL-9
Quartz rich whitish mortar	B	FRL-2 FRL-6D	FRL-8 D	FRL-7-ii FRL-4 FRL-12
Shell & basaltic brown mortar	C	FRL-11-i FRL-11-ii FRL-15 FRL-17 FRL-18 FRL-19D		
Binder rich upper layers	D	FRL-6U FRL-10U FRL-19U	FRL-8U	

5.1 Raw materials

In the case of raw materials, mortar samples can be discussed with two main constituents namely, binder and aggregates, all together provide effective information to reveal the raw materials of the mortar samples from the Roman villa of Frielas.

5.1.1 Binder

Based on the results obtained from OM, XRD, TGA, and SEM-EDS, mortar samples from the Roman villa of Frielas were in general, made with a calcitic lime binder. The significant amount of calcite detected by XRD (GF as well as FF) associated with the TGA thermogram, showing greater mass losses in the characteristic range between temperature 600-900°C as well as the presence of Ca on elemental maps of EDS points to a binder with calcitic composition. Moreover, the acid attack analysis allows the determination of the soluble fraction. Though, the partially dissolved carbonate aggregates (e.g., shell fragments) might have been overestimated the amount of calcium carbonate present in the samples. The amount of calcium carbonates from acid attack (soluble fraction), XRD, and TGA can be compared to see the differences.

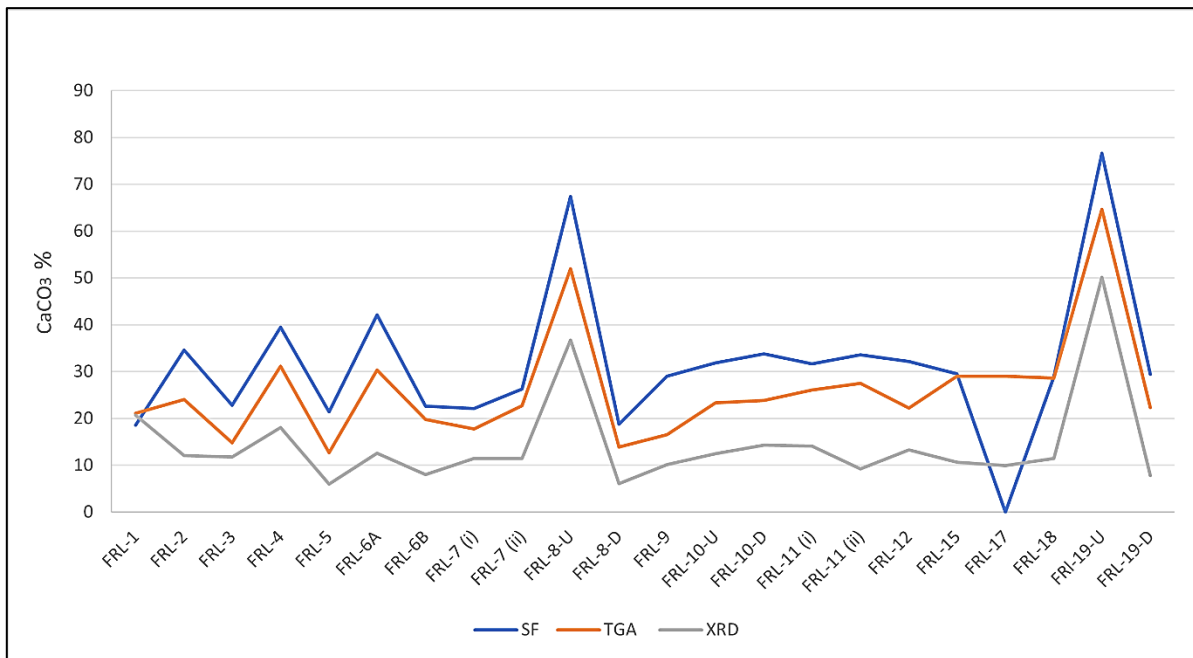


Figure 5. 1- Amount of CaCO_3 (weight %) of the studied samples. Comparison of TGA, acid attack (Soluble fraction), and XRD. XRD is giving fragile quantitative analysis from GF (Global fraction). Sample- FRL-17, could not perform the acid attack analysis due to insufficient materials therefore soluble fraction (SF) curve (blue) showed 0 percentage.

To determine major differences between the different types of binder two facts can be considered, (1) the temperature of the firing process that controls the quality and reactivity of the starting binder. (2) the nature of the starting material that determines the chemical reaction pathway. The temperature needed to produce CaO (eq.1), should be ~850°C, though due to the grain sizes temperature can vary, and the decomposition reaction of the carbonate can also proceed at slightly lower temperatures (780-800°C) in reducing conditions (Rodriguez-Navarro *et al.*, 2009).

Most of the samples from Frielas show in thermograms (Tab. 4.10), the decomposition of calcium carbonate in the range of 600-800°C in the TG curve. While the First Derivative Thermogravimetric curve (DTG) with respect to temperature, allows plotting the most representative changes within the sample during the heating process, in which the peaks will indicate the maximum mass losses due to the characteristic physical or chemical decomposition of the distinct materials in function of temperature (Middendorf *et al.*, 2005a; Stuart, 2007; Földvári, 2011). In the case of studied samples, a peak of decomposition by DTG within 750-800°C were observed (appendix-8.7). And the samples with a whitish upper layer show a slightly higher temperature peak at 800-820°C (DTG), which confirms the presence of calcitic aggregates.

A fundamental difference concerning the nature of the reaction processes of lime binders is whether they involve simple absorption of CO₂ from the atmospheric air to produce carbonates (aerial carbonation), or whether they also involve more complex processes of dissolution of alumino-silicate phases and precipitation of hydrated calcium-aluminum-silicate phases ('pozzolanic' reactions). The former is known as aerial binders because they set in contact with the atmosphere. The latter are called hydraulic binders because they may harden even underwater (Artioli *et al.*, 2019).

In the binder, there is some presence of impurities detected during the elemental mapping employing SEM-EDS analysis. The presence of Mg, Si, and Al was detected with the predominance of Ca in the binder (Fig. 5.2). The presence of Si, Mg, and in the case of ceramic rich samples Fe, is mainly due to the influence of various silicates and ceramic fragments.

The lime lumps present in a few samples provide information about raw materials used for calcination during the binder preparation. Lime lumps can occur due to several causes in the binder, inhomogeneously slaked lime putty forming portlandite (Ca (OH)₂) lumps that underwent late calcination process or reprecipitated late calcite, also lime lumps can be present due to their preexistence in the mixture as slaked lime during the production, and they were not properly mixed with the inert due to lack of water (Bakolas *et al.*, 1995; Artioli *et al.*, 2019). The analysis on the lime lumps of the samples indicates the presence of Ca, O, and C, which represents calcium carbonate (CaCO₃) thereby indicating a calcitic areal binder.

The color of the binder is in general white, but samples with ceramic fragments have reddish hue effects due to fine crushed ceramic fragments (*cocciopesto*) and the quartz-rich samples (group-B) have whitish binder (e.g., sample FRL-4, and FRL-12). The samples from the third group (group C) containing shell and basaltic grains have a brownish binder.

In studied samples, there is no significant pozzolanic reaction, no zoning sign or formation of new mineralogy were detected in the binder composition. This can be due to the presence of low burn ceramic aggregates. The best ceramic-material yielding pozzolanic reaction is the very fine-grained kaolinite-rich pottery in which meta kaolinite-type phases were formed by firing in the temperature range 600–900°C (Bellotto *et al.*, 1995). The use of clay minerals in the production of the ceramics as well as firing at higher temperatures induce the formation of less reactive phases, such as mullite (Gualtieri *et al.*, 1995, Gualtieri and Bellotto, 1998), and thus reduced pozzolanic reactivity (Artioli *et al.*, 2019).

The outer layers of stratified samples contain a high amount of calcitic areal binder. Sample FRL-8-U is a bedding layer of tesserae, where the binder to aggregate ratio is 1:1 and the amount of calcium carbonate is 51.9 %. FRL-19-U, have the amount of calcium carbonates of 64.6 % (Tab-4.10). Both samples showed the decomposition of calcium carbonates in the range of 820°C temperature at the DTG peak, which can be due to the decomposition of carbonates such as limestones. Moreover, detection of calcite in XRD analysis (GF powder) and petrographic observation suggests that the outer layer of this sample was with the crystalline carbonates. And sample FRL-19-U has crushed limestone intentionally added for decorative purposes to make the layer more whitish while the pinkish upper layer of sample FRL-6-U is due to the admixture of fine ceramic particles in the binder.

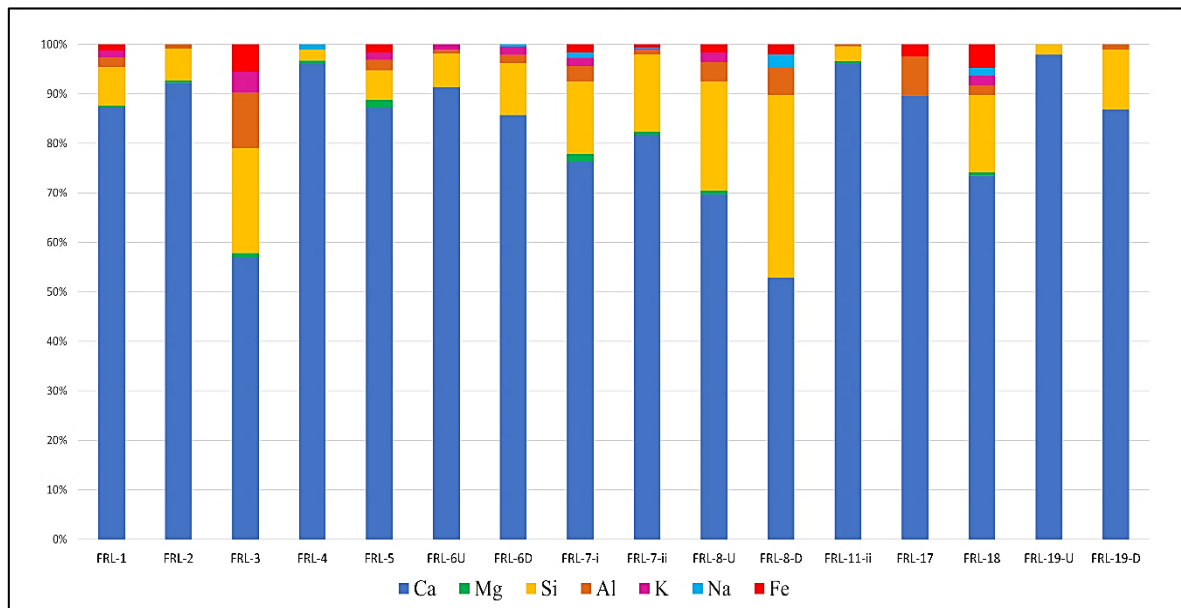


Figure 5. 2- Representative % of elements present in binder results from EDS analysis; Ca (blue), Mg (green), Si (yellow), K (pink), Na (light blue), and Fe (red). Samples that are not presented in the chart, due to lack of information and unavailability of the instrument.

5.1.2 Aggregates

The aggregates show some differences in their composition between the different types of mortars which allowed their grouping. Group-A has ceramic fragments. Group-B contains only siliceous aggregates whereas group- C, contains siliceous aggregates associated with shell and basaltic rock fragments.

In group A, the samples containing crushed ceramic fragments correspond to the water channel structure as their functions are associated with a waterproofing mortar and *opus signinum* (Silva, 2000; Siddall, 2011). The size of the big, crushed ceramic in sample FRL-1 (water channel bottom surface) was similar to other *opus signinum* samples (FRL-9, and FRL-7-i). During sample collection, the intention was to compare both sides of the water channel wall. The inner faces of the two walls are coated with *opus signinum*, functioning as a waterproofing element (FRL-3 and FRL-5) that contains ceramic fragments (> 4mm). While a layer (FRL-2) adjacent to the FRL-3 has a rough or uneven texture, seems prepared for receiving a final layer, perhaps stucco (Silva, 2000). The results indicate the samples FRL-3 and FRL-5, show similar characteristics, while sample FRL-2 (group-B) shows different features. Sample FRL-2, have a predominance of siliceous minerals aggregates, associated with very few and smaller random crushed ceramic fragments. That indicates a different preparation of mortars that can be a later renovation which is left unfinished. On the other hand, as *opus signinum*, FRL-9 contains big, crushed ceramics (2-3 cm) like FRL-1 and FRL-7-i. While FRL-10-D contains smaller (0.25-0.125 mm and >4mm) ceramic fragments than others.

Sample FRL-7-i was collected from the overlapped layer of the mosaic floor. During the collection, FRL-7-i and FRL-7-ii had similar look surface, after cleaning they appear adjacent to each other with completely different compositions of aggregates. FRL- 7-i, (group-A) is like other *opus signinum* mortars, while FRL-7-ii (group-B) contains only siliceous aggregates. Although collected as the same sample and side by side, these samples show differences between them, which might indicate as random mortar fragments used to fill the floor gapping or pits for renovation purposes on the remains of the mosaic floor (Silva, 2012).

The great variability of ceramics found in the various mortars (Tab -4.2 and Tab-4.3) is in accordance with the reuse of different types of construction materials, varied ceramics (bricks, tiles). Five different types of ceramic were observed with a stereo zoom microscope and their frequency were visually estimated. The large, crushed ceramics are found and categorized as dark brown and red ceramics, where red and orange ceramics are found in smaller fragments. Few black ceramic fragments were also observed in samples as fewer amounts. Repetition of ceramics with similar characteristics within the samples, and their visually estimated distribution indicates the use of construction materials intentionally from the same available sources.

The second group (group B) contains siliceous aggregates, mainly quartz, and feldspar. Sample FRL-4 and FRL-12 were from the two walls of the peristyle as filler mortar. In comparison, they appeared quite similar to each other as their functionality was the same. The grain sizes and shape were similar, the abundance of grains profound in both samples was 1-0.5mm. The main aggregates were observed in the insoluble residue of this group were white quartz (milky) and transparent quartz (hyaline) associated with K-feldspar (orthoclase and microcline), confirmed with XRD and petrographic analysis.

FRL-6, as a render mortar, was collected from the same peristyle wall showing similar characteristics with FRL-4 and FRL-12 in the lower layer (FRL-6-D), while the upper layer contains fine quartz and fine ceramic fragments (mainly 0.125-0.063mm) that gave the layer a pinkish hue. The mortar sample associated with the tesserae (FRL-8-D) also belongs to group-B, due to essentially quartz and feldspar as aggregates.

According with several authors (Kaplan, 2013; Caldeira *et al.*, 2019) the roman mosaic floor composition, have several mortar layers (Fig-5.3), the layer containing tesserae called '*Tessellatum*', (1) the second layer as '*bedding*' (2) which is a thin layer rich in lime, applied fresh in a small and regular portion where the mosaic design usually being marked, and the tesserae design inserted before the mortar get hardened. The third layer '*Nucleus*' (3) is an impermeable mortar layer of powdered pottery and lime, to protect the mosaic from the soil water (humidity), and the fourth layer towards the surface '*Rudus*' (4) are mainly a layer of gravel to level the floor, while the last layer '*Statumen*' (5) as a preparatory layer containing large stones.

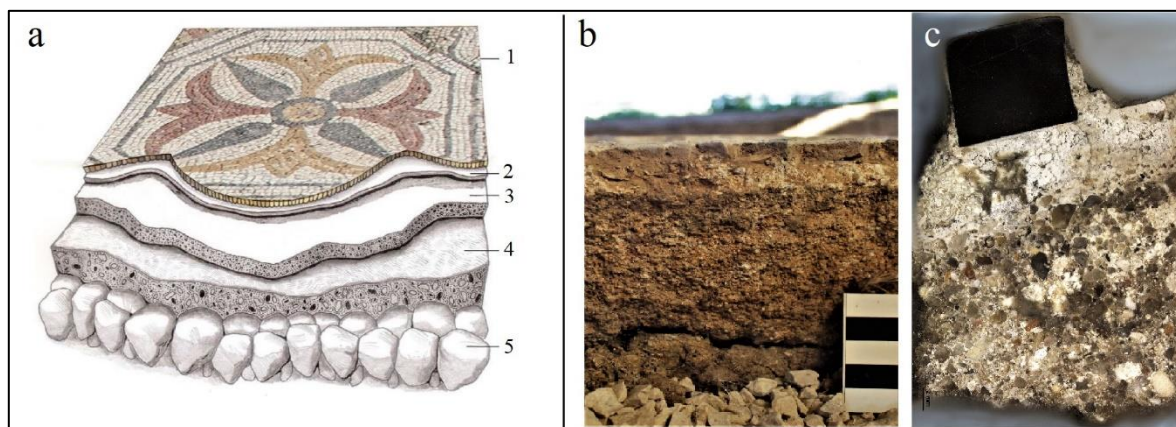


Figure 5. 3- a) shows the Stratigraphy of a Roman mosaic floor according to Vitruvius's description. (Adapted from Caldeira *et. al.*, 2019). 1. Tessellatum, 2. Bedding, 3. Nucleus, 4. Rudus, 5. Statumen, b) section view of the sample FRL-8 (mosaic floor) in situ, from the site, c) prepared polished section of the sample FRL-8, containing stratigraphic layers of the floor.

The results obtained for the mosaic sample (FRL-8) were different from the typical layering described above. Evolving the tesserae, the upper layer is composed of a lime-rich layer with light minerals (quartz and feldspar) which correspond to the '*bedding*' layer. And the lower layer was made of compacting siliceous aggregates (quartz and feldspar) with the absence of ceramic fragments. According to Vitruvius, the roman mosaic floor needs to follow certain layering procedure (Fig-5.3) as described before. A layer with powdered pottery and lime

was essentially needed to protect the mosaic from the humidity or soil water. In the visual and petrographic observation, the studied sample (FRL-8) shows differences, mainly in the layering and absences of ceramic in 'Nucleus' layer.

The third group (group C) demonstrates a different aggregates assembly within the samples, most of the samples of this group are from mural painting wall, and sample FRL-15 is from the compartment- 'a', inner facing wall (see section 2.3.2). The predominance of siliceous aggregates in this group is as similar as former groups with the presence of quartz and feldspar, associated with calcitic shells and rounded basaltic grains. The basalt grain was confirmed with the results from XRD and SEM-EDS, as well as petrographic analysis.

The rounded shape of these basaltic rock fragments indicates transportation from the geological origin, while the siliceous aggregates from all the groups are generally sub-angular to a poorly rounded shape suggesting less transportation.

The granulometric analysis of the previously grouped samples shows patterns (Fig-4.25) of particle size among the samples as grain size distribution plotted in grain chart. Sample with the ceramic as group-A has an abundance in grain size of greater than 4mm (weight %), where the rest of the sample (Group-B and C) shows similarity that has abundance in grain size of 1-0.5mm (weight %). These samples are described as 'Bimodal' and 'Unimodal' for the other groups of samples as observed from GRADISTAT software analysis (Tab-4.11). The textural group of the ceramic rich samples complies with 'sandy gravel' while the rest of the groups are in the 'gravelly sand' group according to Wentworth's classification (Wentworth, 1922).

5.2 Provenance study

For the determination of the provenance study of the samples from the Roman villa of Frielas, mineralogical data was obtained from archaeometry analysis and complementary information. Considering its geological context and vicinity as a primary source of raw materials for binder and aggregates will be the fact of discussion compared with Vitruvius recommendation.

As previously discussed, the lime used in the mortars of the Roman villa of Frielas is calcitic in nature, thus corresponding to an aerial lime. The degree of purity of the lime, without a significant siliceous (detrital) contribution, suggests limestones as the raw material been used. This lithology according to available cartography (Almeida, 1991; Manuppella *et al.*, 2011) is abundant in the surrounding geological context. Namely represented by limestones of formations from '*Calcário de Alforneiros*' and '*Formação de Bica calcário*' (section 2.4 and Fig- 2.6). Some of these limestone occurrences are currently used in the cement and

ornamental industry. Also, in addition to the limestone formations, the villa is based on the Benfica formation which is according to (Carvalho & Romariz, 1972; Manuppella *et al.*, 2011) present limestone intercalations (formation of Arranó). Thus, within a distance radius of 5 km, it is possible to obtain the limestone compatible with the lime composition. A more exact confirmation would imply the analysis of these raw materials, which was not the objective of this work.

As previously discussed, most of the samples have a predominance of siliceous aggregates (quartz and feldspar) (group B). Some samples have the shell and basaltic rock fragments (group-C) and some are containing ceramic fragments (group-A). Besides, as aggregates limestones, sandstone and, quartzite fragments are found in terms of mineralogical and petrographic analysis. The morphology of these aggregates is mainly angular to sub-angular or even poorly rounded. The basaltic rock fragments are observed almost in rounded shape confirming by SEM-EDS, petrographic and visual observation. These rounded basaltic rock fragments indicate significant transportation from their source of origin. In geological context, the “Formação de Benfica” is based on volcanic discontinuity over the Complexo Vulcânico de Lisboa (CVL). Since it is in the vicinity of the studied site that conforms the possible geological sources of these basaltic rock fragments can be from CVL (Fig-5.4).

The quartz and feldspar are in angular to sub-angular shape that might indicate a short distances transportation from their source of origin but in the geological context and surroundings of the villa, it is difficult to find any possible sources. So, quartz and feldspar, together with quartzites, would be transportation associated with Tagus River.

According to Zbyszewski, 1964, sand, and gravel have the available source on the left bank of the Tagus River, occasionally, in quaternary deposits. On the right bank of the Tagus River, sand is available in the lower Miocene units between *Lumiar*, *Ameixoeira*, *Aeroporto*, *Charneca*, and *Camarate*. Several other, sources can be the Middle and Upper Miocene in the regions of *Sacavém*, *Póvoa de Santa Iria*, and *Alverca*. Therefore, it can be assumed that the possible sources of sand (quartz and feldspar) are from the right bank of the Tagus River (Fig. 5.4).

Samples with shell and basalts were previously described as group C. Some samples (FRL-11-ii, FRL-15, and FRL-17) from group C contain carbonated organic materials e.g., shell fragments confirm by the obtained results from SEM-EDS, petrographic and visual observations. Their sources can be assumed from a similar deposit with higher influence of CVL and presence of shells. No evidence was found to an intentional addition of these aggregates to the siliceous sand has been observed. These can be justified with small variations in sedimentary deposits.

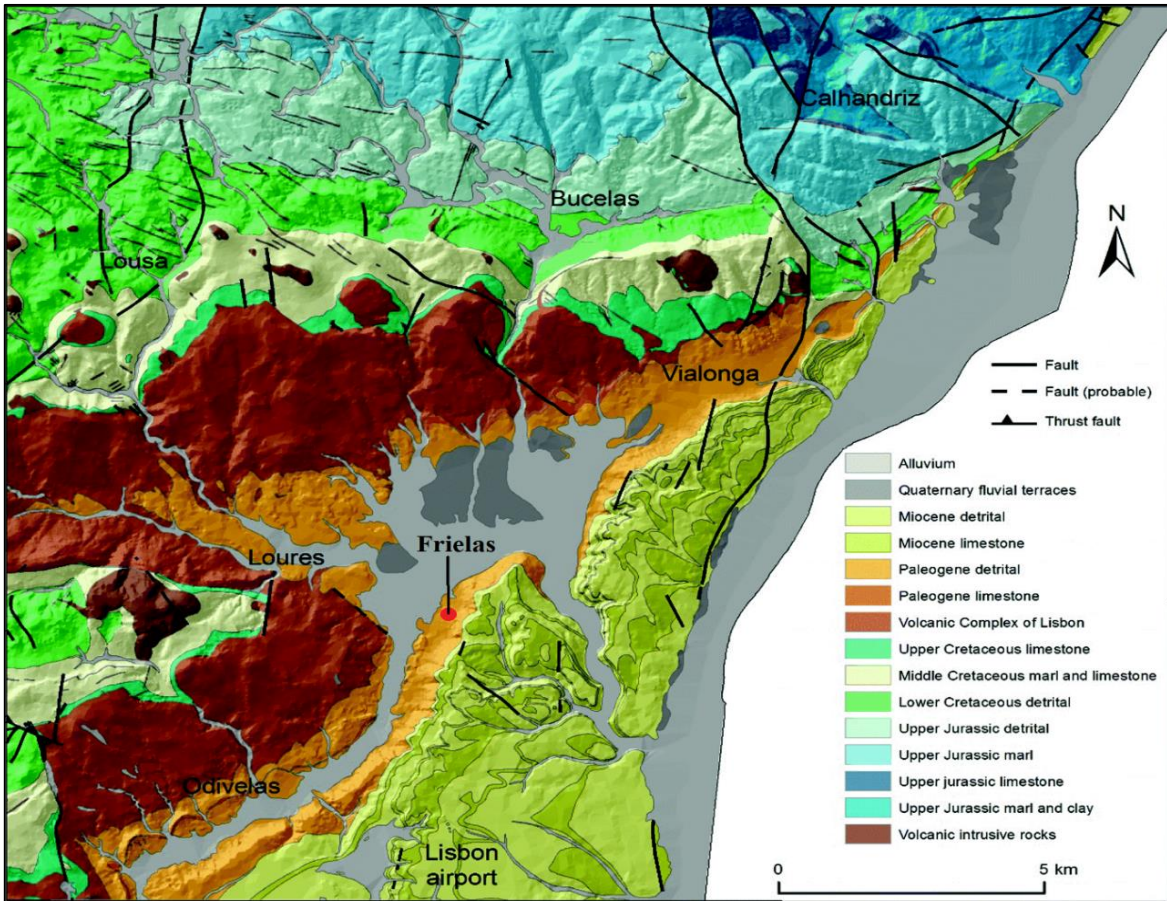


Figure 5. 4- Lithographic map of Loures: Formation of Benfica (yellow) and Miocene limestone (lemon green), Lisbon volcanic complex (LVC) in brown. (Zêzere, 2020)

On the other hand, the presence of white carbonated aggregates (e.g. FRL-19), with angular shapes, suggests an intention to use this type of material. Limestone fragments, eventually crushed and sieved, must have been used to obtain a whitish color.

The sample with ceramic fragments previously described as group A is mainly with angular to sub-angular shaped crushed ceramics corresponding to the hydraulic structure and *Opus signinum*. Their size and shape differ from the functionality of the mortar. These ceramic fragments are assumed as brick and tiles fragments.

5.3 Production Technology

To reveal the production technology of mortar, it can be assumed that the Roman masons must have followed some certain procedure to construct their buildings or any structures holding Roman architectural features. And undoubtedly, the roman recipes were followed and used, widely in the great roman period and even after Roman time. The Vitruvius descriptions are considered major sources of information regarding Roman building techniques for reconstructing architectural evidence or understanding ancient mortar. Because they are the only architectural treatise surviving from classical antiquity and from the Renaissance through the end of the nineteenth century. Vitruvius' *De Architectura* was immensely popular and became the conceptual reference for most Western architecture (Artioli *et al.*, 2019).

To evaluate mortar's production technology, two main attributes were investigated. Based on the soluble fraction and insoluble residue produced by following acid dissolution and the number of carbonates determined by TGA analysis. The technique described by Jedrzejewska was used to determine the binder to aggregate ratios (Jedrzejewska, 2014). The simplified composition of the mortar is summarized in Tab. 5-2. The second aspect studied was the hydraulicity of the mortars, based on mass losses in the samples from structurally bound water and carbon dioxide derived from TGA findings.

Different binder to aggregate proportions depending on the types of sand used was suggested by Vitruvius in his work. In the case of pit sand, three parts of sand should be combined with one part of lime (1:3); in the case of river or sea-sand, two parts of sand and one part of lime (1:2); and for a "better composition," the third part of sieved powdered brick might be used (Book II, Chapter V, Vitruvius). He also suggests aging the slaked lime to get a better combination.

Based on the results from the acid attack and TGA analysis, which were used to determine the aggregates and binder ratio (Tab-5.2). The ratios obtained from the results show two different patterns, while most of the samples show the proportions as 1:3, the rest of the samples vary from 1:1 to 1:7. According to Vitruvius's description, 1:3 can be an 'ideal proportion' in the case of pit sand. While the studied samples are resulting in the analysis that can comply with the river sand. No certain conclusions can be made based on the assessment employed for the binder aggregate ratios. Nevertheless, some assumptions can be made depending on the results, archeological context, structure, and functionality of the mortar samples.

The samples representing the binder to aggregate ratio 1:3 can be considered as a pattern of contemporary structural mortar which might be prepared following roman recipe, while the rest of the samples, with other proportions, can be an indication of repair, rebuild (extension), or renovation of the structures.

The archeological context can give supportive evidence, for this assumption. In the case of sample FRL-3 (1:6) and FRL-5 (1:7) ceramic-rich mortar from water channel, containing similar characteristics as previously described. Sample FRL-2 (1:3) was adjacent with FRL-3 (group-A), which was prepared for receiving a final layer (Fig. 5.5.a), perhaps stucco (Silva, 2000) which is left unfinished that can be a indication of repair as discussed before.

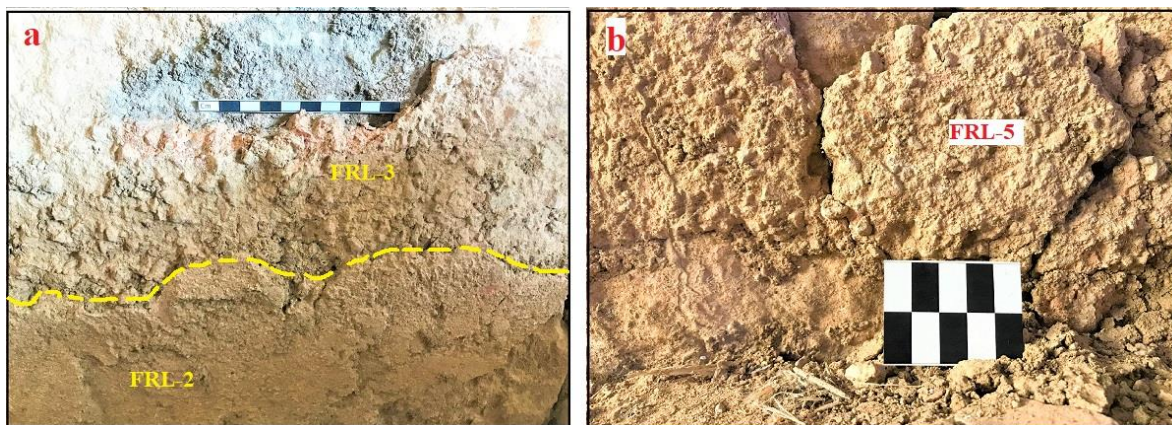


Figure 5. 5-water channel parallel wall (inner), a) one side of the wall showing two layers (FRL-2 & FRL-3), b) another side of the wall (FRL-5, similar to FRL-3 of the other wall)

Sample FRL-8-U (1:1) contains tesserae with lime-rich bedding layer, have the expected amount of binder to aggregates ratio while the lower layer (FRL-8-D) has 1:6. The different ratio of binder to aggregate in both layers and different preparations of mosaic floors does not have similarities with the typical roman mosaic floor as described previously (Fig-5.3).

In the case of sample FRL-6 (group-B), render mortar from peristyle wall (south-facing) coated with pinkish upper layer (1:2), contains fine ceramic fragments and siliceous aggregates. While the lower layer (1:4) comprising with only siliceous aggregates. Both upper and lower layer (FRL-6-U and D) shows different binder to aggregate ratio. The lower layer (FRL-6-D) could have been similar with sample FRL-12 (filler mortar) whereas being in the same wall, it shows a binder to aggregates ratio of 1:3. Sample FRL-4 (filler mortar) is also from the peristyle wall (east-facing) and has the binder to aggregate ratio of 1:2. Both filler mortars (FRL-4 and 12) have similarities in terms of siliceous aggregates and grain size (abundance in 1-0.5mm) distribution, but different binder to aggregate ratios.

The peristyle wall (south-facing) has three columns (Fig. 2.5). In the Archaeological context, it seems that the columns of this peristyle wall were in an unusual position. Likely to be engaged, attached, or embedded column on the wall which is rarely seen in Roman architecture whether if it is not for the purpose of a pilaster. Vitruvius describes in his 'Ten books of Architecture' about the columns. In his third and fourth book, Vitruvius described the different styles of columns and how they are used in different structures. In general, the columns of a portico should have precisely calculated proportions (Noghani, *et al.*, 2012). In the case of the Roman villa of Frielas, an Ionian shaft was found in an archaeological context thus, the remaining base of this column might have been the Ionian column base (Appendix-8.2).

A great example of the Ionian column can be seen in the Roman colosseum (in Rome), on the 2nd level (Turner, 1996). which is not attached to the wall as the studied columns of Frielas (Fig. 5.6). Considering these facts, it can be assumed that the peristyle wall is an indication of quick renovation, rebuilding, or inexperienced masonry work.

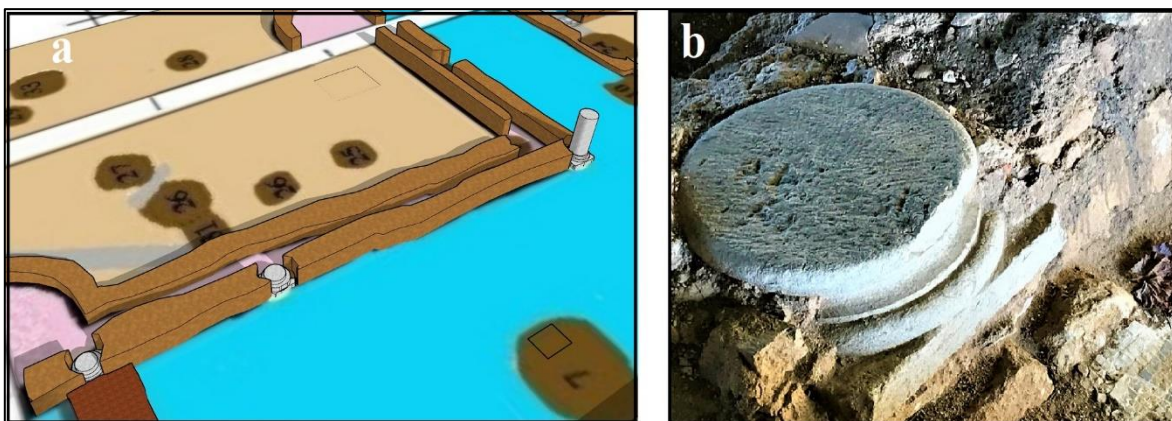


Figure 5. 6-Peristyle wall (south-west facing) with embedded column and pinkish wall surface. a) 3D demonstration of the wall and column location (image is not according to scale, made just to indicate the column position), b) showing the position of the column as embedded in the wall from the site.

On the other hand, Marcus Vitruvius Pollio, in his Book II indicates clearly that the proportion of lime and sand must be increased if the poor quality or marine sand is used as aggregate (Artioli, *et al.*, 2019). Considering Vitruvius's description, if the studied samples were containing poor quality or marine sand, suppose the proportion of aggregates had been increased. And so, the samples (Tab-4.10) are showing a 1:4 to 1:7 ratio of binder to aggregates. Reviewing the results obtained from multi-analytical techniques confirms sample showing random binder to aggregates ratio does not provide evidence of marine sand as aggregate in the samples. The marine sand is usually finer and more rounded.

The samples from group A, have a high ratio of aggregates that can be obtained due to the additives of ceramic fragments within the binder. And samples from group D show a binder to the aggregate ratio of almost 1:1, which can be a functional characteristic of the mortar to avoid shrinkage and cracks.

The inaccuracy of the proportions of aggregates added to the mixture can also be due to the inaccessibility to traditional recipes and a construction based on empiric and intuitive knowledge and a “trial and error” practice or the result of an inexperienced laborer. The remoteness of this rural environment might have influenced the lack of qualified masons, who were most likely to live in the bigger cities (Valdez, 2019, Borsoi *et al.*, 2019). The building methods would have been more faithful to the traditional recipes given in Roman treatises, as evidenced by previous works from the Roman site of Pisões, which showed that Vitruvian rules for mortars were followed, and brick fragments were also included to increase water retention and form pozzolanic products. (Borsoi *et al.*, 2019).

Table 5. 2- Sample composition (mass %) and binder to aggregate ratio by Jedrzejewska method (Jedrzejewska, 1960)

Sample	Aggregates		Total Aggregates % ³	Binder	Binder to aggregates ratio ⁵
	Soluble fraction % ¹	Insoluble residue % ²		CaCO ₃ wt. % ⁴	
FRL-1	-2.4*	81.3	78.9	21.1	1:4
FRL-2	10.6	65.4	76.0	24	1:3
FRL-3	8.1	77.1	85.2	14.8	1:6
FRL-4	8.4	60.5	68.9	31.1	1:2
FRL-5	8.7	78.6	87.3	12.7	1:7
FRL-6-U	11.8	57.8	69.7	30.3	1:2
FRL-6-D	2.8	77.3	80.2	19.8	1:4
FRL-7 (i)	4.5	77.8	82.3	17.7	1:5
FRL-7 (ii)	3.6	73.6	77.3	22.7	1:3
FRL-8-U	15.5	32.5	48.1	51.9	1:1
FRL-8-D	4.9	81.1	86.1	13.9	1:6
FRL-9	12.6	70.8	83.5	16.5	1:5
FRL-10-U	8.6	68.1	76.7	23.3	1:3
FRL-10-D	10.1	66.1	76.2	23.8	1:3
FRL-11 (i)	5.7	68.2	73.9	26.1	1:3
FRL-11 (ii)	6.1	66.4	72.5	27.5	1:3
FRL-12	10.1	67.7	77.8	22.2	1:3
FRL-15	0.6	70.4	71.0	29	1:2
FRL-17	-	-	-	29	1:2**
FRL-18	0.45	70.9	71.4	28.6	1:3
FRL-19-U	12.1	23.3	35.4	64.6	2:1
FRL-19-D	7.2	70.5	77.7	22.3	1:3

1. Soluble = 100- Σ (insoluble residue + carbonates).

2. Insoluble residue percentage from Acid attack analysis.

3. Total aggregates = Insoluble residue percentage (Acid attack analysis) + calculated soluble fraction¹

4. Calculated wt. % of CaCO₃ (from TGA analysis)

5. Binder (considered to be carbonate fraction): aggregate (sand + soluble fraction).

*The calculated negative value can be due to the heterogeneity of the samples obtained from both analyses (acid attack and TGA).

** In the case of Sample FRL-17, was calculated only depending on the carbonates % obtained from TGA, due to unavailability of enough sample for an acid attack.

Samples were also studied in terms of their level of hydraulicity. The hydraulicity of the mortars was calculated based on the results obtained by TGA analysis, the ratio between carbon dioxide (CO₂) to structurally bound water (H₂O) in relation to carbon dioxide (CO₂) to make a correlation with the hydraulic degree of the mortars (Tab-5.3). The hydraulicity of different types of mortars has been studied (Moropoulou *et al.*, 2005) and it was determined that the “inverse trend of hydraulicity of mortars is being augmented exponentially with CO₂”, in which the lower the ratio is, the higher the hydraulicity. If the ratio of CO₂/H₂O is between 1 and 10, mortars can be accepted as hydraulic (Bakolas,1998; Moropoulou *et al.*, 2000).

Results indicate that most of the samples plotted (Tab-5.3) is in the same assemblage (Fig-5.7) depending on the relationship between CO₂ to structurally bonded water ratio versus CO₂ mass losses (Tab-5.3) according to their hydraulic characteristic. The calculation of CO₂/H₂O in relation to CO₂ most of the samples including ceramic-rich samples have hydraulic characteristics.

Though sample FRL-19-U and FRL-8-U show different positions in the chart, due to their high amount CO₂ (%) and low H₂O percentages which is because of their binder-rich properties that comply with their functionality.

Table 5. 3- Weight loss percentages of structurally bound water in the temperature range 200-600 °C, and CO₂ (600-900 °C) for understanding the hydraulic characteristic of the samples.

Sample	H ₂ O %	CO ₂ %	CO ₂ /H ₂ O
FRL-1	2.96	9.31	3.1
FRL-2	2.02	10.60	5.4
FRL-3	3.20	6.55	2.0
FRL-4	1.81	13.72	7.5
FRL-5	2.08	5.60	2.7
FRL-6-U	1.79	13.27	7.4
FRL-6-D	1.17	8.72	7.4
FRL-7-i	2.43	7.79	3.2
FRL-7-ii	0.89	10.0	11.2
FRL-8-U	3.38	22.70	6.7
FRL-8-D	1.25	6.12	4.8
FRL-9	3.18	7.30	2.2
FRL-10-U	2.04	10.26	5.0
FRL-10-D	2.62	10.47	4
FRL-11-i	2.15	11.52	5.3
FRL-11-ii	1.68	12.11	7.2
FRL-12	1.42	9.77	6.9
FRL-15	0.63	12.79	20.3
FRL-17	1.24	12.76	10.2
FRL-18	0.71	12.60	17.5
FRL-19-U	0.57	28.42	49.8
FRL-19-D	1.21	9.81	8.1

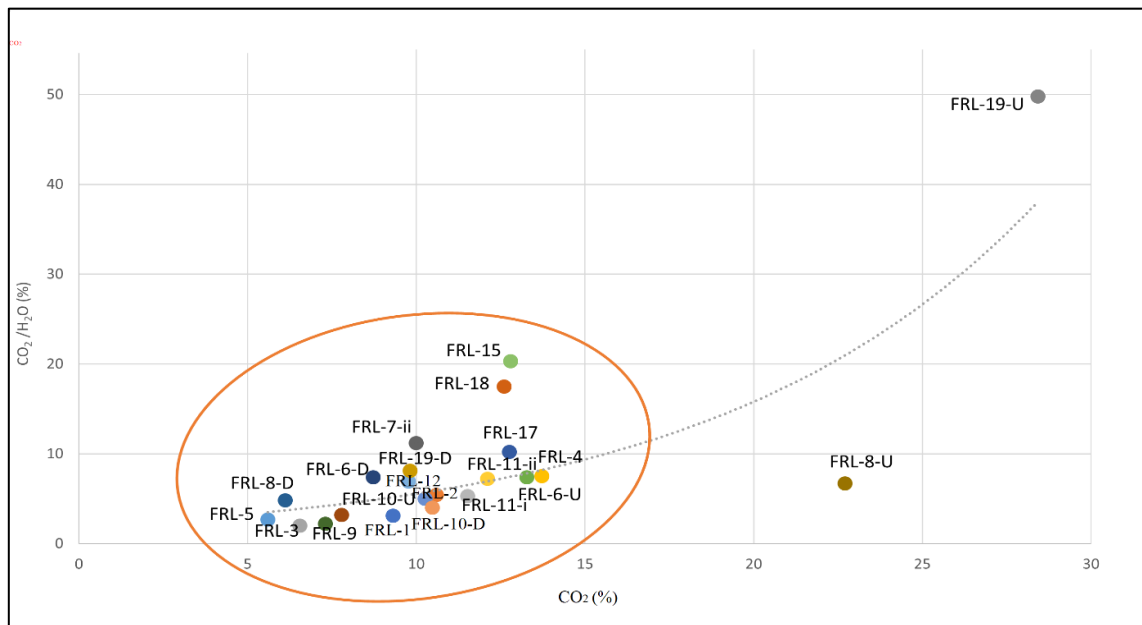


Figure 5. 7- Carbon dioxide vs Carbon dioxide / Structurally bound water.

6 CONCLUSIONS

The study aimed to provide a better understanding of mortars from the Roman villa of Frielas in correlation with the chronological sequence through the investigation. It was necessary to characterize the materials in terms of their binder and aggregates to provide evidence for the characterization of raw materials used in the mortar, as well as their provenance, and to establish a chronology among the structures. Besides that, valuable information about their production techniques was obtained and compared to the ancient recipes given by Vitruvius, which can be used for a future outlook in the consolidation and repair of their structures.

A total of eighteen samples representing the Roman villa of Frielas, were examined through a multi analytical approach. They were analyzed by using Optical Microscopy (OM, stereo zoom, and petrographic microscope), X-ray Diffraction (XRD), Scanning Electron Microscopy coupled with Energy Dispersive X-ray Spectroscopy (SEM-EDS), Thermogravimetric Analysis (TGA-DTG). Acid Attack and Granulometric Analysis were also performed to determine the binder to aggregate ratios of the mortars, as well as the particle size distribution of the insoluble residue and to hypothesize on the production techniques employed in the mortars' manufacture.

On the basis of the results obtained, samples were divided into 4 groups; 1) Samples with ceramic fragments which are associated with water channel structures and the other *Opus signinum*, 2) Samples that contain only siliceous aggregates (quartz and feldspar) corresponding to the peristyle wall and portico's passage floor, 3) Samples with shell and basaltic rock fragments, from the compartments outer wall (mural painting) and inner wall as well as some detached wall fragments, and 4) The upper layers of the stratified samples were divided to make the discussion easier. The characterization of the materials demonstrates a similar composition of the mortars amongst the groups in terms of their binder properties. A little differentiation was observed in terms of aggregates, though that varies because of their functionality.

The first group of samples (Group-A) was mainly rendered, and filler mortar was collected from the water channel and *opus signinum* structure. Analysis revealed that the binder composition of this group was similar to others, high amount of Ca in the binder composition with a very low percentage of Mg, and the presence of other elements such as K, Al, Na, and Si may be from aggregates or even ceramic fragments. TGA and acid attack analysis show the amount of calcium carbonate present in this group of samples varies from 12.7 to 23.8 weight % that indicating a calcitic lime binder.

The calculated calcium carbonate represents binder to aggregate 1:3 to 1:7. The aggregates ratio is higher in this group than the others. These samples have a predominance of crushed ceramic fragments followed by sub-angular to poorly rounded siliceous aggregates (quartz and feldspar). To give the mortars a hydraulic property, ceramic fragments were used as an artificial pozzolan. The functionality of this group of samples also indicates their use related to water-resistant structures. Though in elemental and mineralogical analysis no pozzolanic reaction or new formation mineralogical changes were observed. It is assumed that the ceramic used in the mortar was low burned ceramic which can be a factor in resisting pozzolanic reaction. According to the calculated hydraulic index, this group of samples has hydraulic characteristics.

The second group of (Group-B), related to the villa's peristyle wall and mosaic floor as render and filler mortars. The binder of this group of samples is similar as discussed before. The amount of calcium carbonate varies from 19.8 to 31.1 weight % which represents the binder to aggregate ratio is 1:2 to 1:6. This group contains predominance in siliceous aggregate as quartz and feldspar. The morphology of the aggregates among the sample of this group are similar, angular to sub-angular shape, their predominant grain sizes are 1.05mm and 2-1mm.

The third group of samples is related to the compartments' inner and outer walls (mural painting) as well as detached wall fragments. The samples are mainly rendered mortar, and few of them have the chromatic layer with pigmentation. This group of samples can be differentiated from the other groups depending on their small variation in aggregates. The sample from this group contains shell fragments and basaltic rock fragments. They also contain siliceous aggregates as quartz and feldspar. The morphology of aggregates is similar to other groups, the predominant grain sizes of this group are 1-0.5mm and 2-1mm.

The basaltic rock fragments are rounded shape that indicates their significant source of origin. The calcium carbonate percentage of this group is 22.3 to 29 weights % that represents the binder to aggregates ratio 1:2 to 1:3. The presence of carbonated organic materials as shell fragments can cause the overestimated calcium carbonate percentage in the samples.

The hydraulicity index of this group of samples are showing the level of hydraulicity as calculated based on the ratio between CO₂ to structurally bounded water (H₂O) (TGA analysis) in relation to CO₂, which indicates this group has the hydraulic characteristic.

The upper layers of chromatic samples were divided and grouped separately, to make the assessment and the discussion easier. Three render mortars and one floor (mosaic) mortar are included in this group as sub-samples. These samples are mainly binder-rich upper layers, they contain a high amount of binder. The obtained result from TGA analysis, and acid attack analysis this group of sub-samples are containing percentages of calcium carbonates 23.3 to 64.6 weight %, as their binder to aggregate ratio is 1:1 to 1:3. The binder to aggregate ratio is compliant to their functions. They contain siliceous aggregates as quartz and feldspar in general. In a specific sample FRL-6-U (pinkish layer) contain ceramic fragments that give the layer a pinkish hue. Sample FRL-19-U have angular to sub-angular-shaped crushed lime fragments in Ca-rich binder to make the layer more whitish. The morphology of aggregates

is as similar as other groups, while this group of sub-samples has a predominant grain size in 0.25mm to 0.125mm and in the case of FRL-19-U, 1-0.5mm to 2-1mm.

In terms of raw materials, all the samples indicate the binder used in the samples from the Roman villa of Frielas is a calcitic areal binder. The aggregates of the samples are showing uniformity in terms of siliceous aggregates as quartz and feldspar. Besides, some samples are consisting of ceramic fragments, some are with shell and basaltic rock fragments.

The provenance of the raw materials can be assumed as local. The studied site is in the geological 'Formation of Benfica' and 'limestone of alforlenos' formation region. The limestones or the lime used for the binder can be quarried from near-far sources of the site that is within a radius of 5 km. The sources of sand as aggregates can be from the bank of river Tagus, as near-far sources.

The result demonstrated that the binder to aggregate ratio was 1:1 to 1:7 among the samples. The ratio of binder and aggregates shows a range of varieties and therefore the 'ideal proportions' ('1:3' for pit sand, and '1:2' river sand) of the binder to aggregates according to Vitruvius as the roman recipe in the case of studied samples does not help to make any conclusion. The calculated hydraulicity of the samples are resulting from that the samples are with hydraulic characteristics.

Finally, it can be concluded that the studied mortars are presenting uniformity in terms of the chemical, mineralogical, and microstructural composition according to their structures. There are no differences that would indicate a distinct manufacturing chronology; thus, they are presumed to be contemporaneous. It is clear that the Vitruvius rules were not followed in terms of production. It is reasonable to assume that masons were familiar with the ancient recipes for construction, given the fact that homogeneous mixtures of the traditional materials used were employed for every specific purpose, but this knowledge was always related to their intuition and availability of supplies.

7 REFERENCES

- Adriano, P., A. Santos Silva, R. Veiga, J. Mirão, and A. E. Candeias. (2009). “*Microscopic Characterization of Old Mortars from the Santa Maria Church in Évora.*” *Materials Characterization* 60(7):610–20.
- Almeida, I. M., (1991)– *Características geotécnicas dos solos de Lisboa*. Dissertação de Doutoramento na Especialidade de Geotecnia, Universidade de Lisboa, 391p
- Antunes, M.T. (1967)- *Dépôts paléogènes de Coja: nouvelles donnés sur la Paléontologie et la Stratigraphie. Comparaison avec d'autres formations paléogènes*. Rev. Fac. Ciências, Univ. Usboa, 2" série, C, X:V (1), 69-111.
- Antunes, M.T. (1979)- *Ensaio de slntese crítica acerca do Cretácico terminal e do Paleogénico de Portugal*. Ciências da Terra (UNL), 5, 145-174. Lisboa.
- Artioli, G. (2010). *Scientific methods and cultural heritage. An introduction to the application of materials sciences to archaeometry and conservation science*. New York, US: Oxford University Press.
- Artioli, G., Michele Secco, and Anna Addis. (2019). “*The Vitruvian Legacy: Mortars and Binders before and after the Roman World.*” *European Mineralogical Union Notes in Mineralogy* 20:151–202.
- Azevêdo, T. M., Carvalho, A. M. G.; Oliveira, M. S.; Romariz, C. (1991) – *O “Complexo de Benfca” na Região de Lisboa, Estudo Sedimentológico*. Comunicação do Serviço Geológico de Portugal, t. 77. Lisboa, pp. 103-120.
- Bakolas, A., Biscontin, G., Moropoulou, A., & Zendri, E. (1995). ‘*Characterization of the lumps in the mortars of historic masonry.*’ *Thermochimica Acta* 269/270, 809-816. Bellotto et al., 1995
- Bakolas, A., Biscontin, G., Moropoulou, A., Zendri, E., (1998), *Characterization of Structural Byzantine Mortars by Thermogravimetric Analysis*, *Thermochimica Acta*, 321/1-2, 151-160.
- Borsoi, G., A. Santos Silva, P. Menezes, A. Candeias, and J. Mirão. (2019). “*Analytical Characterization of Ancient Mortars from the Archaeological Roman Site of Pisões (Beja, Portugal).*” *Construction and Building Materials* 204:597–608.
- Caldeira, B., Oliveira, R. J., Teixidó, T., Borges, J. F., Henriques, R., Carneiro, A., and Peña, J.A., (2019), ‘*Studying the Construction of Floor Mosaics in the Roman Villa of Pisões (Portugal) Using Noninvasive Methods: High-Resolution 3D GPR and Photogrammetry*’, *Remote Sensing*. MDPI.
- Cardoso, I., M. F. Macedo, F. Vermeulen, C. Corsi, A. Santos Silva, L. Rosado, A. Candeias, and J. Mirao. (2014). “*A Multidisciplinary Approach to the Study of Archaeological Mortars from the Town of Ammaia in the Roman Province of Lusitania (Portugal).*” *Archaeometry* 56(1):1–24.
- Carneiro, A. (2014). *OTIVM, materialidade e paisagem nas villae do Alto Alentejo português em época romana. Espacio, tiempo y forma 27. Serie II, Historia antigua*, 207-231.
- Carneiro, A. (2016). *A villa romana, entre a construção literária e a realidade construída. Anales de arqueología cordobesa* pp. 27, 77-96.

- Carneiro, A. (2017). *Lusitania Romana: del pasado al presente de la investigación*. Mérida: Museo Nacional de Arte Romano.
- Carneiro, A. (2017). *O final das Villae na Lusitânia romana. O exemplo da Horta da Torre (Fronteira)*. *Urbs Regia*, Nº2, 56-59.
- Carneiro, A. (2017). *Urbs in Rure: Decorative Programmes and Architectural Models in Lusitania's Villae*. *Journal of Mosaic Research* 10, 117-127.
- Carvalho, A. M. G. & Romariz, C (1972) – *Estudo Paleogénico da região de Lisboa e arredores*. Centro de Est. de Geol. Pura e Aplicada, F.C.L Proj. de Inv. LMG-1, Instituto de Alta Cultura.
- Carvalho, A. M. G. (1968)- Contribuição para o Conhecimento Geológico da Bacia Terciária do Tejo. *Mem. Ser. Geol. Portugal*.
- Choffat, P. (1950) – *Geologie du Cenozoique du Portugal*. Obra póstuma. Comunicação dos Serviços Geológicos de Portugal, supl. Tomo XXX, Lisboa, 182p.
- Delatte, N. (2001). *Lessons from Roman Cement and Concrete*. *Journal of professional issues in engineering education and practice*, 109-115.
- Elsen, Jan, Koenraad Van Balen, and Gilles Mertens. (2013). “*Hydraulicity in Historic Lime Mortars: A Review*.” *RILEM Bookseries* 7(September):125–39.
- Elsen, Jan. (2006). “*Microscopy of Historic Mortars-a Review*.” *Cement and Concrete Research* 36(8):1416–24.
- Ergenç, Duygu and Fort González, Rafael. (2019). “*Multi-Technical Characterization of Roman Mortars from Complutum, Spain*.” *Measurement* 147:106876.
- Földvári, Mária. (2011). “*Handbook of the Thermogravimetric System of Minerals and Its Use in Geological Practice*.” Vol. 213, Central European Geology. Budapest: Geological Institute of Hungary Geologia Económica, Especialização em Geotecnia. Departamento de Geologia da Faculdade de Ciências da Universidade de Lisboa, 294p. Valdez Madrid, Dulce Elizabeth. 2019. “*Characterisation of Mortars Associated with the Hydraulic System of Roman Villa Horta da Torre*.” Master Thesis. University of Evora, ARCHMAT. Evora. Franquelo *et al*, 2008
- Groot, C., Bartos, P., & Hughes, J. (1999). *Historic mortars: characteristics and tests - Concluding summary and State of-the-art*. International RILEM Workshop on Historic Mortars: characteristics and Tests, (pp. 443-454). Paisley.
- Gualtieri, A. and Bellotto, M. (1998) ‘*Modelling the structure of the metastable phases in the reaction sequence kaolinite-mullite by X-ray scattering experiments*. *Physics and Chemistry of Minerals*, 25, 442452.
- Gualtieri, A., Bellotto, M., Artioli, G. and Clark, S.M. (1995) *Kinetic study of the kaolinite-mullite reaction sequence. Part II: mullite formation*. *Physics and Chemistry of Minerals*, 22, 215222.
- Jedrzejewska, H. (2014). ‘*Old Mortars in Poland: A New Method of Investigation*.’ *Studies in Conservation*, 5:4, 132- 138
- Jedrzejewska, Hanna. 1960. “*Old Mortars in Poland: A New Method of Investigation*.” 5(4):132–38.

- Kaplan,Z., Ipekoglu,B., (2013) *Characteristics of Mortars of Mosaics From A Roman Villa in Antandros Ancient City, Turkey.*
- Krumnacher, P. (2001). *Lime and Cement Technology: Transition from Tradition to Standardized Treatment methods. Msc Thesis, Virginia Polytechnic Institute, USA.*
- Lopes, I. M. F. (2001) – Avaliação das condições geológicas e geotécnicas para a caracterização do risco sísmico. Aplicação à colina do Castelo de S. Jorge. Dissertação de Mestrado em
- Middendorf, B., Hughes, J. J., Callebaut, K., Baronio, G., & Papayianni, I. (2005). *Investigative methods for the characterization of historic mortars- Part 1: Mineralogical characterization.* Materials and Structures 38, 761-769.
- Middendorf, B., Hughes, J., Callebaut, K., Baronio, G., & Papayianni, I. (2005). *Investigative methods for the characterization of historic mortars- Part 2: Chemical characterization.* Materials and Structures 38, 771-780.
- Moropoulou, A., A. Bakolas, and S. Anagnostopoulou. (2005). “*Composite Materials in Ancient Structures.*” Cement and Concrete Composites 27(2):295–300.
- Moropoulou, A., Bakolas A., Bisbikou K., (2000), *Investigation of the Technology of Historic Mortars*, Journal of Cultural Heritage, 1,), 45-48.
- Noghani,J., Anderson, E.F.,Liarokapis, F., (2012), *Towards a Vitruvian Shape Grammar for Procedurally Generating Classical Roman Architecture*, The 13th International Symposium on Virtual Reality, Archaeology, and Cultural Heritage VAST.
- Quaresma, (2017), ‘*A villa de Frielas na Antiguidade Tardia: evolução estratiográfica entre c. 410 e 525-550 d.C*’ Mediaeval Sophia. Studi e ricerche sui saperi medievali.
- Reis, R. P., Cunha, P. P., Dinis, J.L., ‘Trincão, P.R. (2000) - *Geologic evolution of the Lusitanian Basin (Portugal) during the Late Jurassic. In: Proc. 5th Intern. Symp. on Jurassic system*’. *GeaRes. Forum, Transtec Publ., Zurich*, 6, 345-356.
- Reis, R. P., Cunha, P. Proença (1989)- ‘*Comparación de los relleños terciarios en dos regiones del borde occidental del Macizo Hespérico (Portugal Central)*’. Paleogeografía de la Meseta norte durante el Terciario. (C. J. Dabrio, Ed.), *Stv. Geol. Salamanca*, vol. esp. 5, 253-272.
- Riccardi, Maria Pia, Marco Lezzerini, Federico Carò, Marco Franzini, and Bruno Messiga. (2007). “*Microtextural and Microchemical Studies of Hydraulic Ancient Mortars: Two Analytical Approaches to Understand Pre-Industrial Technology Processes.*” *Journal of Cultural Heritage* 8(4):350–60.
- Robador, M. D., & Arroyo, F. (2013). ‘*Characterization of Roman coatings from the a Roman house in Mérida (Spain)*’. *Journal of Cultural Heritage* 14S, S52-S58.
- Robador, M., Pérez-Rodríguez, J., & Duran, A. (2010). ‘*Hydraulic structures of the Roman Mithraeum house in Augusta emerita, Spain*’. *Journal of Archaeological Science* 37, 2426-2432.
- Rodríguez-Navarro, C. (2009). ‘*Binders in historical buildings: Traditional lime in conservation*’. *Seminario SEM 09*, 91-112

- Rodríguez-Navarro, Carlos. (2012). “*Binders in Historical Buildings: Traditional Lime in Conservation.*” Seminarios SEM 9:91–112.
- Schnabel, Lorraine. (2008). “*Mortar Analysis Part 1: Mortar-Making Materials.*” APT Bulletin 39(1):1.
- Siddall, R. (2011). ‘*From kitchen to bathhouse: the use of waste ceramics as pozzolanic additives in Roman mortars.*’ Pp. 152-168 in: *Building Roma Aeterna* (A. Ringbom and R.L. Hohlfelder, editors). (Proceedings) The Finnish Society of Sciences and Letters, Helsinki.
- Silva, A. R. (2000). ‘*A estação arqueológica de Frielas.*’ In *Actas do 30 Congresso de Arqueologia Peninsular. VI. Arqueologia da Antiguidade na Península Ibérica.* Porto: ADECAP, p. 481-489.
- Silva, A. R. (2001). ‘*A terra Sigilata da villa de Frielas.*’ pp. 431-454
- Silva, A. R., (2004), ‘*A villa Romana de Frielas – espaço, tempo e funcionalidade.*’, in *Arqueologia como Documento, Catálogo de Exposição, Câmara Municipal de Loures.*
- Silva, A. R. (2012), ‘*A villa romana de Frielas.*’, in *Actas da Mesa Redonda de Olisipo a Ierabriga*, in “*Cira-Arqueologia.*”
- Silva, A., Paiva, M., Ricardo, J., Salta, M., Monteiro, A., & Candeias, A. (2006). ‘*Characterisation of roman mortars from the archaeological site of Tróia (Portugal).*’ *Materials Science Forum - MATER SCI FORUM*, 1643-1647
- Stefanidou, Maria, Vasiliki Pachta, Stavroula Konopissi, Fotini Karkadelidou, and Ioanna Papayianni. (2014). “*Analysis and Characterization of Hydraulic Mortars from Ancient Cisterns and Baths in Greece.*” *Materials and Structures/Materiaux et Constructions* 47(4):571–80.
- Stuart, Barbara H. (2007). “*Analytical Techniques in Materials Conservation.*” John Wiley & Sons, England. ISBN: 0-470-01280-3
- Turner, J., (1996) “*Architectural Orders.*” *The Dictionary of Art*, vol. 23, Grove, pp. 477–494.
- Velosa, A., Coroado, J., Veiga, M., & Rocha, F. (2007). ‘*Characterization of roman mortars from Coimbra with respect to their repair.*’ *Materials Characterization* 58, 1208-1216
- Wentworth, C. (1922). ‘*A Scale of Grade and Class Terms for Clastic Sediments.*’ *The Journal of Geology*, Vol. 30, No. 5, 377-392
- Zbyszewski, G. (1963) – ‘*Carta Geológica dos Arredores de Lisboa, à escala 1:50 000, Notícia Explicativa, folha 4-Lisboa.*’, *Serviços Geológicos de Portugal*, 93p.
- Zbyszewski, G. (1964) – ‘*Carta Geológica dos Arredores de Lisboa, à escala 1:50 000, Notícia Explicativa, folha 2-Loures.*’, *Serviços Geológicos de Portugal*, 93p.
- Zêzere J.L. (2020), ‘*The North of Lisbon Region—A Dynamic Landscape.*’ In Vieira G., Zêzere J., Mora C. (eds) *Landscapes and Landforms of Portugal.* *World Geomorphological Landscapes.* Springer, Cham.

8 APPENDICES

Appendix 8. 1-The Roman villa of Frielas, east to west orientation view.



Appendix 8. 2- The Roman villa of Frielas, west to north orientation view.



Appendix 8. 3-The Roman villa of Frielas. South-east corner, 1st phase structures.

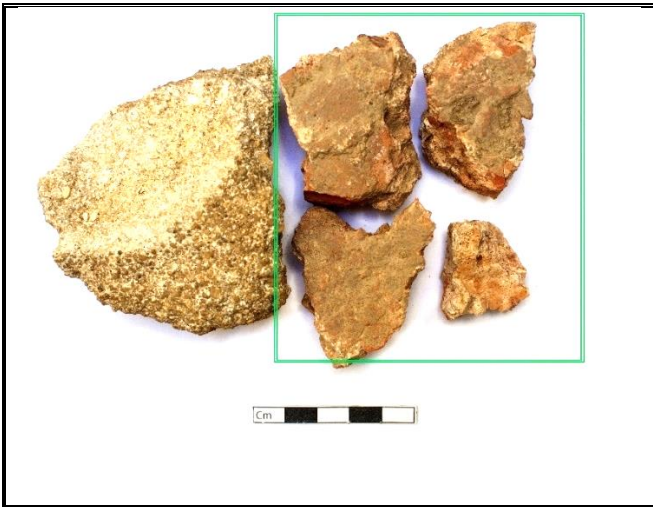


Appendix 8. 4-Peristyle wall with the column, surrounded by mosaic floor and the portico.



Appendix 8. 5- Photographs of collected samples from the Roman Villa of Frielas, after cleaning.





FRL-7-i



FRL-7-ii



FRL-8



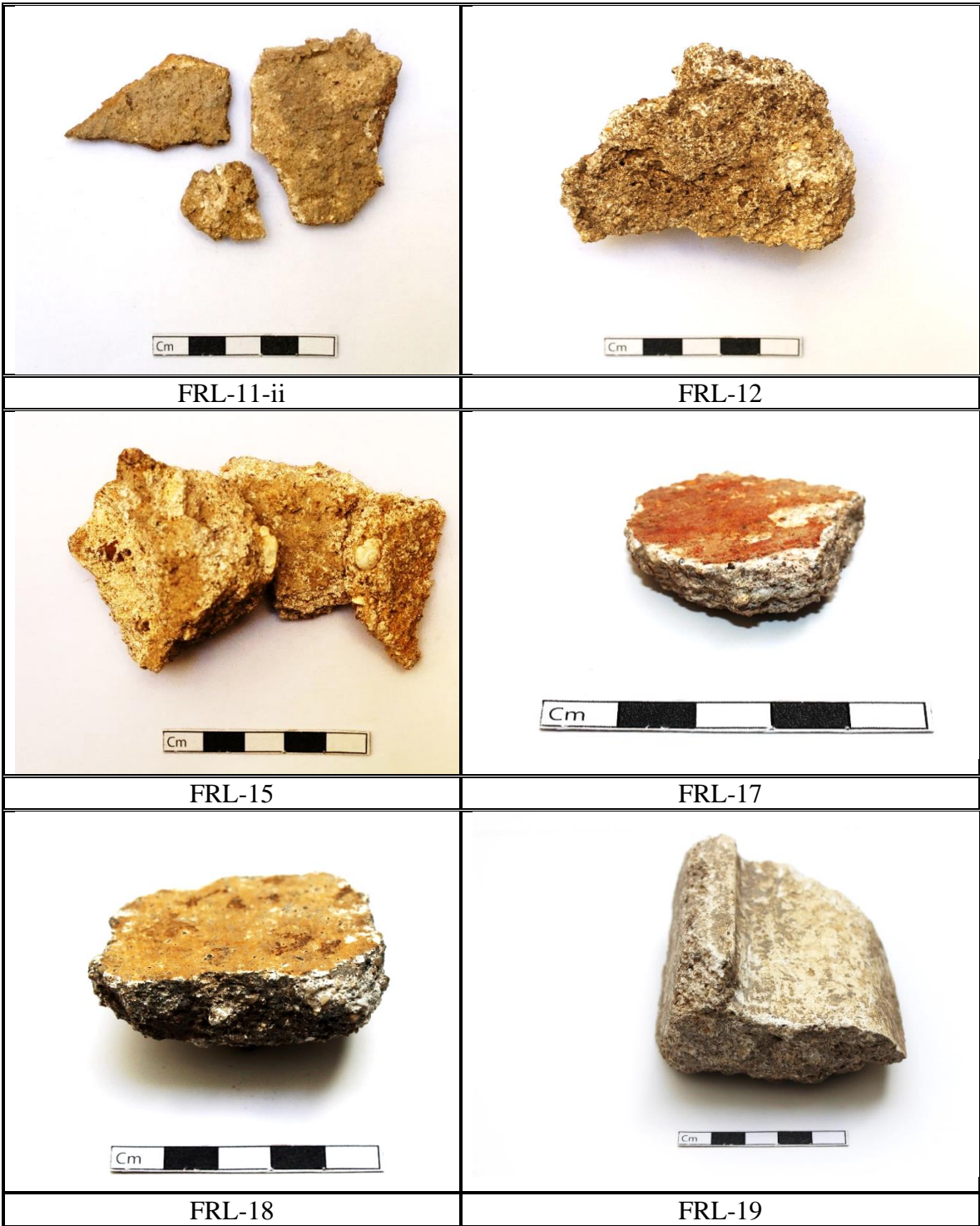
FRL-9



FRL-10



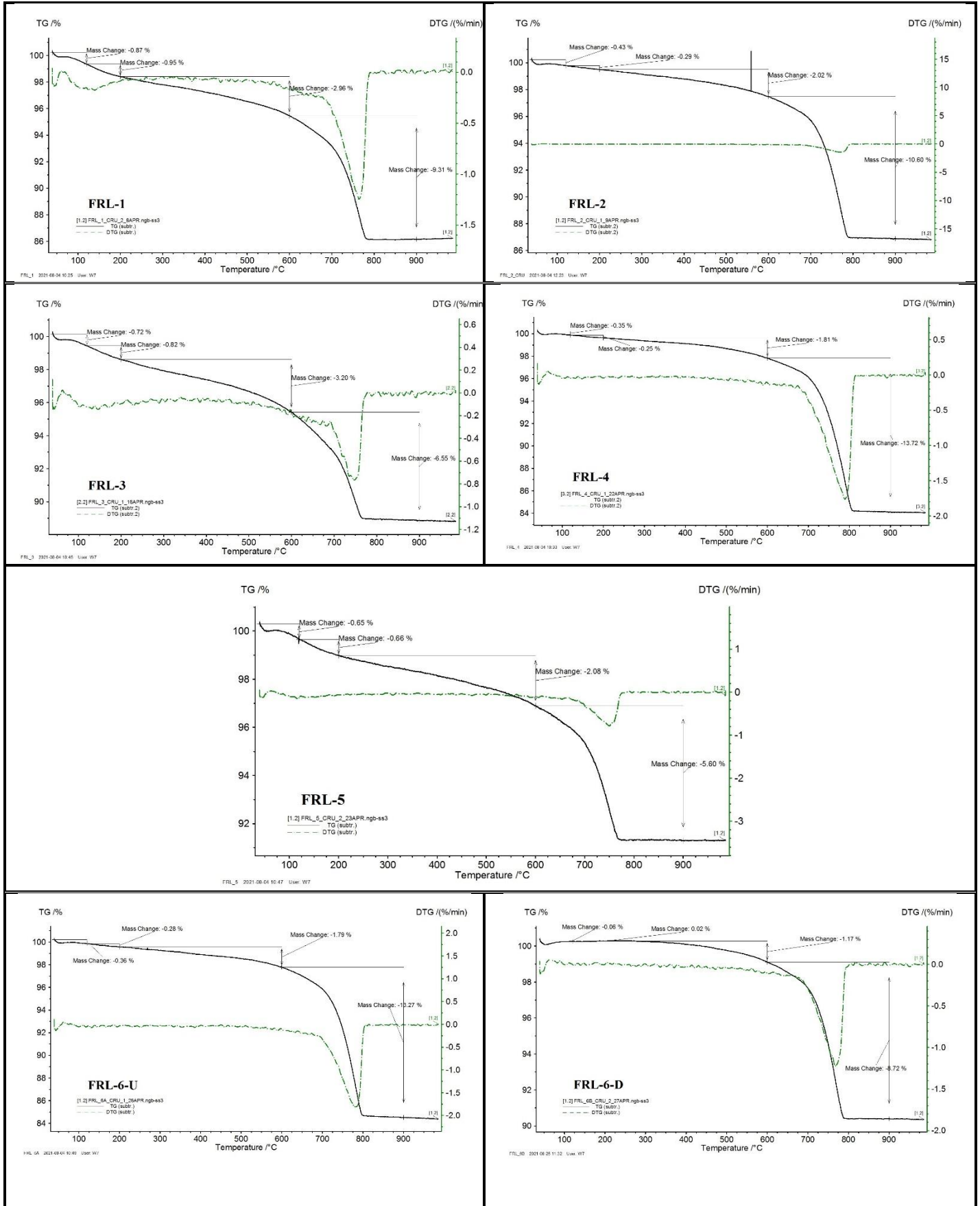
FRL-11-i

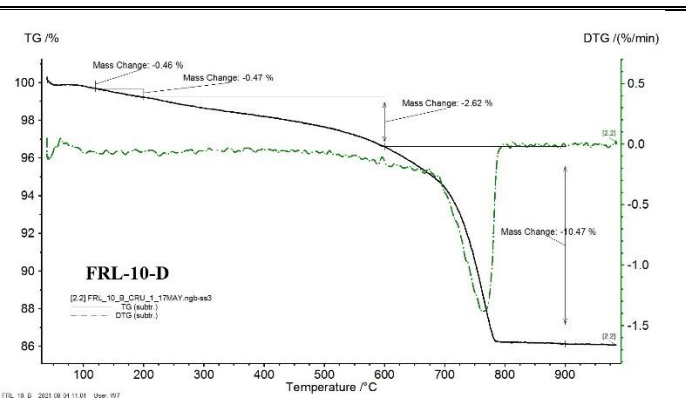
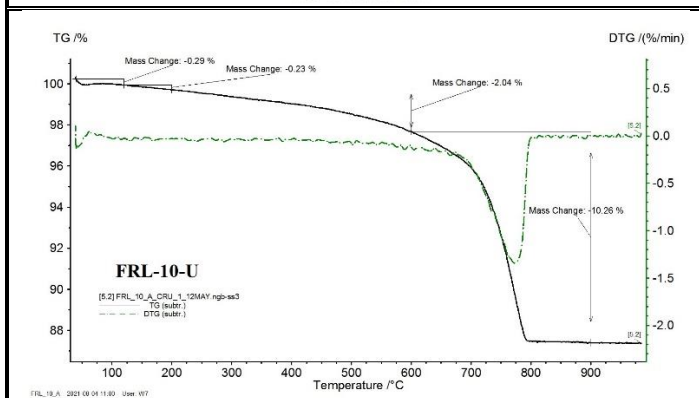
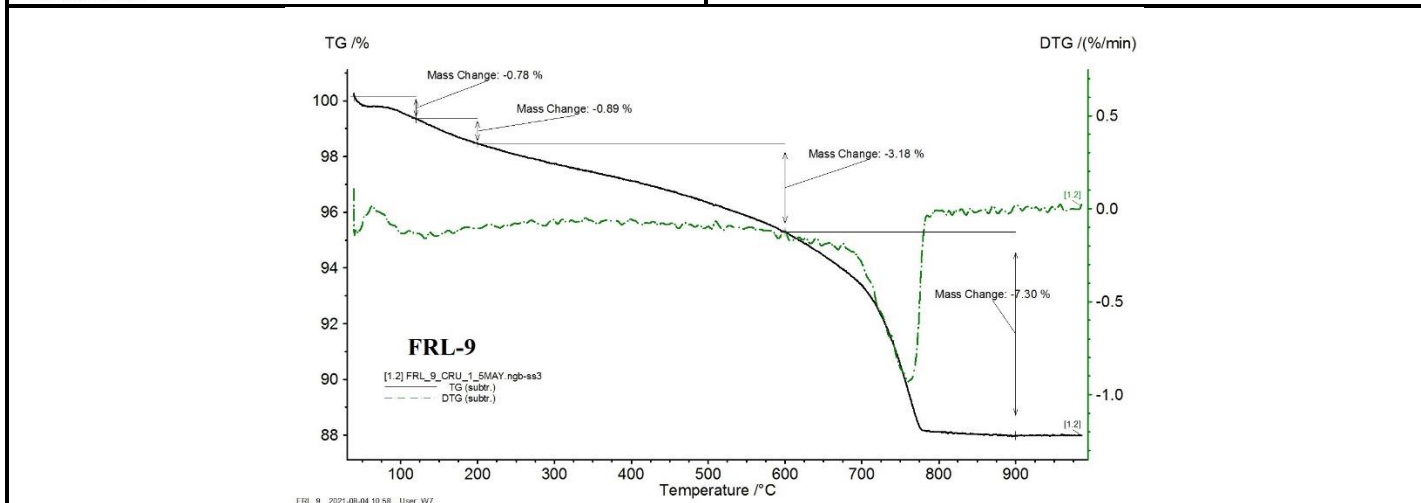
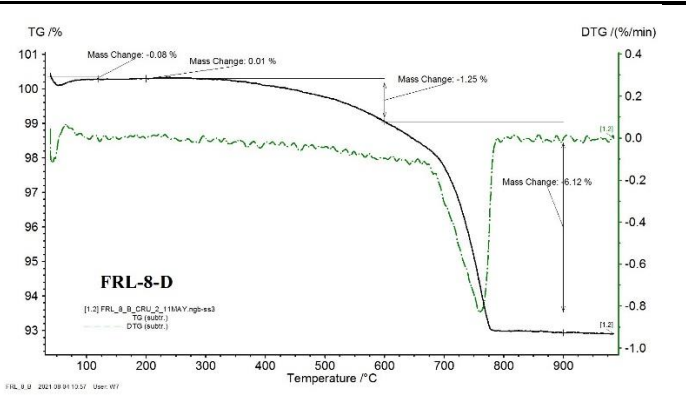
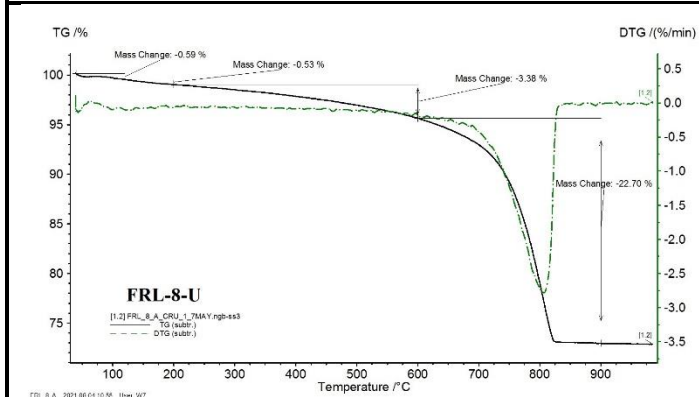
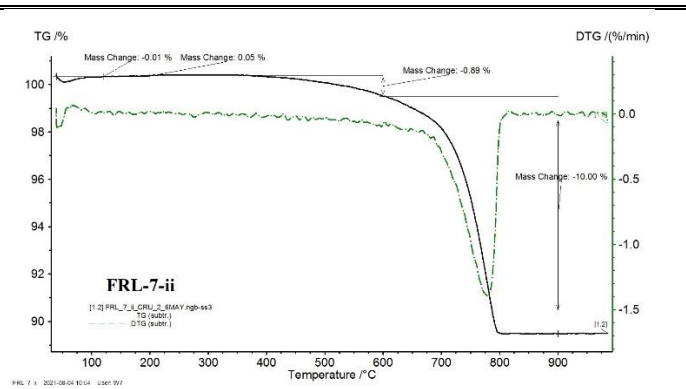
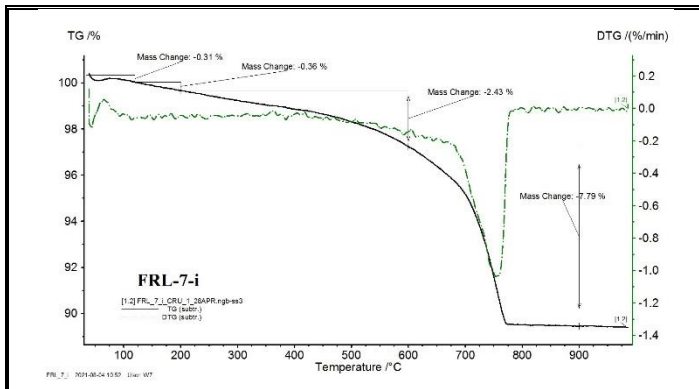


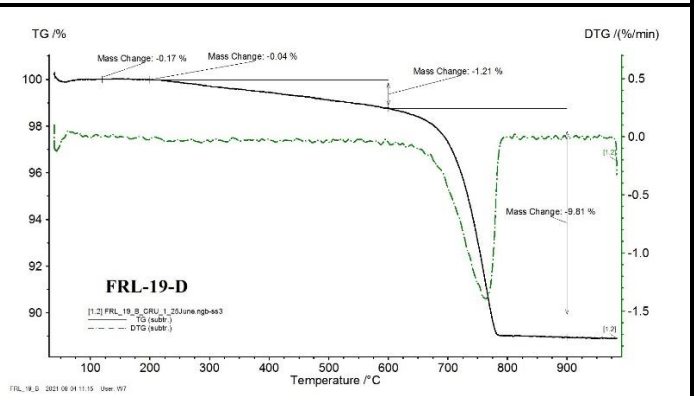
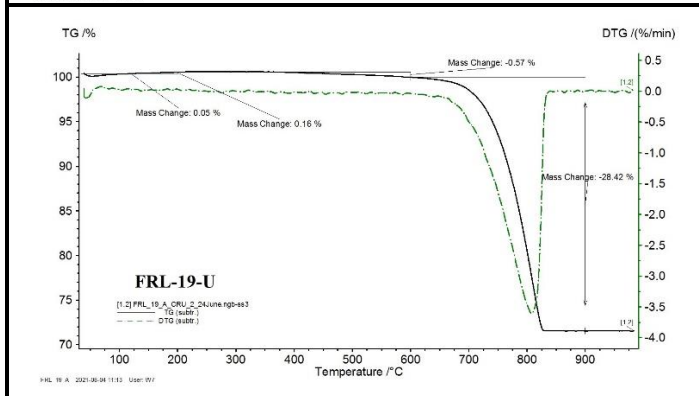
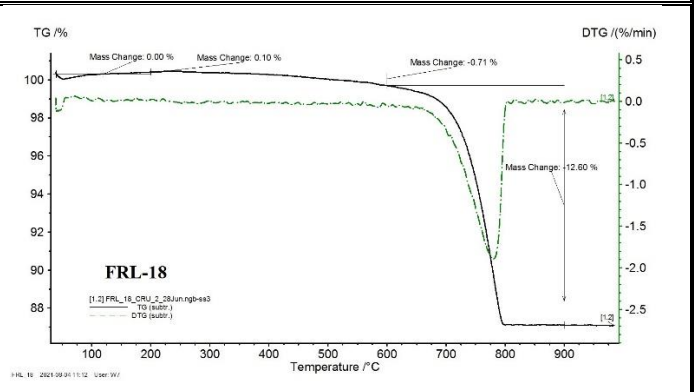
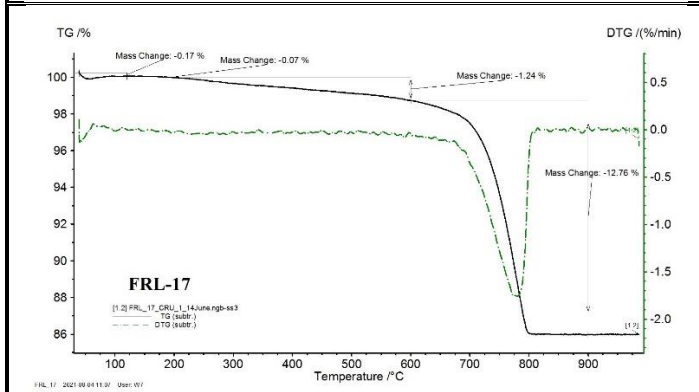
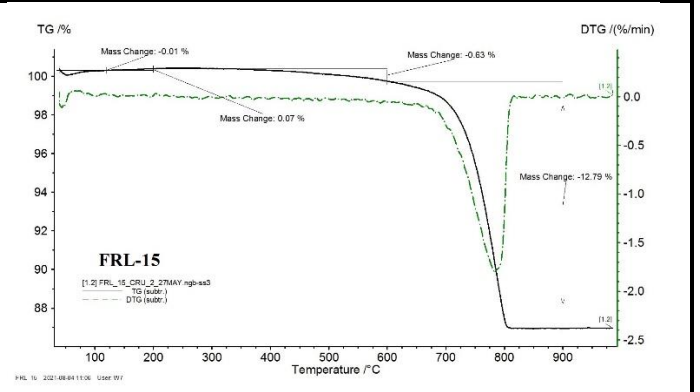
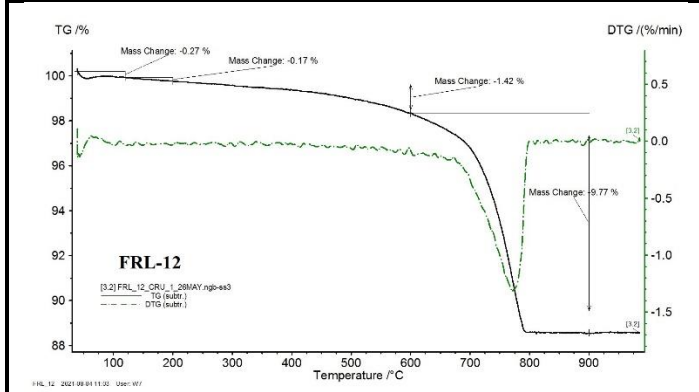
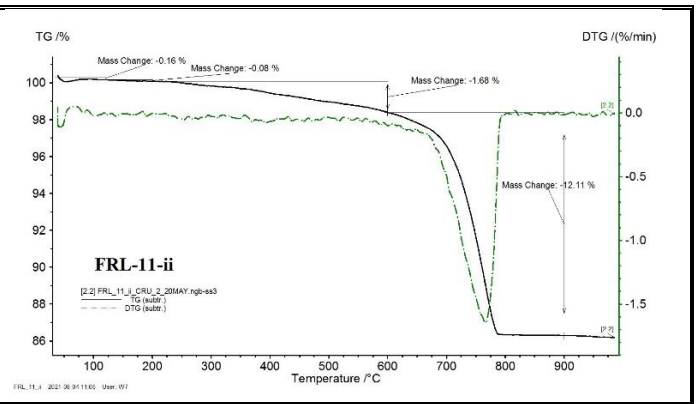
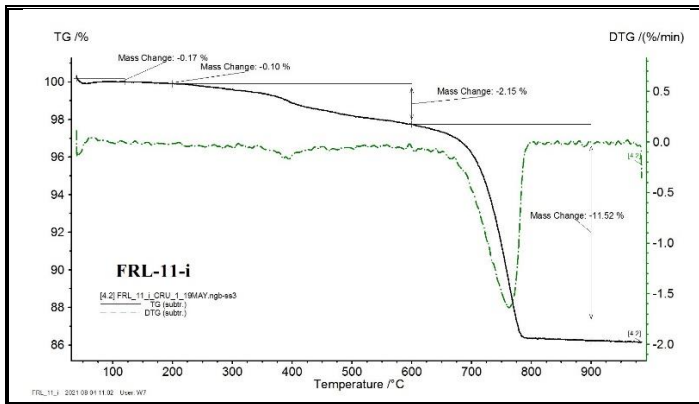
Appendix 8. 6-Results of soluble and insoluble fractions after acid attack, and granulometric analysis performed in insoluble fractions.

ID		Weight		Fraction (%)		Grain Size (%)								
No	Sample	Test	Initial	Final	Soluble	Insoluble	>4mm	4-2mm	2-1mm	1-0.5mm	0.5-.250	.25-.125	.125-.063	< 0.063
1.	FRL-1	A	11.5	9.57	17.1	82.8	80.7	4.10	2.70	2.50	3.10	3.70	2.40	0.20
		B	12.3	9.86	20.0	79.9	74.5	4.90	4.70	4.50	3.90	4.70	2.10	0.10
2.	FRL-2	A	14.6	9.80	32.9	67.1	8.80	9.10	15.1	22.8	22.0	13.3	7.10	1.40
		B	14.8	9.46	36.3	63.7	7.70	7.50	14.5	25.6	24.6	13.3	5.50	0.80
3.	FRL-3	A	17.6	13.6	22.4	77.5	40.1	20.9	10.3	6.30	5.10	7.10	7.10	2.90
		B	16.9	13.0	23.3	76.7	28.5	19.4	10.4	9.0	7.60	9.60	9.70	4.60
4.	FRL-4	A	9.55	5.78	39.5	60.5	1.60	4.20	23.9	36.5	17.3	10.5	5.10	0.20
		-	-	-	-	-	-	-	-	-	-	-	-	-
5.	FRL-5	A	15.4	11.9	22.5	77.5	33.9	14.2	8.90	8.70	12.9	10.8	8.00	2.40
		B	16.0	12.7	20.2	79.7	39.3	12.0	9.70	8.60	10.6	9.90	7.60	2.10
6.	FRL-6-U	A	13.5	7.79	42.4	57.5	1.50	6.10	9.80	10.8	17.5	23.7	24.1	5.90
		B	12.7	7.44	41.9	58.2	0.60	8.20	11.3	12.2	17.6	22.5	22.2	3.50
7.	FRL-6-D	A	15.6	12.0	23.3	76.7	1.40	11.0	29.4	27.9	18.7	8.30	2.20	0.20
		B	15.3	12.0	21.9	78.0	2.20	14.8	27.7	25.05	16.9	8.20	4.10	0.30
8.	FRL-7-i	A	10.7	8.22	23.6	76.4	51.5	16.5	8.90	6.10	5.20	5.40	4.40	1.10
		B	10.7	8.49	20.7	79.2	54.9	12.5	6.40	4.20	5.00	6.60	7.40	2.00
9.	FRL-7-ii	A	10.0	7.41	26.3	73.6	0.00	8.40	29.3	37.6	12.0	6.30	4.90	0.60
		B	10.0	7.43	26.2	73.7	0.00	7.90	28.8	36.0	14.3	6.40	4.80	1.10
10.	FRL-8-U	A	13.9	4.69	66.4	33.5	0.00	1.20	11.3	19.8	20.5	29.9	15.6	0.90
		B	14.3	4.55	68.3	31.6	0.00	1.10	9.60	16.8	26.8	36.2	8.10	0.30
11.	FRL-8-D	A	16.5	13.8	16.3	83.6	0.00	12.3	33.0	31.5	12.6	8.60	1.50	0.05
		B	14.5	11.4	21.2	78.7	0.90	7.30	33.6	33.9	14.1	8.70	0.90	0.05
12.	FRL-9	A	11.4	8.29	27.9	72.0	26.7	13.6	5.30	4.40	7.60	35.5	5.40	0.70
		B	10.9	8.26	30.2	69.7	26.5	14.7	5.10	4.70	6.20	17.3	18.0	8.40
13.	FRL-10-U	A	11.9	8.21	31.2	68.7	1.40	1.70	12.1	23.5	25.8	21.5	11.5	1.30
		B	11.9	8.09	32.5	67.4	1.90	2.00	13.0	21.7	24.8	27.9	6.90	0.60
14.	FRL-10-D	A	11.1	6.88	38.3	61.7	19.4	12.3	5.50	6.20	8.40	28.7	17.3	1.40
		B	11.1	7.86	29.3	70.6	34.9	18.1	7.30	5.80	7.60	17.5	6.90	0.80
15.	FRL-11-i	A	12.3	8.43	31.7	68.2	0.00	6.90	13.0	29.8	27.9	12.8	7.80	0.70
		B	12.3	8.26	33.2	66.8	0.00	3.10	11.0	28.2	27.5	19.7	9.50	0.19
16.	FRL-11-ii	A	12.2	8.11	33.9	66.1	2.70	3.40	10.7	26.1	26.7	20.1	9.00	0.39
		-	-	-	-	-	-	-	-	-	-	-	-	-
17.	FRL-12	A	12.3	8.30	33.0	66.9	0.00	5.20	23.2	37.5	14.8	8.30	7.80	2.43
		B	12.0	8.26	31.4	68.5	2.80	5.20	22.6	35.2	14.5	8.60	8.70	1.14
18.	FRL-15	A	12.5	8.95	28.5	71.4	5.60	16.0	21.6	19.3	23.3	6.30	5.00	2.07
		B	12.1	8.41	30.5	69.4	2.80	8.60	20.3	21.9	26.8	8.30	6.80	3.32
19.	FRL-18	A	10.1	7.19	29.0	70.9	4.00	9.30	30.5	37.2	9.70	4.30	3.50	0.27
		B	10.1	7.18	28.9	71.0	0.00	7.30	35.5	38.1	10.9	5.50	1.60	0.44
20.	FRL-19-U	A	10.1	2.36	76.6	23.3	0.00	9.10	32.9	30.4	14.3	6.20	4.50	0.54
		-	-	-	-	-	-	-	-	-	-	-	-	-
21.	FRL-19-D	A	10.0	7.44	25.7	74.2	1.50	17.6	28.3	30.9	13.8	3.40	3.20	0.49
		B	10.6	7.08	33.1	66.8	0.00	15.7	25.1	30.6	14.0	5.60	6.30	1.53

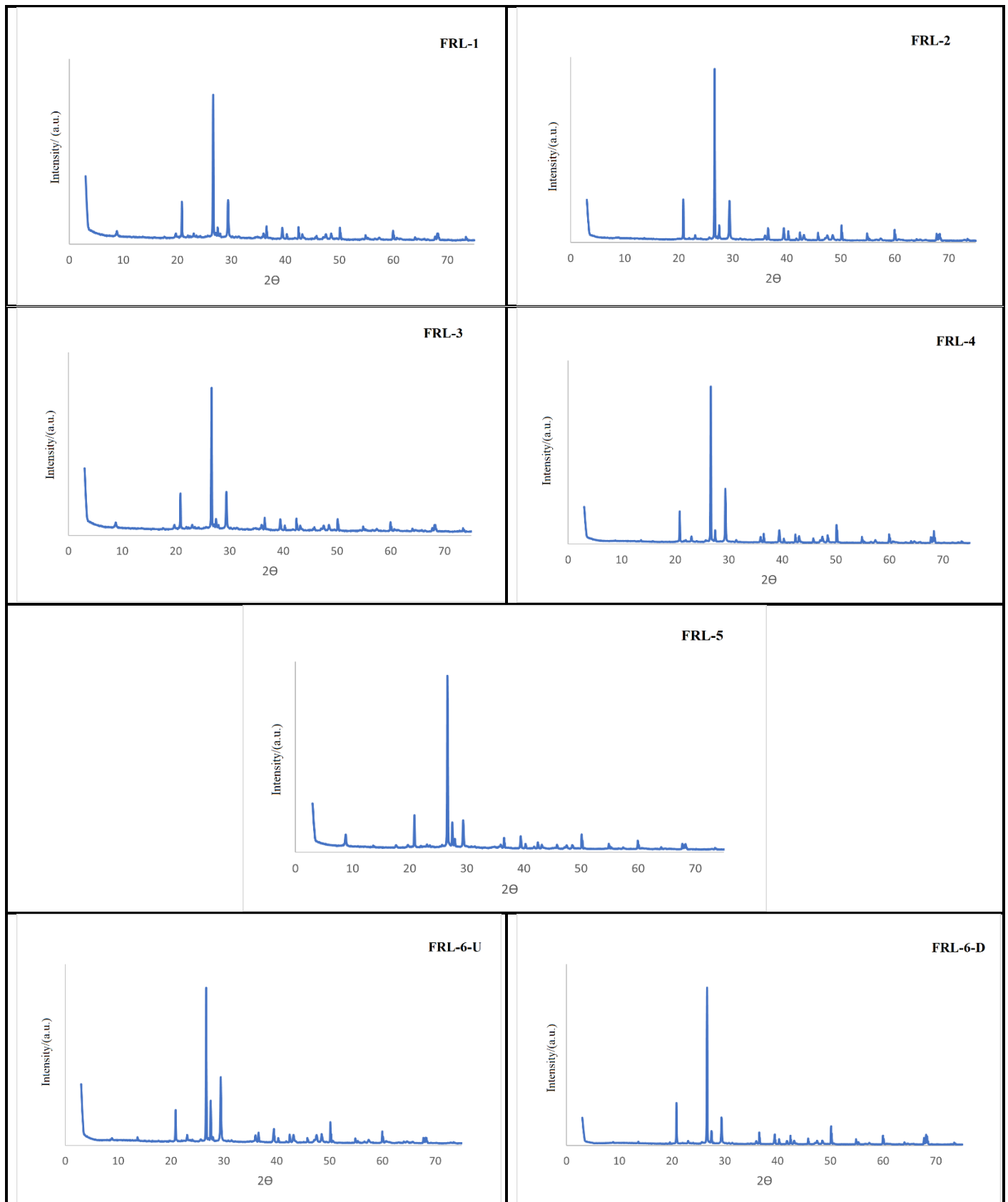
Appendix 8. 7-Thermograms of the results of the global fraction powders of the samples from the Roman villa of Frielas.

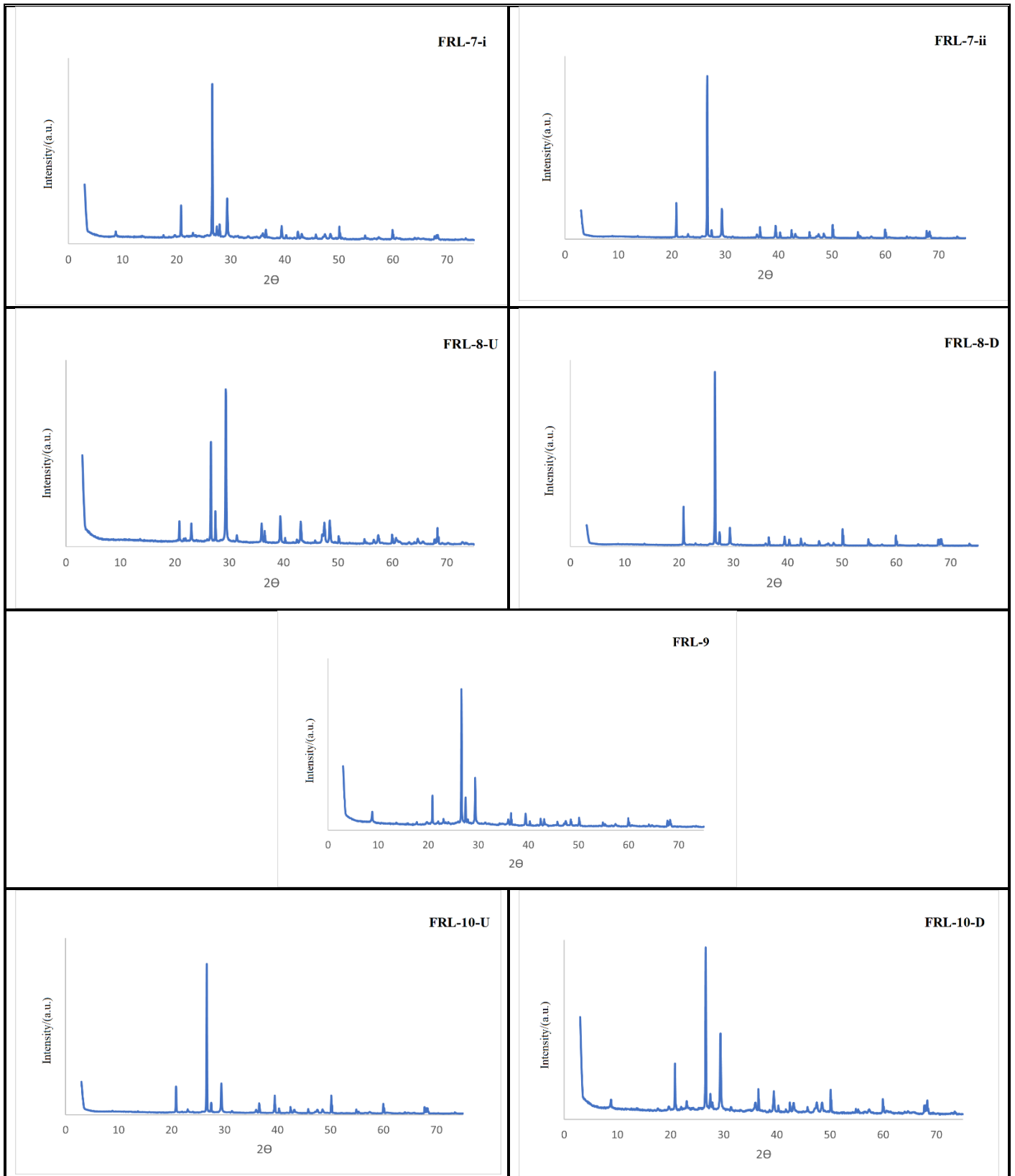


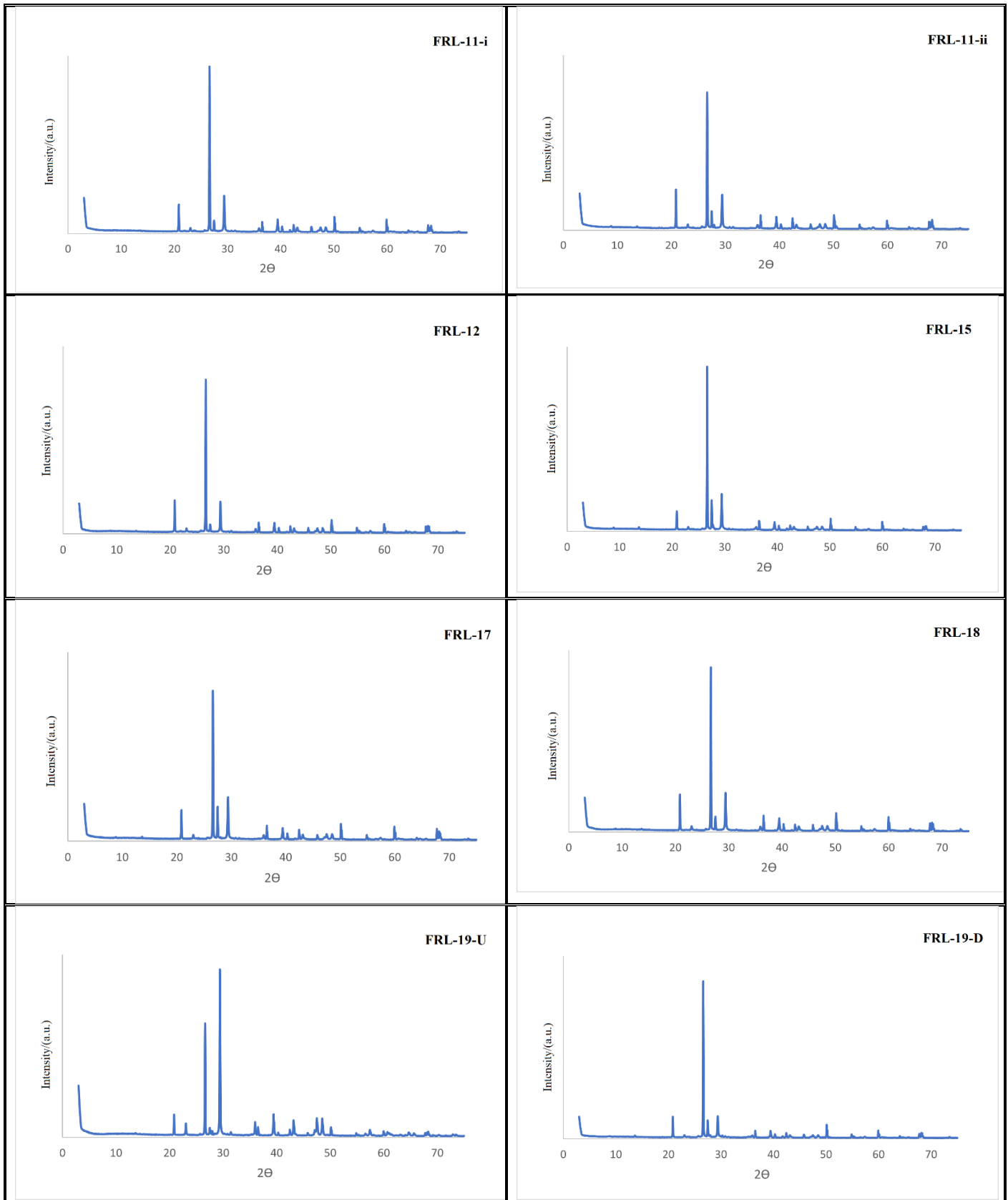















Appendix 8. 8-X-ray Diffractograms of the powdered global fractions of the mortar samples from the Roman villa of Frielas.














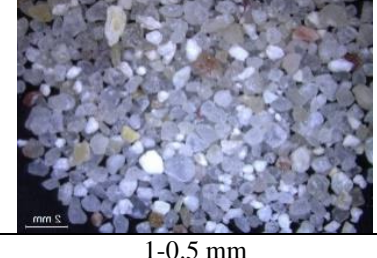
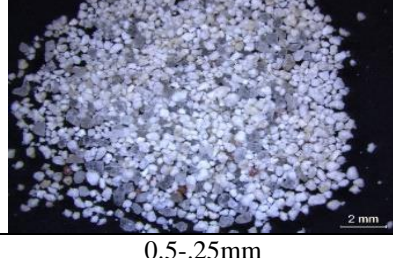























FRL-1		
	>4mm	4-2mm
		
2-1mm	1-0.5 mm	0.5-.25mm
		
0.25-.125mm	0.125-0.063 mm	<0.063mm









FRL-2		
	>4mm	4-2mm
		
2-1mm	1-0.5 mm	0.5-.25mm
		
0.25-.125mm	0.125-0.063 mm	<0.063mm




<p style="text-align: center;">FRL-3</p>		
	>4mm	4-2mm
		
2-1mm	1-0.5 mm	0.5-.25mm
		
0.25-.125mm	0.125-0.063 mm	<0.063mm








<p style="text-align: center;">FRL-4</p>		
	>4mm	4-2mm
		
2-1mm	1-0.5 mm	0.5-.25mm
		
0.25-.125mm	0.125-0.063 mm	<0.063mm








<p style="text-align: center;">FRL-5</p>	 <p style="text-align: center;">>4mm</p>	 <p style="text-align: center;">4-2mm</p>
 <p style="text-align: center;">2-1mm</p>	 <p style="text-align: center;">1-0.5 mm</p>	 <p style="text-align: center;">0.5-.25mm</p>
 <p style="text-align: center;">0.25-.125mm</p>	 <p style="text-align: center;">0.125-0.063 mm</p>	 <p style="text-align: center;"><0.063mm</p>








<p style="text-align: center;">FRL-6-U</p>	 <p style="text-align: center;">>4mm</p>	 <p style="text-align: center;">4-2mm</p>
 <p style="text-align: center;">2-1mm</p>	 <p style="text-align: center;">1-0.5 mm</p>	 <p style="text-align: center;">0.5-.25mm</p>
 <p style="text-align: center;">0.25-.125mm</p>	 <p style="text-align: center;">0.125-0.063 mm</p>	 <p style="text-align: center;"><0.063mm</p>









FRL-6-D	 2 mm	 2 mm
	>4mm	4-2mm
 2 mm	 2 mm	 2 mm
2-1mm	1-0.5 mm	0.5-.25mm
 2 mm	 2 mm	 2 mm
0.25-.125mm	0.125-0.063 mm	<0.063mm









FRL-7-i	 2 mm	 2 mm
	>4mm	4-2mm
 2 mm	 2 mm	 2 mm
2-1mm	1-0.5 mm	0.5-.25mm
 2 mm	 2 mm	 2 mm
0.25-.125mm	0.125-0.063 mm	<0.063mm




<p style="text-align: center;">FRL-7-ii</p>		
	>4mm	4-2mm
		
2-1mm	1-0.5 mm	0.5-.25mm
		
0.25-.125mm	0.125-0.063 mm	<0.063mm








<p style="text-align: center;">FRL-8-U</p>		
	>4mm	4-2mm
		
2-1mm	1-0.5 mm	0.5-.25mm
		
0.25-.125mm	0.125-0.063 mm	<0.063mm









<p style="text-align: center;">FRL-8 -D</p>		
	>4mm	4-2mm
		
2-1mm	1-0.5 mm	0.5-.25mm
		
0.25-.125mm	0.125-0.063 mm	<0.063mm









<p style="text-align: center;">FRL-9</p>		
	>4mm	4-2mm
		
2-1mm	1-0.5 mm	0.5-.25mm
		
0.25-.125mm	0.125-0.063 mm	<0.063mm









<p>FRL-10-U</p>		
	<p>>4mm</p>	<p>4-2mm</p>
		
<p>2-1mm</p>	<p>1-0.5 mm</p>	<p>0.5-.25mm</p>
		
<p>0.25-.125mm</p>	<p>0.125-0.063 mm</p>	<p><0.063mm</p>









<p>FRL-10-D</p>		
	<p>>4mm</p>	<p>4-2mm</p>
		
<p>2-1mm</p>	<p>1-0.5 mm</p>	<p>0.5-.25mm</p>
		
<p>0.25-.125mm</p>	<p>0.125-0.063 mm</p>	<p><0.063mm</p>








<p style="text-align: center;">FRL-11-i</p>		
	<p>>4mm</p>	<p>4-2mm</p>
		
<p>2-1mm</p>	<p>1-0.5 mm</p>	<p>0.5-.25mm</p>
		
<p>0.25-.125mm</p>	<p>0.125-0.063 mm</p>	<p><0.063mm</p>









<p style="text-align: center;">FRL-11 -ii</p>		
	<p>>4mm</p>	<p>4-2mm</p>
		
<p>2-1mm</p>	<p>1-0.5 mm</p>	<p>0.5-.25mm</p>
		
<p>0.25-.125mm</p>	<p>0.125-0.063 mm</p>	<p><0.063mm</p>

FRL-12		
	>4mm	4-2mm
		
2-1mm	1-0.5 mm	0.5-.25mm
		
0.25-.125mm	0.125-0.063 mm	<0.063mm

FRL-15		
	>4mm	4-2mm
		
2-1mm	1-0.5 mm	0.5-.25mm
		
0.25-.125mm	0.125-0.063 mm	<0.063mm

<p style="text-align: center;">FRL-18</p>	 <p style="text-align: right; font-size: small;">2 mm</p>	 <p style="text-align: right; font-size: small;">2 mm</p>
	>4mm	4-2mm
 <p style="text-align: right; font-size: small;">2 mm</p>	 <p style="text-align: right; font-size: small;">2 mm</p>	 <p style="text-align: right; font-size: small;">2 mm</p>
2-1mm	1-0.5 mm	0.5-.25mm
 <p style="text-align: right; font-size: small;">2 mm</p>	 <p style="text-align: right; font-size: small;">2 mm</p>	 <p style="text-align: right; font-size: small;">2 mm</p>
0.25-.125mm	0.125-0.063 mm	<0.063mm

<p style="text-align: center;">FRL-19-U</p>		 <p style="text-align: right; font-size: small;">2 mm</p>
	>4mm	4-2mm
 <p style="text-align: right; font-size: small;">2 mm</p>	 <p style="text-align: right; font-size: small;">2 mm</p>	 <p style="text-align: right; font-size: small;">2 mm</p>
2-1mm	1-0.5 mm	0.5-.25mm
 <p style="text-align: right; font-size: small;">2 mm</p>	 <p style="text-align: right; font-size: small;">2 mm</p>	 <p style="text-align: right; font-size: small;">2 mm</p>
0.25-.125mm	0.125-0.063 mm	<0.063mm

<p>FRL-19-D</p>	 <p style="text-align: right;">2 mm</p>	 <p style="text-align: right;">2 mm</p>
	<p>>4mm</p>	<p>4-2mm</p>
 <p style="text-align: right;">2 mm</p>	 <p style="text-align: right;">2 mm</p>	 <p style="text-align: right;">2 mm</p>
<p>2-1mm</p>	<p>1-0.5 mm</p>	<p>0.5-.25mm</p>
 <p style="text-align: right;">2 mm</p>	 <p style="text-align: right;">2 mm</p>	 <p style="text-align: right;">2 mm</p>
<p>0.25-.125mm</p>	<p>0.125-0.063 mm</p>	<p><0.063mm</p>